UNIVERSITY OF OKLAHOMA

GRADUATE COLLEGE

MECHANISMS OF ENZYMES OF THE α-AMINOADIPATE PATHWAY:

HOMOCITRATE SYNTHASE FROM *Thermus thermophilus*

AND

SACCHAROPINE DEHYDROGENASE FROM *Saccharomyces cerevisiae*

A DISSERTATION

SUBMITTED TO THE GRADUATE FACULTY

In partial fulfillment of the requirement for the

Degree of

DOCTOR OF PHILOSOPHY

By

VIDYA PRASANNA KUMAR

Norman, Oklahoma

2011

MECHANISMS OF ENZYMES OF THE α-AMINOADIPATE PATHWAY:
HOMOCITRATE SYNTHASE FROM *Thermus thermophilus*
AND SACCHAROPINE DEHYDROGENASE FROM *Saccharomyces cerevisiae*


A DISSERTATION APPROVED FOR THE
DEPARTMENT OF CHEMISTRY AND BIOCHEMISTRY




BY




_____
Dr. Paul F. Cook, Chair



_____
Dr. Ann H. West



_____
Dr. Kenneth M. Nicholas



_____
Dr. Susan J. Schroeder



_____
Dr. Michael J. McInerney

I dedicate this dissertation to

Our beloved son

Kaustubh Kasturiranga

# ACKNOWLEDGEMENTS

*Guru Brahma Gurur Vishnu*
*Guru Devo Maheshwaraha*
*Guru Saakshat Para Brahma*
*Tasmai Sree Gurave Namaha*

"The teacher is Brahma, the creator, Vishnu, the preserver; he is also Shiva, the

destroyer.  He is the source of the Absolute. I salute to such a great teacher."

There are few people who get a chance to live their dreams.  I always dreamed to be a Ph. D.  I thank Dr. Paul F. Cook, my advisor who gave my dream wings, my heart a spark of hope and determination to succeed.  I thank him for giving me a chance to work in his laboratory, for sharing the knowledge and spending numerous hours in helping me learn from my data.  I came to the University of Oklahoma with an intension to learn enzyme kinetics as I was fascinated by the subject.  Dr. Cook has strengthened my interest in the subject so much so that I treat my data more like a mystery where I am trying to make sense of every plot, every piece of information that I gather from my experiments.  I am very proud to be Dr. Cook's student.

I am fortunate to have the best graduate committee a student would wish to have.  I am very thankful to Dr. Ann H. West, Dr. Kenneth M. Nicholas, Dr. Susan J. Schoeder and Dr. Michael J. McInerney for their support and guidance during graduate school.  They have encouraged me when I was struggling with my courses and appreciated me when my research was coming along well by attending every annual evaluation in last four years.

I don't have words to thank them but want to say "I love you both". I feel the least I could do is to raise my son to be a fine human being, and providing him with the necessary support to choose and excel in the major of his choice. Though I missed my parents in India, Dr. Cook and Sandra Cook supported me here like one. The pool parties in summer, Thanksgiving dinners and Christmas get-togethers were the highlights of their affection towards us students. Dr. Cook has played multiple roles to help me succeed in graduate school. He has been a friend, a sounding board and has always treated me as his daughter. It is an honor to have been associated with him. I thank both Dr. Cook and Sandra Cook for their love and affection.

Realizing and supporting someone's dream is not an easy task. But my husband has done that. I thank him for the respect that he has given to my wishes and let me come this far to join graduate school. He is one of a kind. I am very grateful to him. I thank my Uncle Raman and Aunt Leela from Texas for their love and guidance. I appreciate their visits to Norman with food and vegetables. I can't thank my friend Raj enough for his friendship and helping me deal with the stress in graduate school and life in a new country. He encouraged me to sing which in turn became the best distressing activity. Giving me an opportunity to assist in organizing karaoke events in NY, NJ and CT brought out another aspect of my personality. I enjoyed the ultimate use of technology. Last but not least I would like to thank my son, Kaustubh, for giving me the joy of life, for being a son that anyone would be proud of, a friend and support in the last few years. Having him around is so much fun.

# TABLE OF CONTENTS

# LIST OF TABLES

# LIST OF ILLUSTRATIONS

# LIST OF SCHEMES

# ABSTRACT

The α-aminoadipate (AAA) pathway for lysine biosynthesis is nearly unique to higher fungi, including human and plant pathogens and euglenoids; an exception is the thermophilic bacterium *Thermus thermophilus*. Knock-out of the genes in this pathway has been shown to be lethal in *Saccharomyces cerevisiae*. It has been shown that scavenging of lysine is insufficient for survival in the host. Thus, enzymes of this pathway could be potential drug targets. The AAA pathway is comprised of eight enzymatic reactions catalyzed by seven enzymes. Homocitrate synthase (HCS) catalyzes the first and regulated step in this pathway, the condensation of acetyl-CoA (AcCoA) and α-ketoglutarate (α-Kg) to give homocitrate and coenzyme A (CoASH). The homocitrate synthase from *Thermus thermophilus* (*Tt*HCS) is a metal activated enzyme with either $Mg^{2+}$ or $Mn^{2+}$ capable of serving as the divalent cation. The enzyme exhibits a sequential kinetic mechanism. The mechanism is steady state ordered with α-Kg binding prior to AcCoA with $Mn^{2+}$, while it is steady state random with $Mg^{2+}$, suggesting a difference in the competence of the E·Mn·α-Kg·AcCoA and E·Mg·α-Kg·AcCoA complexes. The mechanism is supported by product and dead-end inhibition studies. The primary isotope effect obtained with deuterioacetylCoA (AcCoA-$d_3$) in the presence of $Mg^{2+}$ is unity at low concentrations of AcCoA, while it is 2 at high concentrations of AcCoA. Data suggest the presence of a slow conformational change induced by binding of AcCoA that accompanies deprotonation of the methyl group of AcCoA. The solvent kinetic deuterium isotope effect is also unity at low AcCoA, but is 1.7 at high AcCoA, consistent with the proposed slow

conformational change. The maximum rate is pH independent with either $Mg^{2+}$ or $Mn^{2+}$ as the divalent metal ion, while $V/K_{a\text{-}Kg}$ (with $Mn^{2+}$) decreases at low and high pH giving pK values of about 6.5 and 8.0. Lysine is a competitive inhibitor that binds to the active site of $Tt$HCS, and shares some of the same binding determinants as $\alpha$-Kg. Lysine binding exhibits negative cooperativity, indicating crosstalk between the two monomers of the $Tt$HCS dimer. Data are discussed in terms of the overall mechanism of $Tt$HCS.

Saccharopine dehydrogenase (SDH) catalyzes the final reaction in the $\alpha$−aminoadipate pathway, the conversion of L-saccharopine to L-lysine and $\alpha$-ketoglutarate using $NAD^+$ as an oxidant. The enzyme utilizes a general acid-base mechanism to carry out the multistep saccharopine dehydrogenase reaction with a base proposed to accept a proton from the secondary amine in the oxidation step and a second group proposed to activate water to hydrolyze the imine. A pair of thiols in the dinucleotide binding site forms a disulfide in the wild type (WT) enzyme as isolated, which interferes with binding of the dinucleotide substrate. The SDH enzyme with a C205S mutation, has been characterized recently and is referred to as a pseudo-WT enzyme. Crystal structures of an open apo-form of the pseudo-WT SDH (C205S), as well as a closed form of the C205S enzyme with saccharopine and NADH bound have been solved. The structure of a ternary complex between the C205S pseudo-WT enzyme, NADH, and Sacc provided a closed form of the enzyme and a more accurate description of the interactions between enzyme side chains and reactant functional groups. Importantly, the distance between C4 of the nicotinamide ring to C8 of Sacc is 3.6 Å, a reasonable hydride transfer distance. The side chains of H96 and K77 now

appear properly positioned to act as acid-base catalysts. Mutation of K77 to M results in a 145-fold decrease in $V/E_t$ and greater than a three order of magnitude increase in $V_2/K_{Lys}\mathbf{E_t}$ and $V_2/K_{\alpha-Kg}\mathbf{E_t}$. A primary deuterium kinetic isotope effect of 2.0 and an inverse solvent deuterium isotope effect of 0.77 on $V_2/K_{Lys}$ were observed, suggesting that hydride transfer is rate-limiting. The hypothesis was corroborated by the value of 2.0 obtained when the primary deuterium kinetic isotope effect was repeated in $D_2O$. The viscosity effect of 0.8 observed on $V_2/K_{Lys}$ indicated the solvent deuterium isotope effect resulted from stabilization of an enzyme form prior to hydride transfer. The deuterium isotope effect on $V$ is slightly lower than that on $V/K$ and decreases when repeated in $D_2O$, suggesting a contribution to rate limitation of product release, likely release of $NAD^+$. A small normal solvent isotope effect is observed on $V$, which decreases slightly when repeated with NADD, consistent with a contribution from product release to rate limitation. In addition, $V_2/K_{Lys}\mathbf{E_t}$ is pH independent consistent with the loss of an acid-base catalyst and perturbation of the $pK_a$ of the second catalytic group to higher pH, likely a result of a change in the overall charge in the active site. The H96Q mutation results in about a 28-fold decrease in $V_2/\mathbf{E_t}$ and $>10^3$-fold decreases in the second order rate constant. The primary deuterium kinetic isotope effect is within error 1, but a large solvent deuterium isotope effect of 2.4 is observed, suggesting rate limiting imine hydrolysis, consistent with the proposed role of H96 in protonating the leaving hydroxyl as the imine is formed. In agreement, the multiple isotope effects, repeating the primary deuterium effect in $D_2O$ and the solvent effect with NADD, are identical to the individual effect. The pH-rate profile for $V_2/K_{Lys}\mathbf{E_t}$ exhibits the $pK_a$ for K77, perturbed to a value of about 9, which must be unprotonated in order to accept a

proton from the ε-amine of the substrate Lys so that it can act as a nucleophile. The proposed roles of H96 and K77 are corroborated by the nearly 700-fold decrease in $V_2/\mathbf{E_t}$ and $>10^5$-fold decreases in the second order rate constants for the double mutant. Thus, data consistent with an acid-base mechanism in the non-physiologic reaction direction suggest that the K77 side chain initially accepts a proton from the ε-amine of the substrate lysine and eventually donates it to the imino nitrogen as it is reduced to a secondary amine in the hydride transfer step, and then H96 protonates the carbonyl oxygen as the imine is formed.

Lysine13, positioned near the active site base (K77), hydrogen-bonds to a glutamate neutralizing it, contributing to setting the $pK_a$ of the catalytic residues to near neutral pH. Glutamate16 hydrogen-bonds with Nε of R18 which in turn has strong H-bonding interactions with α-carboxylate of α-Kg. Mutation of K13 to M and E16 to Q decreased $k_{cat} \sim$ 15-fold, and primary and solvent deuterium isotope effects measured with the mutant enzymes indicate hydride transfer is rate limiting of SDH reaction. The pH-rate profiles for K13 exhibited no pH dependence, consistent with an increase in negative charge in the active site resulting in the perturbation in the $pK_a$s of catalytic groups. Elimination of E16 affects optimal positioning of R18 for binding and holding α-Kg in the correct conformation for optimum catalysis. As a result, the $\Delta\Delta G^{\circ}$' value of 2.60 kcal/mol for E16 suggests its contribution in binding of Lys.

Overall, data are consistent with the proposed acid-base mechanism in the non-physiologic reaction direction in which the K77 side chain initially accepts a proton from the ε-amine of the substrate lysine and eventually donates it to the imino nitrogen as it is reduced to a secondary amine in the hydride transfer step, and then H96

protonates the carbonyl oxygen as the imine is formed. Lysine13 and E16 play an important role of balancing the charge in the active site and elimination of either of the residues perturbs p$K_a$s of the catalytic residues, positioning of R18 residue for optimum binding of α-Kg is affected and the step contributing to the rate-limitation is changed to hydride transfer while in the case of C205S enzyme neither hydride transfer nor imine hydrolysis was solely responsible for rate-limitation. Thus K13 and E16 are important for favorable binding of Lys and α-Kg and optimum catalysis.

# CHAPTER 1

# Introduction

Amino acid biosynthesis is an important aspect of the living. Microorganisms and plants are capable of synthesizing essential and nonessential amino acids, but mammals acquire the essential amino acids from their diet. Amino acid biosynthesis is broadly divided into five families based on the initial precursor used to synthesize that group of amino acids (*1*). The serine family includes Ser, Cys and Gly and in addition provides intermediates that are diverted to other biosynthetic pathways. The aspartate family includes Asp, Asn, Met, Thr and Lys (except in fungi). These pathways are highly branched with multiple regulatory points along the way. Isoleucine, Val, Ala and Leu belong to the pyruvate family with highly interrelated pathways. Biosynthesis of all the aromatic amino acids are grouped into one family, which consists of a common aromatic pathway leading to biosynthesis of chorismate from which the three aromatic amino acids, Tyr, Trp and Phe are derived. The glutamate family includes Glu, Gln, Pro and Arg biosynthesis. Most fungi and the thermophilic bacterium *Thermus thermophilus* derive lysine (Lys) from $\alpha$-ketoglutarate, which is in equilibrium with glutamate (*1*). Thus, Lys biosynthesis, in these cases, has been included in the Glutamate family. Regulation of the amino acid biosynthetic pathways is at two levels, one at the level of enzyme activity and metabolite concentrations and the second at the level of gene expression.

Lysine has two distinct biosynthesis pathways. The diaminopimelate pathway operates in plants, bacteria and lower fungi while the $\alpha$-aminoadipate pathway is found

in euglenoids and higher fungi, including the human pathogens *Candida albicans,*

*Cryptococcus neoformans, Aspergillus fumigatus,* the plant pathogen *Magnaporthe*

*grisea,* and the thermophilic bacterium *Thermus thermophilus (2-4).* The α-

aminoadipate pathway consists of seven enzymatic reactions in eight steps (Figure 1).

Candidiasis, cryptococcosis and aspergillosis represent a major health threat for patients

with cancer, AIDS, those that received a transplant, and those undergoing

immunosuppressive treatment. With the essentiality of the lysine biosynthetic pathway

reported in *Aspergillus fumigatus in vivo* (*5*)*,* one might expect the pathway to also be

essential in the other human fungal pathogens. Thus, the enzymes of the pathway could

be good targets for anti-fungal drug development (*6, 7*). The kinetic and chemical

mechanisms of all the enzymes have been studied (*8-20*).
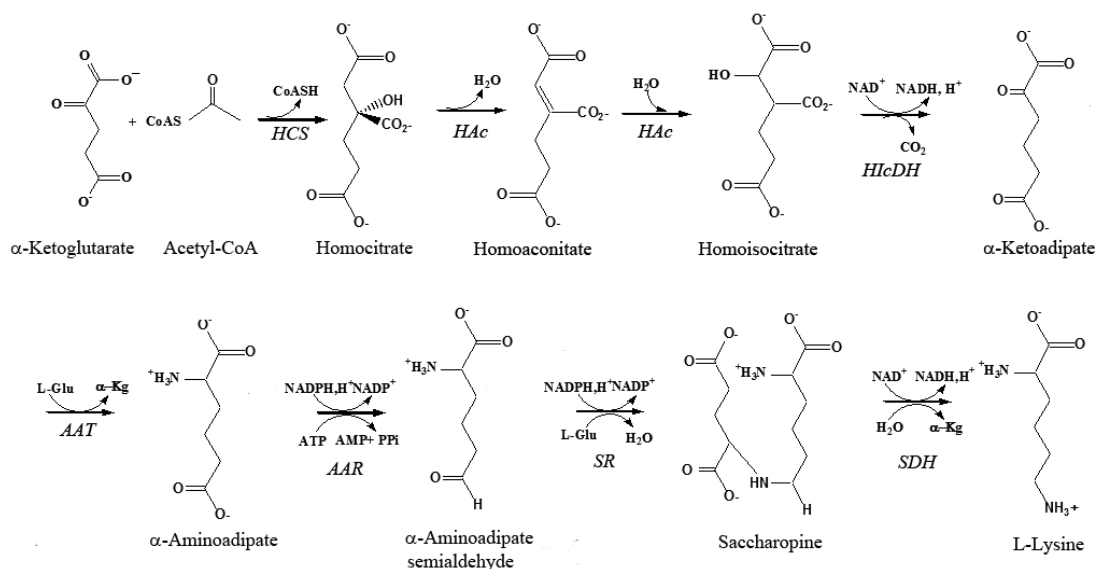


Figure 1.1 The α-aminoadipate pathway for lysine biosynthesis in yeast. The enzymes involved are 1. Homocitrate synthase (HCS; EC 4.1.3.21). 2. Homoaconitase (HAc; EC 4.2.1.36). 3. Homoisocitrate dehydrogenase (HIcDH; EC 1.1.1.87). 4. α-Aminoadipate aminotransferase (AAT; EC 2.6.1.39). 5. α-Aminoadipate reductase (AAR; EC 1.2.1.31). 6. Saccharopine reductase (SR; EC 1.5.1.10). 7. Saccharopine dehydrogenase (SDH; EC 1.2.1.31).

2

The α-aminoadipate pathway begins with HCS catalyzing a Claisen condensation between AcCoA and α-Kg. The methyl of AcCoA attacks the carbonyl of α-Kg. This is followed by hydrolysis of the thioester which traps the product homocitrate. HAc catalyzes the next two reactions in the pathway. In the first reaction homocitrate is dehydrated to form homoaconitate which is then hydrated to form homoisocitrate in the second reaction. The third enzyme in the pathway, HIcDH catalyzes the oxidative decarboxylation of homoisocitrate to α-ketoadipate. In the next step amino group from glutamate is transferred to α-ketoadipate, catalyzed by AAT. Once α-aminoadipate is formed the δ-carboxylate is reduced to an aldehyde by AAR. The aldehyde is then condensed with α-amine of glutamate followed by reduction to give saccharopine which is the direct precursor for lysine; the enzyme catalyzing this reaction is SR. The last reaction in the pathway is catalyzed by SDH which gives lysine and α-Kg via an NAD-dependent oxidative deamination.

The research in this dissertation is directed toward a determination of the mechanism of HCS and SDH. An introduction to these enzymes will be presented in detail below.

## 1.1 HOMOCITRATE SYNTHASE

Homocitrate synthase (HCS) (acetyl-coenzyme A: 2-ketoglutarate C-transferase; E.C. 2.3.3.14) catalyzes the first and regulated step in α-aminoadipate pathway, the condensation of Acetyl-CoA (AcCoA) and α-ketoglutarate (α-Kg) to give homocitrate and CoA (*21, 22*).

Multiple sequence alignment at the amino acid level of HCS from *Saccharomyces cerevisiae, Candida albicans, Aspergillus fumigatus, Schizosaccharomyces pombe* and *Thermus thermophilus* showed highly conserved regions suggesting high similarity in the structure at the active site (Figure 2). In most bacteria, lysine is synthesized from aspartic acid through the diaminopimelate pathway. However, in *T. thermophilus,* lysine is synthesized via the α-aminoadipate pathway (*4, 23, 24*). The *T. thermophilus* HCS (*Tt*HCS) has a 54% sequence identity at the amino acid level to *S. cerevisiae* HCS (*Sc*HCS) and ~53% identity to *C. albicans* HCS (*Ca*HCS). Disruption of the *LYS20* gene (encoding HCS) of *T. thermophilus* resulted in a lysine auxotroph (*4*).

### 1.1.1 Stability and Divalent Metal Ion Requirement.

*Saccharomyces cerevisiae* HCS is unstable as isolated. Careful studies with a variety of solvents and additives were carried out to develop conditions to stabilize the enzyme. A combination of 100 mM guanidine hydrochloride, 100 mM α-cyclodextrin, and 600 mM ammonium sulfate maintained the enzyme active for 2 months when stored at 4 °C (*25*). The *Ca*HCS was also unstable and could be stabilized with the same combination of reagents (Appendix 3).

*Saccharomyces cerevisiae* HCS as isolated was analyzed for bound metal ions by inductively coupled plasma mass spectrometry (ICP-MS) (*9*), which suggested $87 \pm 5$ % $Zn^{2+}$. Only $Zn^{2+}$ could reactivate the enzyme after treatment with EDTA, suggesting that the *Sc*HCS is a Zn-metalloenzyme (*9*). Monovalent ($Li^+$, $Cs^+$, $K^+$ and $NH_4^+$) and divalent ($Mg^{2+}$, $Mn^{2+}$ and $Ca^{2+}$) cations tested exhibited various levels of inhibition. The

best monovalent cation for the activity of *Sc*HCS was K$^+$ which gave only slight inhibition (*26*).

An ICP-MS analysis of *Tt*HCS showed Cu$^{2+}$, Fe$^{2+}$, and Zn$^{2+}$ at 0.25, 0.12, and 0.04 mol/mol, respectively (*27*).

```
SpoHCS  MS----------VSEANG------------TETIKPPMNGNPYGPNP--SDFLSRVNNFS  36
AfHCS   MCPGADNEPNGHTNGANGTVPHPGFTAVETRQNPHPSASRNPYGHNVGVTDFLSNVSRFK  60
ScHCS   --------------------------------MTAAKPNPYAAKP--GDYLSNVNNFQ  24
CaHCS   MVDGYKEVS--------------------ESFDRSKIQHNPYGPNP--GDFLSNVGNFQ  37
TtHCS   ------------------------------------------------------MVE  3
                                                            ..

SpoHCS  IIESTLREGEQFANAFFDTEKKIQIAKALDNFGVDYIELTSPVASEQSRQDCEAICKLGL  96
AfHCS   IIESTLREGEQFANAFFDTEKKIEIAKALDDFGVDYIELTSPCASEQSRKDCEAICKLGL 120
ScHCS   LIDSTLREGEQFANAFFDTEKKIEIARALDDFGVDYIELTSPVASEQSRKDCEAICKLGL  84
CaHCS   LIESTLREGEQFANAFFSTETKIEIAKALDDFGVDYIELTSPVASEQSRKDCEAICKLGL  97
TtHCS   ILDTTLRDGTQGEGVSLSVDDKVAIARRLAAFGIHLIEGGWPGSNPKDAEFFQRMRGVDL  63
        :::::***:*  *  .. :..: *: **: *  **:. **   * :. :. :  : :  :.*

SpoHCS  KCKILTHIRCH--------MDDARVAVETGVDGVDVVIGTSQYLRKYSHGKD-MTYIIDS 147
AfHCS   KAKILTHIRCH--------MDDARVAVETGVDGVDVVIGTSSYLREHSHGKD-MTYIKNT 171
ScHCS   KAKILTHIRCH--------MDDAKVAVETGVDGVDVVIGTSKFLRQYSHGKD-MNYIAKS 135
CaHCS   KAKILTHIRCH--------MDDARVAVETGVDGVDVVIGTSQFLRQYSHGKD-MNYIAQS 148
TtHCS   GAARLAAFGATRRKGLAPEEDPSVLALLEAETPVVVLFGKSWTLHVLEALETSLEENLRM 123
        .  *: : .          *  : :*:  .  * *::*.*  *:  .  : :

SpoHCS  ATEVINFVKSKGIEVRFSSE---DSFRSDLVDLLSLYKAVDKIGVNRVGIADTVGCATPR 204
AfHCS   AIEVIEFVKSKGIEIRFSSE---DSFRSDLVDLLSIYSAVDKVGVNRVGIADTVGCASPR 228
ScHCS   AVEVIEFVKSKGIEIRFSSE---DSFRSDLVDLLNIYKTVDKIGVNRVGIADTVGCANPR 192
CaHCS   AIEVIEFVKSKGIEIRFSSE---DSFRSDLVDLLNIYRTVDKIGVNRVGIADTVGCANPR 205
TtHCS   IEETVAFFARRGRRVVYDAEHFFDGYKEDPAYALATLEAAFRGGADTLVLCDTNGGSLPE 183
         *.: *.  :* .: :.:*  *.::.* .  *     :. : *.: : :.** * : *.

SpoHCS  QVYDLIRTLRG-VVSCDIECHFHNDTGMAIANAYCALEAGATHIDTSILGIGERNGITPL 263
AfHCS   QVYELVRVLRG-VVSCDIETHFHNDTGCAIANAYCALEAGATHIDTSVLGIGERNGITPL 287
ScHCS   QVYELIRTLKS-VVSCDIECHFHNDTGCAIANAYTALEGGARLIDVSVLGIGERNGITPL 251
CaHCS   QVYELVRTLKS-VVKCDIECHFHNDTGCAIANAYTALEGGARLIDVSVLGIGERNGITPL 264
TtHCS   EVYAITKAVVERFPGVRVGIHPHNDADLAVANALAAVRAGATHVQGTINGYGERCGNLNL 243
        :**  : :.:   :   * ***:. *:*** *:..** :: :: * *** * *

SpoHCS  GALLARMYVTDREYITHKYKLNQLRELENLVADAVEVQIPFNNYITGMCAFTHKAGIHAK 323
AfHCS   GGLMARMMVADPEYVKSKYKLEKLKDIEDLVAAAVEVNIPFNNYITGFCAFTHKAGIHAK 347
ScHCS   GGLMARMIVAAPDYVKSKYKLHKIRDIENLVADAVEVNIPFNNPITGFCAFTHKAGIHAK 311
CaHCS   GGLMARMIAADREYVLSKYKVHKLRDIENLVAEAVQVNIPFNNPITGFCAFTHKAGIHAK 324
TtHCS   TSFLPTLVFKYGIPAISPEKLRELREVSHFVDERANLTPNRRAPYVGEAAFAHKAGVHVS 303
        .::. :          *:.::::::..:*   .::   .  .* .**:****:*..

SpoHCS  AILANPSTYEILKPEDFGMSRYVHVGSRLTGWNAIKSRAEQLNLHLTDAQAK-------- 375
AfHCS   AILNNPSTYEIINPADFGMTRYVHFASRLTGWNAIKSRAQQLNIEMTDAQYK-------- 399
ScHCS   AILANPSTYEILDPHDFGMKRYIHFANRLTGWNAIKARVDQLNLNLTDDQIK-------- 363
CaHCS   AILANPSTYEILSPSDFGLTRYIHFANRLTGWNAIKSRVDQLNLHLTDEQCK-------- 376
TtHCS   AVLKNPRTYEHIPPEWVGNQRRFLVS-DVSGRSNLLAKLQELGVDLSKEEARRLLEEVKA 362
        *:* ** *** : *  .*  * . .. ::* . : :: ::*.:.:: : :

SpoHCS  --------------------------------------------ELTVRIKKLADV 387
AfHCS   --------------------------------------------ECTAKIKALADI 411
ScHCS   --------------------------------------------EVTAKIKKLGDV 375
CaHCS   --------------------------------------------EVTNKIKKLGDV 388
TtHCS   LEYEGYAFEGAEASFYLLAHRLKGGSLPFSVEGFSVFVHGRGLSTAWAEATVRVRVGESL 422
                                                     * *  :::    .:

SpoHCS  RTLAMDDVDRVLREYHADLSDADR-----ITKEASA---------------------- 418
AfHCS   RPIAVDDADSIIRAYYRNLKSGENKPLLDLTAEEQAQFAAKEKELAGSGVIA-------- 463
ScHCS   RSLNIDDVDSIIKNFHAEVSTPQVLSAKKNKKNDSDVPELATIPAAKRTKPSA------- 428
```

Figure 1.2 Multiple sequence alignment at the amino acid level of HCS from *Saccharomyces cerevisiae* (*Sc*HCS), *Candida albicans* (*Ca*HCS), *Aspergillus fumigatus* (*Af*HCS), *Schizosaccharomyces pombe* (*Sp*HCS) and *Thermus thermophilus* (*Tt*HCS).  *, fully conserved residue; :, groups of strongly similar properties; ., groups of weakly similar properties.

When treated with EDTA, $Tt$HCS had negligible activity, but addition of $Mg^{2+}$, $Mn^{2+}$ and $Co^{2+}$ restored the activity, suggesting $Tt$HCS required the biologically relevant metal ions $Mg^{2+}$ and $Mn^{2+}$ for its activity (*27*).

## 1.1.2 Kinetic Mechanism.

For $Sc$HCS, an ordered kinetic mechanism was proposed with α-Kg binding to the enzyme prior to AcCoA and with CoA released before homocitrate (Figure 3) (*8*).

Uncompetitive product inhibition by CoA against α-Kg suggested an irreversible reaction consistent with the downhill hydrolysis of the intermediate homocitryl-CoA. Studies with desulfo-CoA and citrate as dead-end inhibitors supported the proposed ordered kinetic mechanism. When initial velocity patterns were obtained over a wide range of AcCoA, competitive substrate inhibition by AcCoA was observed with a $K_{IAcCoA}$ of 0.93 mM, suggesting binding of AcCoA to free enzyme, giving a non-productive E·AcCoA dead-end complex (*26*). Kinetic parameters for the WT enzyme at pH 7.5 were as follows : $K_{AcCoA}$, 24 μM; $K_{\alpha-Kg}$, 1.3 mM; and $k_{cat}$, 37 min$^{-1}$ (*8*).
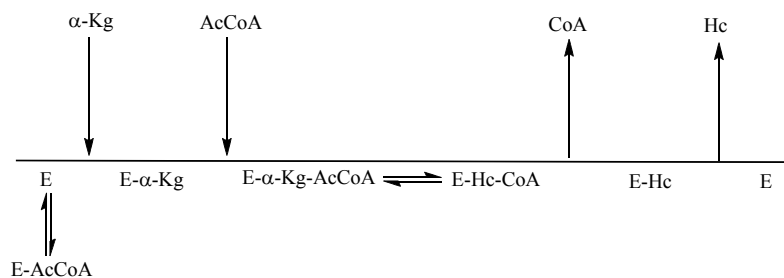


Figure 1.3 Proposed Kinetic Mechanism for *Saccharomyces cerevisiae* Homocitrate Synthase. An ordered kinetic mechanism is shown with a dead-end E-AcCoA complex.

Other than kinetic parameters, there is little information available for the *Schizosaccharomyces pombe* HCS. Kinetic parameters for WT *Sp*HCS were as follows: $K_{AcCoA}$, 11 μM; $K_{\alpha\text{-}Kg}$, 0.16 mM; and $k_{cat}$, 300 min$^{-1}$(*28*).

### 1.1.3 Chemical Mechanism.

A general acid-general base, Lewis acid chemical mechanism has been proposed for *Sc*HCS (figure 4) (*9*). α-Ketoglutarate binds to the enzyme with its α-carboxylate and α-oxo groups coordinated to the active site Zn. At this point Zn is coordinated with two imidazoles, a glutamate, the α-carboxylate and α-oxo groups of α-Kg and a water molecule. The general acid (B$_1$H) hydrogen bonds to the carbonyl of α-Kg, while the C5-carboxylate interacts with a protonated residue on the enzyme (B$_3$H). AcCoA binds with its methyl group positioned near the enzyme residue that will act as a general base (B$_2$). The general base abstracts a proton from the methyl of AcCoA which generates an enolate, this step comes to equilibrium prior to the condensation reaction. A nucleophilic attack of the methyl of AcCoA on the carbonyl of α-Kg is carried out resulting in the alkoxide of homocitryl-CoA, which then accepts a proton from B$_1$H. The resulting homocitryl-CoA is then hydrolyzed by a Zn-activated water molecule, with B$_1$ acting as a base. The products are then released.

### 1.1.4 Site-directed Mutagenesis.

A crystal structure was not available for HCS when the site directed mutagenesis was carried out. The structure of a homolog of HCS, isopropylmalate synthase from

*Mycobacterium tuberculosis* (*Mt*IPMS), was used to guide mutagenesis. *Sc*HCS and

*Mt*IPMS have a 27% sequence identity, and a 39% similarity.
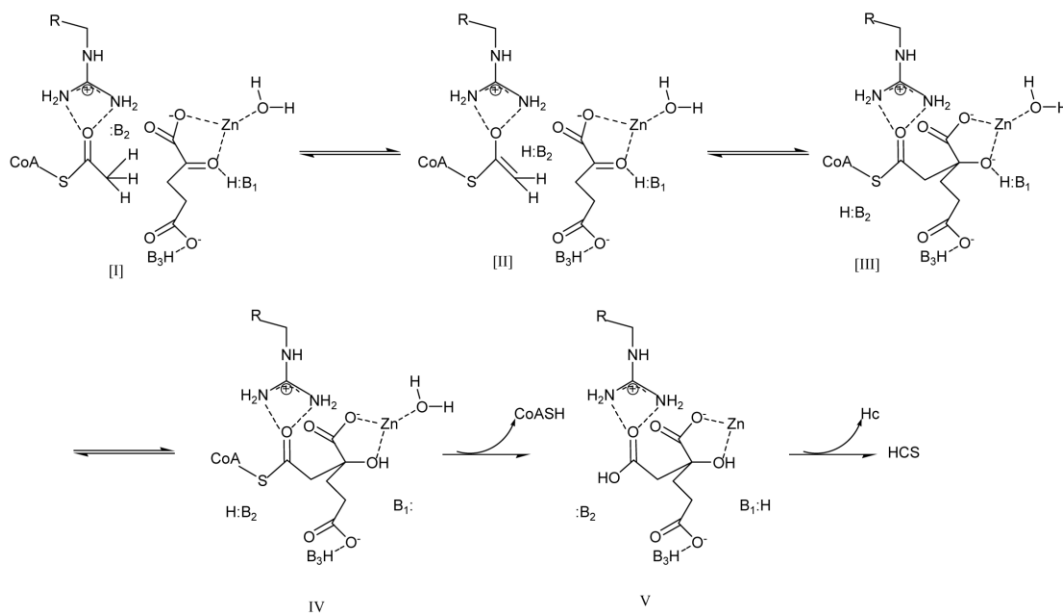


Figure 1.4  Proposed Chemical mechanism for *Saccharomyces cerevisiae* homocitrate synthase (*9*).  [I] α-Kg binds to the enzyme with its α-carboxylate and α-oxo groups coordinated with the active site Zn.  [II] Formation of the enolate.  [III] Formation of the alkoxide of homocitryl-CoA.  [IV] Potonation to give homocitryl-CoA. [V] Hydrolysis to give homocitrate and CoA.

The active site residues, Glu155, His309, and Tyr320, are conserved in all HCSs

for which sequence is available.  On the basis of the proposed chemical mechanism (*9*)

and the crystal structure of *Mt*IPMS (*29*), the roles of Glu155, His309 and Tyr320 were

studied by site-directed mutagenesis (*10*).  From initial velocity and pH studies, it was

suggested that H309 and E155 function as a catalytic dyad to deprotonate the methyl

group of AcCoA, while hydrogen-bonding between E155 and H309 increased the

basicity of H309.  The increased proton affinity would in turn aid in efficiently

accepting a proton from the methyl of AcCoA.  Y320 was believed to aid in correct

positioning of the substrates and/or the catalytic dyad (*10*).

On the basis of the *Sp*HCS structure (*28*), active site residues involved in either binding of substrate and/or catalysis were mutated. The T197S mutant enzyme gave a slight decrease in $k_{cat}$, while T197A gave a 25 fold decrease, suggesting that a hydrogen-bond between the hydroxyl of T197 and the C1 carboxylate of α-Kg contributed to catalysis, likely by properly orienting the substrate. Mutations of R43, which hydrogen-bonds with carboxylate of α-Kg, abolished activity completely, consistent with its role in protonating the carbonyl of α-Kg in the condensation reaction. Mutations in residues interacting with C5 carboxylate of α-Kg impaired or abolished activity, the R163K mutant enzyme showed an increase in $K_{\alpha\text{-}Kg}$ of >150 fold. Data suggested residues interacting with C5 carboxylate are important to α-Kg binding.

### 1.1.5 Location of Slow Steps.

Isotope effects were measured for *Sc*HCS to determine the location of slow steps along the reaction pathway. A solvent deuterium kinetic isotope effect of unity suggested protons were not in flight in the rate-limiting transition state. A small primary kinetic deuterium isotope effect of 1.3 suggested the deprotonation of the methyl of AcCoA came to equilibrium prior to a rate-limiting condensation to form the alkoxide of homocitryl-CoA.

Values of about 1.5 and 2 were estimated for $^D V$ and $^D(V/K_{\text{AcCoA}})$, respectively, for E155A. Data suggested formation of lower amount of the enolate of AcCoA prior to condensation, consistent with E155 increasing the basicity of H309 via direct hydrogen-bonding. Primary kinetic deuterium isotope effects of 1.8 and 1.4 were observed on $V$ and $V/K_{\text{AcCoA}}$ for Y320F mutant enzyme, consistent with the enolization

step being rate limiting at saturating substrate concentration, but with some substrate stickiness on the basis of the smaller isotope effect on $V/K_{AcCoA}$ compared to $V$.


**1.1.6 Mechanism of Regulation**.

The kinetic mechanism of regulation of $Sc$HCS by $Na^+$ and lysine has been studied (*26*). $Na^+$ is an activator at low concentrations and an inhibitor at high concentrations. The inhibition by $Na^+$ is eliminated at high concentrations of AcCoA, and thus, the monovalent cation as an inhibitor is proposed to bind the same site as the AcCoA. Feedback inhibition by lysine was linear competitive against $\alpha$-Kg over the physiological concentration range ($\leq 5$ mM). Binding of lysine to HCS when measured by fluorescent titration was biphasic, consistent with negative cooperativity of binding. In the absence of a crystal structure for HCS, lysine binding to an allosteric site, stabilizing a less active conformer of the enzyme, was suggested.

L-Lysine was also competitive against $\alpha$-Kg and non-competitive against AcCoA for the $Sp$HCS. When the key residues Asp123 and Glu222 interacting with $\varepsilon$-amino group of lysine, were mutated to Asn and Gln, respectively, inhibition by lysine was abolished (*30*).


**1.1.7 Structural Studies**.

The structure HCS from *S. pombe* was the first one solved (*28*). The $Sp$HCS is a homodimer with N-terminal and C-terminal domains. The N-terminal domain forms an $(\alpha/\beta)_8$ TIM barrel, while the C-terminal domain consists of two subdomains, 1 and 2. Subdomain 1 has a $\beta$ sheet with three consecutive $3_{10}$ helices forming a lid motif, while

subdomain 2 consists of a 3-helix bundle.  The C-terminal lid domain of monomer A closes on the TIM barrel of monomer B. The active site of *Sp*HCS is located within the C-terminal end of the TIM barrel. The divalent cation in the active site has octahedral geometry and is coordinated to E44, H224, H226 and the α-carboxylate and  α-oxo groups of α-Kg.  Upon binding of α-Kg, pronounced structural changes occur in the linker between β4 and α4 of the TIM barrel, which is disordered in apoenzyme. Superimposition of the active sites of the apo-enzyme and α-Kg-bound closed complex showed the carboxylate groups of D123 and E222 rotating away from the site to accommodate C5 of α-Kg, while H103, R43, R163 and S165 re-orient towards the center of the β barrel to form hydrogen bonds and/or salt bridges with α-Kg.  The α-carboxyl and α-oxo groups of α-Kg hydrogen bond to T197 and R43, firmly positioning the substrate (Figure 1.5).

A molecular basis for the feedback regulation by lysine was proposed on the basis of a comparison of the lysine-bound structure with that of the α-Kg-bound structure and/or that of the free enzyme.  With lysine bound, the structure (*30*) was similar to the substrate bound structure (*28*) with a few important differences.  The lid motif from the C-terminal domain, which regulates the substrate access to the neighboring active site, was in a closed conformation.  When the active sites were compared, the positions of the four key residues, H103, D123, R163, and E222 were significantly different in the lysine and α-Kg bound structures. Histidine-103 and R163 were rotated towards α-Kg (*28*) forming hydrogen bonding with its C5-carboxylate, while in the lysine-bound structure these residues moved away and D123 and E222

were rotated inwards forming hydrogen-bonds and/or salt bridges with the ε-amine group of lysine. These findings were supported by kinetic data which showed that L-lysine was competitive against α-Kg.
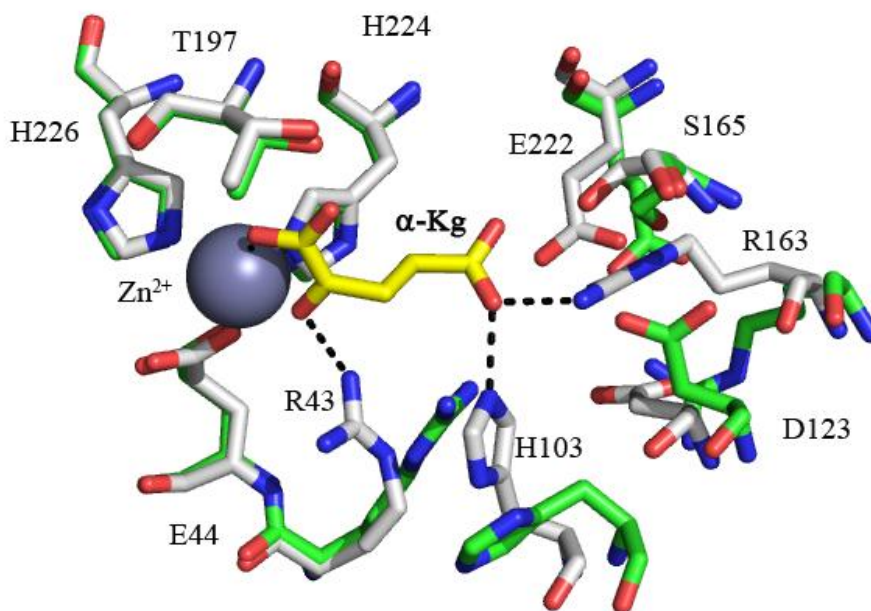


Figure 1.5 Superimposition of the active sites of the *Sp*HCS apo- and α-Kg bound enzymes. Active site residues of the apo-enzyme (PDB code 3IVS) are shown as green carbons and α-Kg bound enzyme (PDB code 3IVT) as gray carbons. The active site $Zn^{2+}$ is shown as a sphere in gray. Hydrogen bonds are shown as dashed lines in black.

The structure of *Tt*HCS has also been solved (*27*). The binary complex of enzyme and α-Kg had a metal ion which was identified as $Cu^{2+}$ on the basis of the electron density. The enzyme-homocitrate complex, derived from the addition of α-Kg and AcCoA to the crystallization medium with enzyme had the same metal ion. A third structure, E•α-Kg•$Mg^{2+}$ was derived from apo-enzyme (treatment with EDTA), with the addition of $Mg^{2+}$ and α-Kg during crystallization. *Tt*HCS has an overall structure similar to that of *Sp*HCS. The α-carboxylate and α-oxo groups of α-Kg are coordinated

to the bound divalent metal ion and the α-carboxylate accepts a hydrogen bond from T166, while the α-oxo group interacts with the guanidium group of R12. The side chains of A164 and L94 make van der Waals contact with the C3 and C4 atoms of α-Kg, and the C5-carboxylate is stabilized by hydrogen bonds and ionic interactions with H72 and R133 and, via a water molecule, interacts with S135. Lysine bound to the active site of *Tt*HCS exhibits the same interactions as α-Kg with the divalent metal ion, T166, A164 and L94. However, the α-amino of lysine is also within hydrogen bonding distance to Tyr297* (the * indicates the residue is from the other subunit of the dimer), and the ε-amino group of lysine is stabilized by interactions with D92 and E193 (see Chapter 2 for figure). The most significant difference in binding of α-Kg and lysine is in the displacement of residues surrounding the C5-carboxylate of α-Kg to accommodate binding of the ε-amino group. The overall rearrangement includes: 1) movement of R133 away from the active site, forming an ion pair with E43; and 2) movement of H72, which formed a hydrogen bond to the C5-carboxylate of α-Kg, to stack with the side chain of R12, which formed a hydrogen bond to the α-oxo group of α-Kg. Overall, there is a 44 Å displacement of the position of the α11 helix, which includes Y297*, moving it closer to the active site (*27*).

## 1.2 SACCHAROPINE DEHYDROGENASE

The last reaction in the AAA pathway is catalyzed by saccharopine dehydrogenase (SDH, *N*6-(glutaryl-2)-L-lysine: nicotinamide adenine dinucleotide (NAD) oxidoreductase (L-lysine forming); (EC 1.5.1.7)). The enzyme catalyzes the reversible pyridine nucleotide dependent oxidative deamination of saccharopine (Sacc)

to generate α-Kg and Lys using NAD as an oxidant (Figure 1) (*3*).  The enzyme from *Saccharomyces cerevisiae* (*Sc*SDH) is a monomer with a reported molecular weight of ~39 000 with one binding site for reactants (*31*).

### 1.2.1 Kinetic Mechanism.

A sequential kinetic mechanism has been proposed for *Sc*SDH with binding of NAD followed by Sacc, while release of the products, α-Kg and Lys is random and precedes release of NADH (*18*).  Competitive inhibition by lysine verses NADH indicated formation of a dead-end E·Lys complex, and α-Kg gave substrate inhibition that was uncompetitive versus NADH at saturating Lys concentration, suggesting the presence of a dead-end E·NAD·α-Kg complex; this inhibition requires the E·NAD complex to exist in the steady-state, i.e. release of NAD must contribute to rate limitation.  Results from the product and dead-end inhibition experiments were consistent with the proposed mechanism (Figure 6)
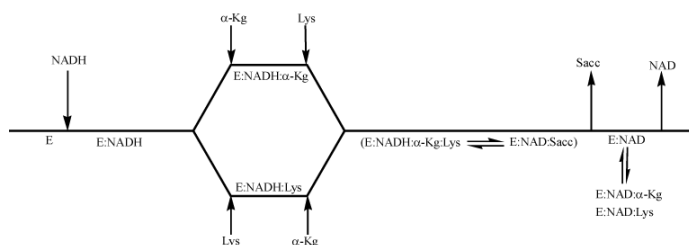


Figure 1.6 Proposed Kinetic Mechanism of *Sc*SDH.  The reaction is shown in the non-physiological direction with NADH binds prior to α-Kg and Lys.  Ordered release of Sacc prior to NAD is shown.

The substrate dependence of isotope effects, e.g. primary deuterium isotope effects, provides information on kinetic mechanism.  In the case of an ordered

mechanism *V/K* for the first substrate bound is equal to the on-rate for the reactant, which is not sensitive to isotopic substitution, and $^D(V/K)$ will be equal to 1. On the other hand, $^D(V/K_b)$ will be finite if the isotopic step contributes to rate limitation. In the case of a random kinetic mechanism, values of $^D(V/K_a)$ and $^D(V/K_b)$ will be finite. If the values of $^D(V/K_a)$ and $^D(V/K_b)$ are equal, data would suggest either a rapid equilibrium random mechanism, or that both reactants are equally sticky suggesting a steady state random mechanism. If they are not equal, reactant with the larger $^D(V/K)$ provides an indication of preferential release from the central complex. (*32*). For *Sc*SDH, $^D(V_2/K_{NADH})$ was close to unity at neutral pH, supporting the proposed ordered binding of NADH to free enzyme (*18*). However, $^D(V_2/K_{Lys})$ and $^D(V_2/K_{\alpha-Kg})$ had finite values suggesting random addition of these two substrates. A larger value was observed for $^D(V_2/K_{\alpha-Kg})$, suggesting that $\alpha$-Kg is preferentially released from E·NADH·Lys·$\alpha$-Kg complex prior to Lys. In addition, $^D(V_2)$ was similar to $^D(V_2/K_{Lys})$ suggesting the off-rate for lysine from the E·NADH·Lys·$\alpha$-Kg complex is similar to off-rate for NAD from the E·NAD complex, corroborating the existence of E·NAD in the steady state (*18*).

The $K_{eq}$ for *Sc*SDH was experimentally determined by carrying out the reaction at fixed concentrations of all the reactants except for NAD, and monitoring change in absorbance at 340 nm. The empirical value of $K_{eq}$ estimated was $3.9 \times 10^{-7}$ M, similar to the value determined by the Haldane relationship (*18*).

**1.2.2 Use of Inhibitors to Map the Active Site.**

Extensive kinetic studies with substrate analogs were carried out to map the interaction between the functional groups on the substrates and the residues in the substrate binding pocket (*33*).  Inhibition by a number of nucleotide analogs suggested that most of the binding energy came from the AMP portion of the molecule, and that the conformation generated upon binding of oxidized and reduced dinucleotide might be different.  The presence of a 2'-phosphate had an adverse effect on binding of substrates.  A hydrophilic binding pocket was suggested for the nicotinamide ring on the basis of a decreased affinity for 3-acetylpyridine adenine dinucleotide compared to NAD.  The α-Kg binding pocket was studied using aromatic and aliphatic keto acid analogs.  An optimal length of three carbons from the α-keto group up to and including the side chain carboxylate was estimated.  The distance between the C1, C2 unit and the C5 carboxylate was important and the α-oxo contributed a factor of about 10 to affinity. The α-Kg binding pocket is larger and more flexible than the lysine binding pocket, which is more hydrophobic. Lysine was the only substrate found; ornithine was not a substrate.  Extensive inhibition studies using aliphatic amino acids suggested that the amino acid binding pocket could accommodate a branch at the γ-carbon, but not at the β-carbon (*33*).

**1.2.3 Chemical Mechanism.**

The pH dependence of kinetic parameters provides information on the optimal protonation state of groups on reactant and enzyme involved in binding and/or catalysis. The pH dependence of *V* is determined at saturating substrate concentrations, while *V/K*

is obtained at saturating concentrations of all substrates but one which is maintained limiting. Thus, the $V$ profile reflects the groups involved in catalysis and $V/K$ reflects groups on enzyme and/or substrate involved in binding and/or catalysis (*32*).

A proton shuttle mechanism was suggested for the *Sc*SDH (Figure 7) with two groups on enzyme proposed as acid-base catalysts. Once NAD and Sacc are bound, a group with a p$K_a$ of 6.2 accepts a proton from the secondary amine of Sacc as it is oxidized to the imine [II]. The conjugate acid then does not participate further until Lys is formed. The general base, possibly a Lys or His residue with a p$K_a$ of 7.2 accepts a proton from $H_2O$ as it attacks the Schiff base carbon forming a carbinolamine intermediate [III]. The same residue then donates its proton to the carbinolamine nitrogen to form a protonated carbinolamine [IV]. Collapse of the carbinolamine occurs with the conjugate base of the group with a p$K_a$ of 7.2,.accepting the proton from the hydroxyl of the carbinolamine and generating $\alpha$-Kg and Lys [V]. The amine nitrogen of Lys is then protonated by the residue that accepted a proton from secondary amine of Sacc in the very first step [VI] (*19*).

### 1.2.4 Isotope Effects and Chemical Mechanism.

Primary deuterium isotope effect (*19*) for $V_2/K_{NADH}$ was unity while finite values of $1.56 \pm 0.05$ and $1.9 \pm 0.1$ for $^D(V_2/K_{Lys})$ and $^D(V_2/K_{\alpha\text{-}Kg})$ respectively, were observed. $^D(V_2/K_{\alpha\text{-}Kg}) > {}^D(V_2/K_{Lys})$ suggested preferential release of $\alpha$-Kg from E·NADH·Lys·$\alpha$-Kg complex. The value of $1.45 \pm 0.07$ for $^D(V_2)$ was similar to that for $^D(V_2/K_{Lys})$ suggesting steady state existence of E·NAD. Finite values for the primary deuterium isotope effects reflected hydride transfer contributing to rate limitation. $^D(V_2)$ was pH

independent but $^D(V_2/K_{Lys})$ decreased as pH was increased. The data suggested that pH and isotope sensitive steps were not the same and hydride transfer step was not completely rate limiting in the overall reaction. Isotope insensitive step contributed to $V_2$ at low pH.
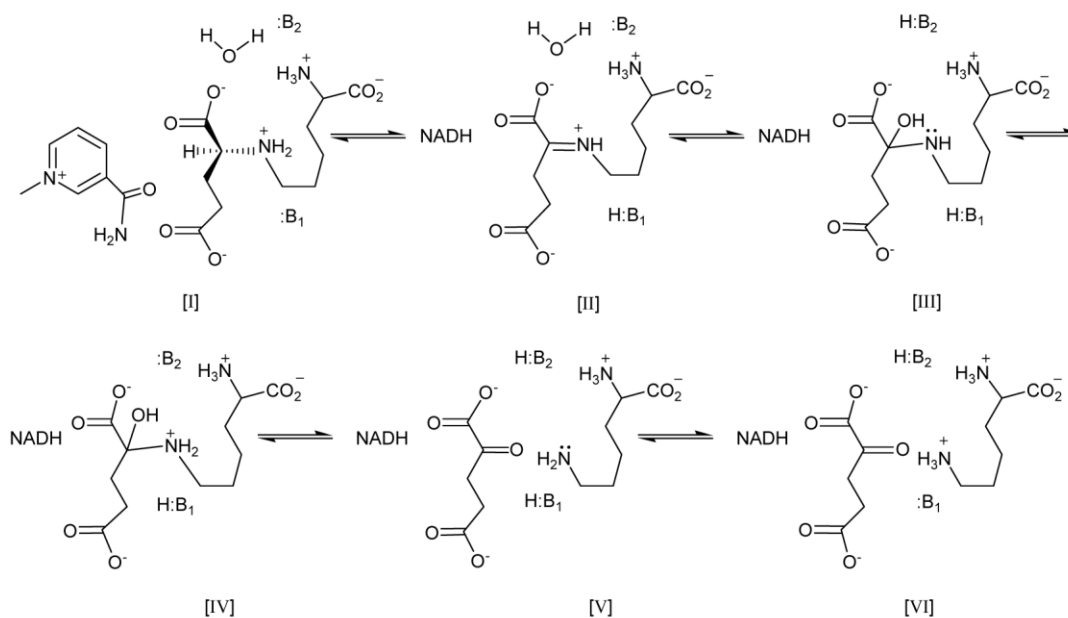


Figure 1.7 Proposed Chemical Mechanism for *Saccharomyces cerevisiae* SDH (*19*). [I] Central complex E•NAD•Sacc once NAD and Sacc bind; [II] Schiff base intermediate; [III] Carbinolamine intermediate; [IV] Protonated carbinolamine; [V] Central complex E•NADH•α-Kg•Lys; [VI] Protonated Lys. With the exception of Sacc, no stereochemistry is implied.

The solvent deuterium isotope effects were finite with $^{D2O}V_2$ and $^{D2O}V_2/K_{Lys}$ of 2.2 ± 0.1 and 1.9 ± 0.1, suggesting significant contribution of proton transfer steps to rate limitation of the overall reaction. Larger solvent isotope effects as compared to primary kinetic isotope effects suggest imine hydrolysis step contributing more to rate-limitation than hydride transfer step.

In order to determine whether the substrate and solvent isotope effects were on the same step along the reaction pathway, multiple isotope effects were carried out. If

the isotope sensitive step is completely rate-limiting, then isotope effects will not change in presence of the second isotope. An increase in the isotope effects will be seen if the step is not completely rate-limiting. If the substrate and solvent isotope effects are on two different steps, then deuteration of the substrate would make the deuterium-sensitive step more rate-limiting as a result decreasing the observed solvent isotope effect.

Multiple isotope effects can be carried out in two ways 1) primary substrate deuterium isotope effect in $D_2O$; 2) solvent isotope effects with NADD as the dinucleotide (*32*). In the case of *Sc*SDH, both multiple isotope effects were measured on $V_2$ and $V_2/K_{Lys}$. There was no change in the solvent isotope effects when obtained using NADD as compared to NADH, $^{D2O}(V_2)_D = 1.76 \pm 0.08$ and $^{D2O}(V_2/K_{Lys})_D = 1.86 \pm 0.08$. Similarly, there was no change in primary isotope effects on $^D(V_2)$ and $^D(V_2/K_{Lys})$ when measured in $D_2O$ as against $H_2O$, $^D(V_2)_{D2O} = 1.50 \pm 0.15$ and $^D(V_2/K_{Lys})_{D2O} = 1.55 \pm 0.14$. Data suggested a concerted proton and hydride transfer that is completely rate-limiting in the overall reaction. However, the isotope effect on $V_2/K_{\alpha\text{-}Kg}$ was greater than that observed for $V_2/K_{Lys}$ at pH 7. Moreover, with decrease in pH, $^D V_2/K_{Lys}$ increased and $^{D2O}(V_2)_D$ decreased as compared to $^{D2O}(V_2)_H$, suggesting that hydride transfer was not the only rate-limiting step. Thus, hydride transfer had a proton transfer step in addition to another proton transfer step such as hydrolysis of imine (*19*).

When pre-steady-state kinetic studies were carried out in the direction of lysine production, a prominent burst was observed at the beginning of the progress curve. The calculated burst rate was $8.8 \pm 1.0$ s$^{-1}$ and this was followed by a steady-state rate of $0.8 \pm 0.1$ s$^{-1}$, similar to $V/\mathbf{E_t}$. The calculated burst amplitude was about 30% of $\mathbf{E_t}$. The

burst indicated a slow step occurred after the formation of NADH (*34*). The pH dependence of isotope effects suggested that a step other than hydride transfer becomes rate limiting as the pH was increased (*19*). It was proposed that the slow step was protonation/deprotonation of carbinolamine nitrogen formed as an intermediate in imine hydrolysis (*34*).

### 1.2.5 Structure of *Sc*SDH.

The structure of the apo-enzyme form of *Sc*SDH was solved at 1.64 Å resolution. The enzyme is comprised of two domains, an N-terminal domain and a C-terminal domain with a narrow cleft between them (*35*). The two domains were structurally similar and include a Rossmann fold. The crystal structure also showed a disulfide bond between C205 and C249 at the center of the Rossmann fold in the dinucleotide binding site. It was suggested that this disulfide bridge might be physiologically significant, since its presence did not significantly change the conformation of the surrounding residues, and the two cysteines were conserved among all known fungal SDHs. A molecular model of the ternary complex of *Sc*SDH, NAD and Sacc suggested K77 and E122 were potentially important in substrate binding and/or catalysis (*35*).

Additional structural information was obtained from three subsequent crystal structures of *Sc*SDH with sulfate, AMP or the α-Kg analog oxalylglycine (OG) bound, respectively (*36*). In the sulfate bound structure, the sulfate ion mimics a substrate carboxylate and binds in the cleft between the two domains. Binding induced a rotation of 11.8° between the domains leading to 65% closure of the active site. Oxalylglycine

binds with its carboxylates bound to R18 and R131, and its carbonyl oxygen within hydrogen-bonding distance to K77 and H96. The structure corroborates the prediction from kinetic data (*33*) that the optimum number of carbon atoms between R18 and R131 is five. In the E·AMP structure, AMP is bound to the dinucleotide binding domain via eight hydrogen bonds and hydrophobic interactions resulting in domain I rotating by 3.9° with regard to domain II. On the basis of the pH dependence of $K_i$ for AMP (*33*), two functional groups on the enzyme (one protonated and one unprotonated) were involved in the binding of AMP. From structural studies the unprotonated group was proposed to be D227, which accepts a hydrogen bond from the AMP ribose. The AMP-bound structure also showed that the two cysteines were in close proximity to the phosphate moiety of AMP. It was proposed that AMP binds only to the dithiol form of the enzyme, which is catalytically active.

The two active site thiols, C205 and C249, form a disulfide bridge in the sulfate- and OG-bound structure, but are present as the reduced dithiol in the AMP-bound structure.

On the basis of sulfate-, AMP- and OG-bound structures a semiempirical model of the active site was constructed with NAD- and Sacc-bound. The model did not consider the conformational change that must occur on binding of both substrates, but predicted electrostatic and hydrogen-bonding interactions between Sacc and active site residues that were used to guide site directed mutagenesis (see section **Dissecting the Active Site**) (*36*).

## 1.2.6 Role of Active Site Thiols.

As discussed above, a pair of thiols was observed in the dinucleotide binding site as a disulfide in the structure of apo-enzyme, but as a dithiol in the AMP-bound structure (*36*). When treated with 5,5'-dithiobis (2-nitrobenzoate) (DTNB), 1.2 – 1.5 thiols/mol enzyme were modified, and NADH protected against modification (*37*). A RedOx titration of the WT enzyme with monobromobimane (mBBr) gave an average $E'_0$ value of -200 ± 10 mV at pH 7.0.
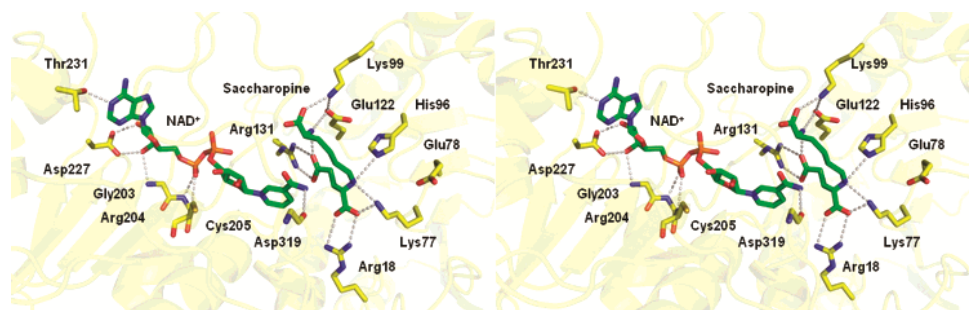


Figure 1.8 Semiempirical Model of the *Sc*SDH·NAD·Sacc Ternary Complex. The interactions between the enzyme residues and substrates are shown as dashed lines in gray. Glutamate 78 or E122 (:B$_1$ in Figure 7) and K77 or H96 (:B$_2$ in Figure 7) were proposed to be the catalytic residues. It was also proposed that Sacc might form an intramolecular electrostatic bond, thus folding itself to accommodate the highly hydrophilic active site. NAD presents its *pro-R* face for hydride transfer. Reprinted with permission from Andi, B., Xu, H., Cook, P. F., and West, A. H. (2007) Crystal Structures of Ligand-Bound Saccharopine Dehydrogenase from *Saccharomyces cerevisiae*, *Biochemistry 46*, 12512–12521. Copyright 2007 American Chemical Society.

A mutant enzyme where C205, one of the thiols, was replaced by S, gave the mutant enzyme a much higher $V/\mathbf{E}_t$ and $V/K\mathbf{E}_t$ in both reaction directions at pH 7 compared to the WT enzyme. The kinetic mechanism of C205S remained similar to the WT enzyme. The primary kinetic and solvent isotope effects were larger than those of WT enzyme. Thus, the slow step in the reaction catalyzed by WT enzyme must be

faster in the reaction catalyzed by C205S. However, the multiple isotope effects for C205S were similar to WT suggesting that hydride transfer and imine hydrolysis contribute more to rate limitation in C205 but the relative rates of the two steps to one another are the same.

At pH 6, a >10 fold higher rate was observed for the WT enzyme treated with tris(2-carboxyethyl)phosphine (TCEP) as compared to untreated enzyme. On the basis of maximum rates, it was proposed that WT had 10-20% of dithiol form of enzyme and the disulfide form seemed to lock the enzyme in a less active conformation.

In the highly reducing environment of the cytoplasm, the possibility of forming a disulfide bridge is low. In addition, the presence of thioredoxin reductase in the cytoplasm may prevent disulfide bond formation (*38*).

### 1.2.7 Dissecting the Active Site.

On the basis of semiempirical model of the E•NAD•Sacc complex (*35, 36*) a number of ionizable residues are found in the active site. An alignment of the primary sequences from *C. albicans, Pichia guilliermondii, S. cerevisiae, A. fumigatus,* and *C. neoformans* SDHs indicates all ionizable residues in the active site are conserved, suggesting they are important to the overall reaction. To determine the contribution of each of these residues to binding and/or rate enhancement, individual mutations of each residue were made, and double mutants were also made to estimate the interrelationship between the residues.

The role of E78 and E122 was studied by changing these residues to either Q or A, alone and as a pair where both residues were mutated to Q. The kinetic mechanism

was qualitatively similar to that of WT SDH with the exception that for E78A, $\alpha$-Kg binds to free enzyme and the E·NADH complex (*39*). There was not much change in $V/\mathbf{E}_t$ for any of the mutants, but $V/K_{Lys}\mathbf{E}_t$ decreased significantly suggesting a decrease in the affinity for Lys. This result suggested that absence of E122 and E78 affected the binding constant for Lys (*39*). Isotope effects were similar to those of WT for the E122Q, E87Q and E122Q/E87Q mutants suggesting chemistry still contributed to rate limition. The pH dependence of kinetic parameters changed drastically with p$K_a$ values shifted to low and high pH by $\geq 1.5$ pH units suggesting an effect on the basicity of the catalytic residues.

The role of another conserved residue K99 was studied by changing it to M (*40*). K99 was proposed to hydrogen-bond to the $\alpha$-amine of Sacc (*36*). When mutated to M, the charge balance of the active site is lost resulting in poor binding of the substrates indicated by a decrease in $V/K$ values as compared to those of the C205S enzyme. The primary deuterium isotope effects on $V$ and $V/K_{Lys}$ increased, while solvent isotope effects decreased suggesting a change in the partition ratio of the imine intermediate to favor hydrolysis.

Aspartate319 is close to the carboxamide side chain of nicotinamide ring of NAD. Changing D319 to A reduced the negative charge and increased the positive charge of the active site. A 33-fold decrease in $V/K_{Lys}$ suggested D319 was involved in binding of the substrate. A decrease in isotope effects compared to C205S suggested a non-isotope sensitive step had become slower in D319A mutant enzyme. The slower step was proposed to be a conformational change that occurs on binding of NADH.

**1.3 MAIN PROJECTS AND OTHER CONTRIBUTIONS.**

In this dissertation, two projects are discussed. The first one is on the mechanism of homocitrate synthase from *Thermus thermophilus*. The second project concerns the roles of active site residues of saccharopine dehydrogenase from *Saccharomyces cerevisiae*. In chapter 2, the kinetic mechanism of HCS from *T. thermophilus* is discussed. This chapter also has a report on the slow steps along the reaction pathway and regulation by lysine. In chapter 3, the roles of K77 and H96, two of the two active site residues, are determined. Lysine77 and H96 were proposed as catalytic residues for SDH from *S. cerevisiae*. In chapter 4, the role of K13 and E16 was probed. Although not directly involved in catalysis, the residues are essential for optimum charge distribution and positioning of the catalytic residues.

I have also contributed to a number of other published studies that are not discussed in the dissertation. Publications that resulted from the additional studies are listed below.

1. Bobyk, K. D., Kim, S. G., Kumar, V. P., Kim, S. K., West, A. H., and Cook, P. F. (2011) The Oxidation State of Active Site Thiols Determines the Activity of Saccharopine Dehydrogenase at Low pH. *Arch. Biochem. Biophys.* 513, 71-80.

2. Wickham, S. E., Regan, N., West, M. B., Kumar, V. P., Thai, J., Li, P. K., Cook, P. F., and Hanigan, M. H. (2011) Divergent Effects of Compounds on the Hydrolysis and Transpeptidation Reactions of Gamma-Glutamyl Transpeptidase. *J. Enz. Inhib. Med. Chem.* doi:10.3109/14756366.2011.597748.

3. Mozzarelli, A., Bettati, S., Campanini, B., Salsi, E., Raboni, S., Singh, R., Spyrakis, F., Kumar, V. P., and Cook, P. F. (2011) The multifaceted pyridoxal

5'-phosphate-dependent O-acetylserine sulfhydrylase. *Biochim. Biophys. Acta. 1814*, 1497-1510.

4. Tyapochkin, E., Kumar, V. P., Cook, P. F., and Chen, G. (2011) Reaction product affinity regulates activation of human sulfotransferase 1A1 PAP sulfation. *Arch. Biochem. Biophys. 506*, 137-141.

5. Tian, H., Guan, R., Salsi, E., Campanani, B., Bettati, S., Kumar, V. P., Karsten, W. E., Mozzarelli, A., and Cook, P. F. (2010) Identification of the structural determinants for the stability of substrate and aminoacrylate external Schiff bases in *O*-acetylserine sulfhydrylase-A. *Biochemistry 49*, 6093-6103.

## 1.4 REFERENCES.

1. Umbarger, H. E. (1978) Amino Acid Biosynthesis and its Regulation, *Annu Rev Biochem. 47*, 532-606.

2. Zabriskie, T. M., and Jackson, M. D. (2000) Lysine biosynthesis and metabolism in fungi, *Nat. Prod. Rep. 17*, 85-97.

3. Xu, H., Andi, B., Qian, J., West, A. H., and Cook, P. F. (2006) The α-aminoadipate pathway for lysine biosynthesis in fungi, *Cell Biochem. Biophys. 46*, 43-64.

4. Kosuge, T. a. H., T. (1998) The alpha-aminoadipate pathway for lysine biosynthesis is widely distributed among *Thermus* strains., *FEMS Microbiol. Lett. 169*, 361 − 367.

5. Liebmann, B., Muhleisen, T. W., Muller M, Hecht, M., Weidner, G., Braun, A., Brock M., and Brakhage, A. A. . (2004) Deletion of the *Aspergillus fumigatus* lysine biosynthesis gene lysF encoding homoaconitase leads to attenuated virulence in a low-dose mouse infection model of invasive aspergillosis., *Arch Microbiol. 181*, 378 - 383.

6. Garrad, R. C., and Bhattacharjee, J. K. (1992) Lysine biosynthesis in selected pathogenic fungi: Characterization of lysine auxotrophs and the cloned LYS1 gene of *Candida albicans*, *J. Bacteriol. 174*, 7379-7384.

7.      Ye, Z. H., and Bhattacharjee, J. K. (1988) Lysine biosynthesis pathway and biochemical blocks of lysine auxotrophs of *Schizosaccharomyces pombe*, *J. Bacteriol. 170*, 5968-5970.

8.      Andi, B., West, A. H., and Cook, P. F. (2004) Kinetic mechanism of histidine-tagged homocitrate synthase from *Saccharomyces cerevisiae*, *Biochemistry 43*, 11790-11795.

9.      Qian, J., West, A. H., and Cook, P. F. (2006) Acid-base chemical mechanism of homocitrate synthase from *Saccharomyces cerevisiae*, *Biochemistry 45*, 12136-12143.

10.     Qian, J., Khandogin, J., West, A. H., and Cook, P. F. (2008) Evidence for a catalytic dyad in the active site of homocitrate synthase from *Saccharomyces cerevisiae*, *Biochemistry 47*, 6851-6858.

11.     Beinert, H., Kennedy, M. C. and Stout, C. D. (1996) Aconitase as Iron-Sulfur Protein, Enzyme, and Iron-Regulatory Protein, *Chem. Rev. 96*, 2335-2373.

12.     Jia, Y., Tomita, T., Yamauchi, K., Nishiyama, M., and Palmer, D. R. (2006) Kinetics and product analysis of the reaction catalysed by recombinant homoaconitase from *Thermus thermophilus*, *Biochem J. 396*, 479-485.

13.     Lin, Y., Alguindigue, S. S., Volkman, J., Nicholas, K. M., West, A. H., and Cook, P. F. (2007) Complete kinetic mechanism of homoisocitrate dehydrogenase from *Saccharomyces cerevisiae*, *Biochemistry 46*, 890-898.

14.     Miyazaki, J., Asada, K., Fushinobu, S., Kuzuyama, T., and Nishiyama, M. (2005) Crystal structure of tetrameric homoisocitrate dehydrogenase from an extreme thermophile, *Thermus thermophilus*: involvement of hydrophobic dimer-dimer interaction in extremely high thermotolerance, *J Bacteriol. 187*, 6779-6788.

15.     Ehmann, D. E., Gehring, A. M., and Walsh, C. T. (1999) Lysine biosynthesis in *Saccharomyces cerevisiae*: mechanism of alpha-aminoadipate reductase (Lys2) involves posttranslational phosphopantetheinylation by Lys5, *Biochemistry 38*, 6171-6177.

16.     Vashishtha, A. K., West, A. H., and Cook, P. F. (2008) Overall kinetic mechanism of saccharopine dehydrogenase from *Saccharomyces cerevisiae*, *Biochemistry 47*, 5417–5423.

17.     Vashishtha, A. K., West, A. H., and Cook, P. F. (2009) Chemical mechanism of saccharopine reductase from *Saccharomyces cerevisiae*, *Biochemistry 48*, 5899–5907.

18. Xu, H., West, A. H., and Cook, P. F. (2006) Overall Kinetic Mechanism of Saccharopine Dehydrogenase from *Saccharomyces cerevisiae*, *Biochemistry 45*, 12156-12166.

19. Xu, H., Alguindigue, S. S., West, A. H., and Cook, P. F. (2007) A proposed proton shuttle mechanism for saccharopine dehydrogenase from *Saccharomyces cerevisiae*, *Biochemistry 46*, 871-882.

20. Karsten, W. E., Reyes, Z. L., Bobyk, K. D., Cook, P.F. and Chooback, L. . (2011) Mechanism of the aromatic aminotransferase encoded by the Aro8 gene from *Saccharomyces cerevisiae*., *Arch Biochem Biophys.*

21. Tucci, A. F., and Ceci, L. N. (1972) Homocitrate synthase from yeast, *Arch Biochem Biophys 153*, 742-750.

22. Gray, G. S., and Bhattacharjee, J. K. (1976) Biosynthesis of lysine in *Saccharomyces cervisiae*: properties and spectrophotometric determination of homocitrate synthase activity, *Can J Microbiol 22*, 1664-1667.

23. Kobashi, N., Nishiyama, M. and Tanokura, M. (1999) Aspartate kinase-independent lysine synthesis in an extremely thermophilic bacterium, *Thermus thermophilus*: lysine is synthesized via alpha-aminoadipic acid not via diaminopimelic acid., *J. Bacteriol. 181*, 1713 – 1718.

24. Wulandari, A. P., Miyazaki, J., Kobashi, N., Nishiyama, M., Hoshino, T., and Yamane, H. (2002) Characterization of bacterial homocitrate synthase involved in lysine biosynthesis, *FEBS Lett 522*, 35-40.

25. Andi, B., West, A. H., and Cook, P. F. (2004) Stabilization and characterization of histidine-tagged homocitrate synthase from *Saccharomyces cerevisiae*, *Arch Biochem Biophys. 421*, 243-254.

26. Andi, B., West, A. H., and Cook, P. F. (2005) Regulatory mechanism of histidine-tagged homocitrate synthase from *Saccharomyces cerevisiae*. I. Kinetic studies, *J Biol Chem 280*, 31624-31632.

27. Okada, T., Tomita, T., Wulandari, A. P., Kuzuyama, T., and Nishiyama, M. (2010) Mechanism of substrate recognition and insight into feedback inhibition of homocitrate synthase from *Thermus thermophilus*, *J Biol Chem 285*, 4195-4205.

28. Bulfer, S. L., Scott, E. M., Couture, J. F., Pillus, L., and Trievel, R. C. (2009) Crystal structure and functional analysis of homocitrate synthase, an essential enzyme in lysine biosynthesis., *J Biol Chem. 284*, 35769-35780.

29.    Koon, N., Squire, C. J., and Baker, E. N. (2004) Crystal structure of LeuA from *Mycobacterium tuberculosis*, a key enzyme in leucine biosynthesis., *Proc. Natl. Acad. Sci. U.S.A. 101*, 8295−8300.

30.    Bulfer, S. L., Scott, E. M., Pillus, L., and Trievel, R. C. (2010) Structural basis for L-lysine feedback inhibition of homocitrate synthase., *J Biol Chem. 285*, 10446-10453.

31.    Ogawa, H., and Fujioka, M. . (1978) Purification and characterization of saccharopine dehydrogenase from baker's yeast, *J. Biol. Chem. 253*, 3666-3670.

32.    Cook, P. F. a. C., W. W. (2007) *Enzyme kinetics and mechanism*, Taylor & Francis Group, LLC, New York.

33.    Xu, H., West, A. H., and Cook, P. F. (2007) Determinants of Substrate Specificity for Saccharopine Dehydrogenase from *Saccharomyces cerevisiae*, *Biochemistry 46*, 7625-7636.

34.    Xu, H. (2007) Mechanism of Saccharopine Dehydrogenase : The last enzyme in the lysine biosynthetic pathway in *Saccharomyces cerevisiae*, In *Chemistry and Biochemistry*, University of Oklahoma, Norman.

35.    Burk, D. L., Hwang, J., Kwok, E., Marrone, L., Goodfellow, V., Dmitrienko, G. I., and Berghuis, A. M. (2007) Structural studies of the final enzyme in the α-aminoadipate pathway-saccharopine dehydrogenase from *Saccharomyces cerevisiae*, *J Mol Biol. 373*, 745-754.

36.    Andi, B., Xu, H., Cook, P. F., and West, A. H. (2007) Crystal Structures of Ligand-Bound Saccharopine Dehydrogenase from *Saccharomyces cerevisiae*, *Biochemistry 46*, 12512–12521.

37.    Bobyk, K. D., Kim, S. G., Kumar, V. P., Kim, S. K., West, A. H., and Cook, P. F. (2011) The oxidation state of active site thiols determines activity of saccharopine dehydrogenase at low pH., *Arch Biochem Biophys. 513*, 71-80.

38.    Derman, A. I., Prinz, W. A., Belin, D., and Beckwith, J. . (1993) Mutations that allow disulfide bond formation in the cytoplasm of *Escherichia coli*, *Science 262*, 1744-1747.

39.    Ekanayake, D. K., Andi, B., Bobyk, K. D., West, A. H., and Cook, P. F. (2010) Glutamates 78 and 122 in the active site of saccharopine dehydrogenase contribute to reactant binding and modulate the basicity of the acid-base catalysts., *J Biol Chem. 285*, 20756–20768.

40.    Ekanayake, D. K., West, A. H., and Cook, P. F. (2011) Contribution of K99 and D319 to substrate binding and catalysis in the saccharopine dehydrogenase reaction, *Arch Biochem Biophys 514*, 8-15.

# CHAPTER 2

## Mechanisms of Homocitrate Synthase from *Thermus thermophilus*

## 2.1 INTRODUCTION

The α-aminoadipate (AAA) pathway for lysine biosynthesis is nearly unique to higher fungi, including human and plant pathogens and euglenoids; an exception is the thermophilic bacterium *Thermus thermophilus*. The AAA pathway is comprised of eight enzymatic reactions catalyzed by seven enzymes. Homocitrate synthase (HCS) catalyzes the first and regulated step in this pathway, the condensation of acetyl-CoA (AcCoA) and α-ketoglutarate (α-Kg) to give homocitrate and coenzyme A (CoASH) (Scheme 2.1) (*1, 2*). As a result, it is a potential target for the development of new antifungals against human pathogens such as *Candida albicans* and *Aspergillus fumigatus* (*3*).
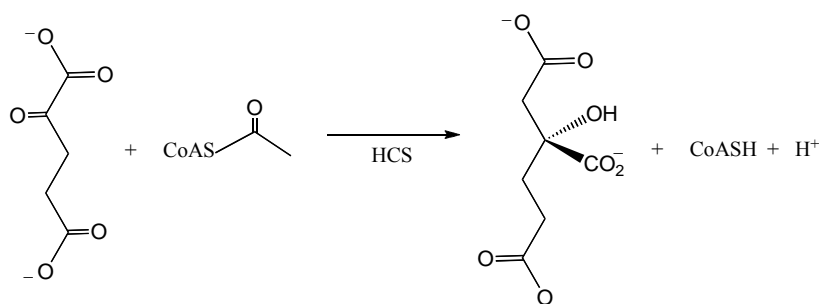


Scheme 2.1  Reaction Catalyzed by Homocitrate Synthase.

The best studied of the homocitrate synthases is that from *Saccharomyces cerevisiae* (*4-8*). The homocitrate synthase from *Saccharomyces cerevisiae* (*Sc*HCS) is

a Zn-metalloenzyme (*8*). The *Sc*HCS and that from *Candida albicans* (*Ca*HCS) are not particularly stable as isolated; but they are stable for at least 2 months at 4 °C in the presence of the additives, guanidine hydrochloride, α-cyclodextrin, and $(NH_4)_2SO_4$ (*5*, Appendix 3). In the absence of the additives, however, the enzymes rapidly lose activity, and this limits the type of experiments that can be carried out, especially structural studies (*5*).

An ordered kinetic mechanism has been proposed for *Sc*HCS and *Ca*HCS with α-Kg binding prior to AcCoA (*4*, unpublished data of VPK in this laboratory). Lysine is a feedback inhibitor of *Sc*HCS, and is competitive *vs* α-Kg. Inhibition was thought to result from binding to an allosteric site, stabilizing a less active conformer of the enzyme.

A chemical mechanism for *Sc*HCS has been proposed in which α-Kg is bound to the active site Zn via its α-carboxylate and α-oxo groups, in the vicinity of the thioester of AcCoA. A general base accepts a proton from the methyl group of AcCoA as it attacks the thioester of AcCoA, and a general acid protonates the carbonyl of α-Kg in the formation of homocitryl-CoA. The general acid then acts as a base in the deprotonation of $Zn-OH_2$ in the hydrolysis of homocitryl-CoA to give homocitrate and CoA (*8*). Isotope effect data suggest the product of the condensation of AcCoA and α-Kg is the alkoxide, which is then protonated by a general acid in the next step (*8*).

Multiple sequence alignment of the residues around the active site of HCS show conservation of *Sc*HCS residues E155, H309* (* indicates a residue from the other monomer), and Y320 in *Tt*HCS, isopropylmalate synthase (IPMS), and citramalate

synthase (CMS). Site-directed mutagenesis indicates that E155 and H309* form the catalytic dyad that is proposed to deprotonate the methyl of AcCoA and Y320 may be involved in orienting the reactants and/or the catalytic dyad for catalysis (*6*).

In most bacteria, lysine is synthesized from aspartic acid via the diaminopimelate pathway. However, in *Thermus thermophilus,* lysine is synthesized via the AAA pathway. Crystal structures of *Tt*HCS recently have been solved (*10*), but a detailed study of the kinetic and/or chemical mechanism of *Tt*HCS has not been carried out. In this manuscript, the *Tt*HCS has been subjected to initial rate, and isotope effect studies, and the pH dependence of kinetic parameters has been measured. Based on these results kinetic and chemical mechanisms are proposed for the *Tt*HCS enzyme and comparisons are made to those proposed for *Sc*HCS.

## 2.2 MATERIALS AND METHODS

### 2.2.1 Chemicals.

α-Ketoglutarate, AcCoA, CoA, DCPIP, oxaloacetate, oxalate, EDTA and Chelex 100 were from Sigma. *N*-oxalylglycine was obtained from Frontier Scientific. Imidazole, KCl, $CaCl_2$, $MgCl_2$, $MnCl_2$, $ZnCl_2$, $CoCl_2$ and $NiCl_2$ were from Fisher Scientific. The buffers, Taps, Hepes, Bis-Tris and Mes, were from Research Organics, while the NiNTA resin was purchased from 5 Prime. MagicMedia used for cell growth was purchased from Invitrogen. Perdeuterioacetic anhydride (98 atom% D) and $D_2O$ (99 atom% D) were purchased from Cambridge Isotope Laboratories, Inc. Deuterioacetyl-CoA was prepared from CoA and perdeuterioacetic anhydride according to the method of Simon and Shemin (*11*).

**2.2.2 Cell Growth and Expression.**

Histidine-tagged homocitrate synthase from *T. thermophilus* was previously cloned into the pET26b$^+$ (Novagen) vector (*12*). The *Tt*HCS clone was transformed into *Escherichia coli* BL21(DE3) RIL star cells and the culture was grown in MagicMedia containing chloramphenicol (34 µg/ml) and kanamycin (10 µg/ml) at 37˚C overnight. Cells were lysed by sonication in 50 mM Hepes, pH 7.5, containing 30 mM KCl, 5 mM imidazole and enzyme was purified using the Ni-NTA resin, with elution at 360 mM imidazole. The enzyme was >95% pure by SDS-PAGE. The enzyme was stored at 4˚C in the elution buffer.

**2.2.3 Enzyme Assay.**

HCS activity was measured using the dichlorophenol indophenol (DCPIP) assay developed previously (*5*), monitoring the decrease in absorbance at 600 nm as DCPIP is reduced by CoASH. Reactions were carried out in quartz cuvettes with a path length of 1 cm and a final volume of 0.5 ml containing 50 mM Hepes, pH 7.5, 0.1 mM dichlorophenol indophenol (DCPIP), and variable concentrations of $\alpha$-Kg and AcCoA. The concentrations of AcCoA and DCPIP were estimated spectrophotometrically, using the following extinction coefficients: AcCoA, $\varepsilon_{260}$ = 16,400 M$^{-1}$ cm$^{-1}$; DCPIP$_{red}$, $\varepsilon_{600}$ = 19,100 M$^{-1}$ cm$^{-1}$. Assays were carried out at 25˚C and reactions were thermally equilibrated to allow completion of the reaction between the small amount of CoA in the AcCoA solution and DCPIP before adding the enzyme to the reaction mixture.

**2.2.4 Divalent Metal Ion Specificity.**

In order to determine the effect of metal ions on $Tt$HCS, apo-enzyme was prepared by dialyzing the isolated enzyme against 50 mM Hepes, pH 7.5 containing 100 mM EDTA, followed by dialysis against 50 mM Hepes, pH 7.5 buffer. All reagents used either for dialysis or enzyme assay, were passed through Chelex resin to remove metal ions. All reagents used in these experiments were stored in polypropylene bottles and tubes. The effect of the presence of divalent cations such as $Mg^{2+}$, $Mn^{2+}$, $Ca^{2+}$, $Ni^{2+}$, $Zn^{2+}$ and $Co^{2+}$ and monovalent cations such as $Na^+$ and $K^+$ on the activity of $Tt$HCS was tested by initial velocity measurements. The enzyme assay was carried out as described above.

**2.2.5 Initial Velocity Studies.**

To determine the kinetic mechanism of $Tt$HCS, initial velocity patterns were obtained by measuring the initial rate as a function of AcCoA concentration at different fixed concentrations of α-Kg (or oxaloacetate). The reaction typically consisted of 50 mM Hepes, pH 7.5, 0.1 mM DCPIP, 200 μM $MgCl_2$, 1 μM $Tt$HCS and variable concentrations of α-Kg and AcCoA. Similar initial velocity patterns were also obtained with 200 μM $MnCl_2$ as the metal ion in place of $MgCl_2$.

Inhibition patterns were obtained by measuring initial rates at different concentrations of one reactant at a fixed concentration of the other (AcCoA was maintained at 50 μM, while α-Kg was maintained at 1 mM) in the absence and presence of inhibitor. Inhibition by CoASH, made use of the disappearance of absorbance at 232 nm (reflecting the thioester bond of AcCoA) using an $\varepsilon_{232} = 4500$ $M^{-1}cm^{-1}$ (*4*). The

apparent inhibition constant for lysine was also measured as a function of pH from 5.9 –
8.8 at fixed concentrations of α-Kg (100 μM) and AcCoA (50 μM) in presence of
MgCl$_2$ (200 μM).

### 2.2.6 pH Studies.

It is important to confirm that the enzyme is stable for the duration of the assay
in the pH range that is being tested.  To test this, the enzyme was pre-incubated at the
given pH and aliquots were removed at regular time intervals and assayed at pH 7.5,
where the enzyme is known to be stable.  The pH dependence of $V$ and $V/K$ was
obtained by measuring the initial rate as a function of one substrate, maintaining the
other at a fixed concentration (α-Kg, 5 mM; AcCoA, 5 μM).  Initial velocity patterns
were obtained over the pH range of 6 – 9 and $K_m$ values estimated for both α-Kg and
AcCoA (not done for Mg$^{2+}$.)  This information determined the concentration range of
substrates to be used over the entire pH range.  Buffers were maintained at 50 mM
concentration in the following pH range; Bis-Tris, 6.0 - 7.0; Hepes, 7.0 - 8.0; Taps, 8.0 -
9.0. The pH of the reaction mixture was recorded before and after the reaction with little
difference noted.  The data were then analyzed by plotting log$V$ or log$V/K$ vs pH.

### 2.2.7 Isotope Effects.

Primary deuterium kinetic isotope effects were measured by direct comparison
of initial velocities, where AcCoA-d$_3$was used as the deuterated substrate and α-Kg was
fixed at saturating concentration (400 μM).  Solvent deuterium isotope effects were
obtained by direct comparison of initial rates as a function of α-Kg at different fixed

35

levels of AcCoA in $H_2O$ and $D_2O$ over the pH(D) range 6 - 9 (around the pH-independent region of the $V$ (or $V/K$) pH-rate profile). For these studies, all the reagents including buffers, substrates and DCPIP were first dissolved in a small amount of $D_2O$, then lyophilized overnight to remove $H_2O$ and re-dissolved in the required volume of $D_2O$. The pH(D) was adjusted using KOD or DCl. The initial rate was measured in $H_2O$ and $D_2O$.

## 2.2.8 Data Processing.

Data were fitted to the appropriate rate equation using the EnzFitter program from BIOSOFT, Cambridge, UK. In some cases data could not be fitted by the computer program, and kinetic parameters were obtained from graphical analysis. Initial velocity data with $MnCl_2$ were fitted to eq. 1. Competitive and uncompetitive inhibition data were fitted using eqs. 2 and 3. Isotope effect data were fitted to eq. 4.

$$v = \frac{V\mathbf{AB}}{K_a \mathbf{B}\left(1 + \frac{\mathbf{B}}{K_{IB}}\right) + K_b\mathbf{A} + \mathbf{AB}} \tag{1}$$

$$v = \frac{V\mathbf{A}}{K_a\left(1 + \frac{\mathbf{I}}{K_{is}}\right) + \mathbf{A}} \tag{2}$$

$$v = \frac{V\mathbf{A}}{K_a + \mathbf{A}\left(1 + \frac{\mathbf{I}}{K_{ii}}\right)} \tag{3}$$

$$v = \frac{V\mathbf{A}}{K_a\left(1 + F_iE_{V/K}\right) + \mathbf{A}\left(1 + F_iE_V\right)} \tag{4}$$

In eqs. 1-4, $v$ and $V$ are initial and maximum velocities, respectively, **A**, **B**, and **I** are substrate and inhibitor concentrations, $K_a$ and $K_b$ are Michaelis constants for substrates A and B, respectively, while $K_{is}$ and $K_{ii}$ are slope and intercept inhibition constants, respectively. In eq. 4, $F_i$ is the atom fraction of deuterium in the labeled component, while $E_{V/K}$ and $E_V$ is the isotope effect minus 1 on the given parameter.

Data for lysine inhibition were fitted to eq. 5 (*13*):

$$\log v = \log \left( \frac{V\left[d\mathbf{A} + \mathbf{A}^2\right]}{c + b\mathbf{A} + \mathbf{A}^2} \right) \tag{5}$$

where b, c, and d are defined in eqs. 6-8.

$$b = d + \frac{SL_o}{INT_o} \tag{6}$$

$$c = d\left\lfloor \frac{SL_\infty}{INT_o} \right\rfloor \tag{7}$$

$$d = \frac{SL_o - SL_\infty}{INT_\infty - INT_o} \tag{8}$$

The parameters $SL_o$ and $SL_\infty$ refer to the slope of the double reciprocal plot with the concentration of A tending toward zero and infinity, while $INT_o$ and $INT_\infty$ refer to the intercept of the double reciprocal plot extrapolating the linear asymptote at low **A** to the ordinate and the ordinate intercept at infinite **A**, respectively.

The pH dependence of $V/K_{AcCoA}$ was fitted to eq. 9, while data for the pH dependence of the apparent $K_{ILys}$ was fitted to eq. 10.

$$\log y = \log\left[C\left(1+\frac{\mathbf{H}}{K_1}+\frac{K_2}{\mathbf{H}}\right)\right] \qquad (9)$$

$$\log y = \log\left[\frac{Y_L + Y_H\left(1+\dfrac{10^{-9.5}}{\mathbf{H}}\right)}{1+\dfrac{10^{-9.5}}{\mathbf{H}}}\right] \qquad (10)$$

In equation 9, $y$ is the observed value of $V/K$ at any pH, $C$ is the pH-independent value of $y$, $\mathbf{H}$ is the hydrogen ion concentration, and $K_1$ and $K_2$ are the acid dissociation constants of functional groups required in a given protonation state on enzyme or substrate for optimal binding and/or catalysis. In eq. 10, y is the value of $1/K_{ILys}$ at any pH, $Y_L$ and $Y_H$ are the pH independent values of $1/K_{ILys}$ at low and high pH, respectively, and the value $10^{-9.5}$ is the acid dissociation constant for the α-amine of lysine.

## 2.3 RESULTS

### 2.3.1 Divalent metal ion specificity.

As isolated, *Tt*HCS has metal ions bound. Treatment with EDTA removed the bound metal ions. The dependence of rate on added metal ion was measured with the EDTA-treated *Tt*HCS. In the absence of any exogenous metal ion, apo-enzyme had negligible activity, Figure 2.1. The enzyme could be reactivated by the addition of

$Mg^{2+}$ or $Mn^{2+}$, while in the presence of $Ni^{2+}$, or $Zn^{2+}$ no detectable activity was observed, Figure 2.1. Slight activity was observed in the presence of $Co^{2+}$, but the stock used was only 97% pure and had significant contamination with other divalent metal ions including $Mg^{2+}$ and $Mn^{2+}$. Reactivation to a lesser extent was found with addition of the monovalent cations, $Na^+$ and $K^+$ (data not shown). It is likely that activation by $Na^+$, and $K^+$ results from contaminating $Mg^{2+}$. A saturating concentration of $Mn^{2+}$ or $Mg^{2+}$ is 200 µM. Dialysis of the Mg-reconstituted enzyme does not result in an appreciable loss of activity, suggesting $Mg^{2+}$ is tightly bound to enzyme.
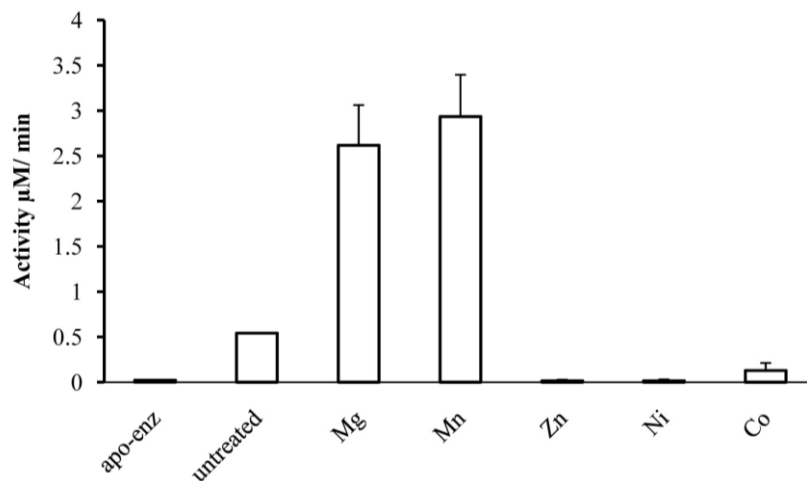


Figure 2.1 Effect of metal ions on *Tt*HCS activity. Apo-enzyme is EDTA-treated *Tt*HCS. All metal ions were tested at 5 mM final concentration in the reaction; $Zn^{2+}$ was also tested at 50 mM and showed no activation of *Tt*HCS (data not shown). Enzyme concentration was maintained at 4 µM.

## 2.3.2 Initial velocity studies.

An initial velocity pattern was obtained in the presence of 200 µM $MnCl_2$ varying the concentration of α-Kg at different fixed concentrations of AcCoA, Figure 2.2. At low concentrations of AcCoA the pattern is nearly parallel, while at concentrations

above 25 µM AcCoA competitive substrate inhibition by AcCoA *vs* α-Kg is observed, Figure 2.2; the slope replot exhibits the inhibition. Kinetic parameters are summarized in Table 2.1.

In the presence of 200 µM $MgCl_2$, the initial velocity pattern differs from that seen with $MnCl_2$. The primary plot with α-Kg as the varied substrate exhibits a set of lines that intersect to the right of the ordinate at low AcCoA, but the slope and intercept increase as the concentration of AcCoA increases, Figure 2.3A. Plotted with AcCoA as the varied substrate, all curves are near parallel at low concentrations, but curve upward at all α-Kg concentrations as the concentration of AcCoA increases, giving a finite intersection point on the ordinate, Figure 2.3B.
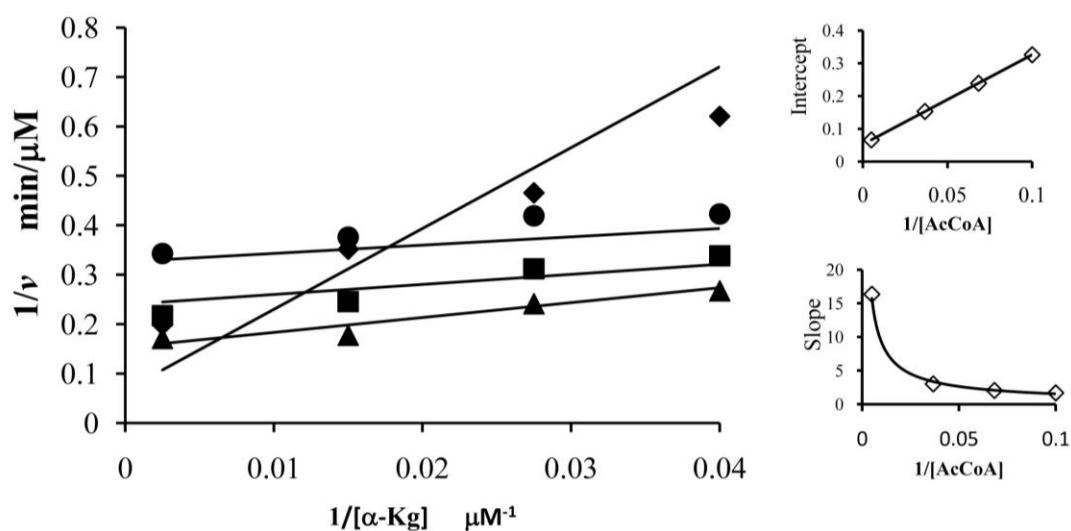


Figure 2.2 Initial Velocity Pattern with $Mn^{2+}$ as the Catalytic Divalent Metal Ion. Initial rates were measured at pH 7.5 and 25 °C as a function of α-Kg at different concentrations of AcCoA as follows: 10 µM (●); 14.6 µM (■); 27.3 µM (▲); and 200 µM (◆). Enzyme concentration was maintained at 1 µM. Graphs on the right hand side are replots of intercepts and slopes obtained from the primary plot *vs* the reciprocal of AcCoA concentration. Note the substrate inhibition exhibited in the slope replot indicating competitive substrate inhibition by AcCoA *vs* α-Kg. Points in the primary plot are experimental, while the solid lines are theoretical based on a fit to eq 1.

Attempts to fit the data in Figure 2.3 were unsuccessful as the equation was not well conditioned to the data. Thus, kinetic parameters were estimated graphically from plots of $V$ and $V/K_{a\text{-}Kg}$ (Figure 2.3C and D) obtained from fits of the individual lines in Figure 2.3A to the Michaelis-Menten equation; parameters are summarized in Table 2.2.

Table 2.1 Summary of Kinetic Parameters with $Mn^{2+}$

| | |
|---|---|
| $V/E_t$ $(s^{-1})$ | $0.068 \pm 0.005$ |
| $V/K_{\alpha\text{-}Kg}E_t$ $(M^{-1}s^{-1})$ | $(4 \pm 2) \times 10^3$ |
| $V/K_{AcCoA}E_t$ $(M^{-1}s^{-1})$ | $(2.5 \pm 0.4) \times 10^3$ |
| $K_{\alpha\text{-}Kg}$ $(\mu M)$ | $16 \pm 7$ |
| $K_{AcCoA}$ $(\mu M)$ | $27 \pm 4$ |
| $K_{I\,AcCoA}$ $(\mu M)$ | $10 \pm 5$ |

Data were obtained at pH 7.5 and 25 $^{o}$C with $Mn^{2+}$ fixed at 200 $\mu M$.

Table 2.2  Summary of Estimated Kinetic Parameters with $Mg^{2+}$

| | Low AcCoA[a] | High AcCoA[a] |
|---|---|---|
| $V/E_t$ $(s^{-1})$[b] | $\geq 0.117 \pm 0.002$ | $\leq 0.035 \pm 0.002$ |
| $V/K_{\alpha\text{-}Kg}E_t$ $(M^{-1}s^{-1})$[b] | $\geq 2300 \pm 380$ | $\leq 880 \pm$ |
| $V/K_{AcCoA}E_t$ $(M^{-1}s^{-1})$[b] | $\geq 7800 \pm 1500$ | $\sim 1400$ |
| $K_{\alpha\text{-}Kg}$ $(\mu M)$ | $50 \pm 8$ | $40 \pm 7$ |
| $K_{AcCoA}$ $(\mu M)$ | $15 \pm 3$ | $\sim 25$ |

[a]Data were obtained at pH 7.5 and 25 $^{o}$C ($Mg^{2+}$ was fixed at 200 $\mu M$).

[b]Kinetic parameters were estimated graphically from plots of $V$ and $V/K_{\alpha\text{-}Kg}$, Figure 2.3C and D.
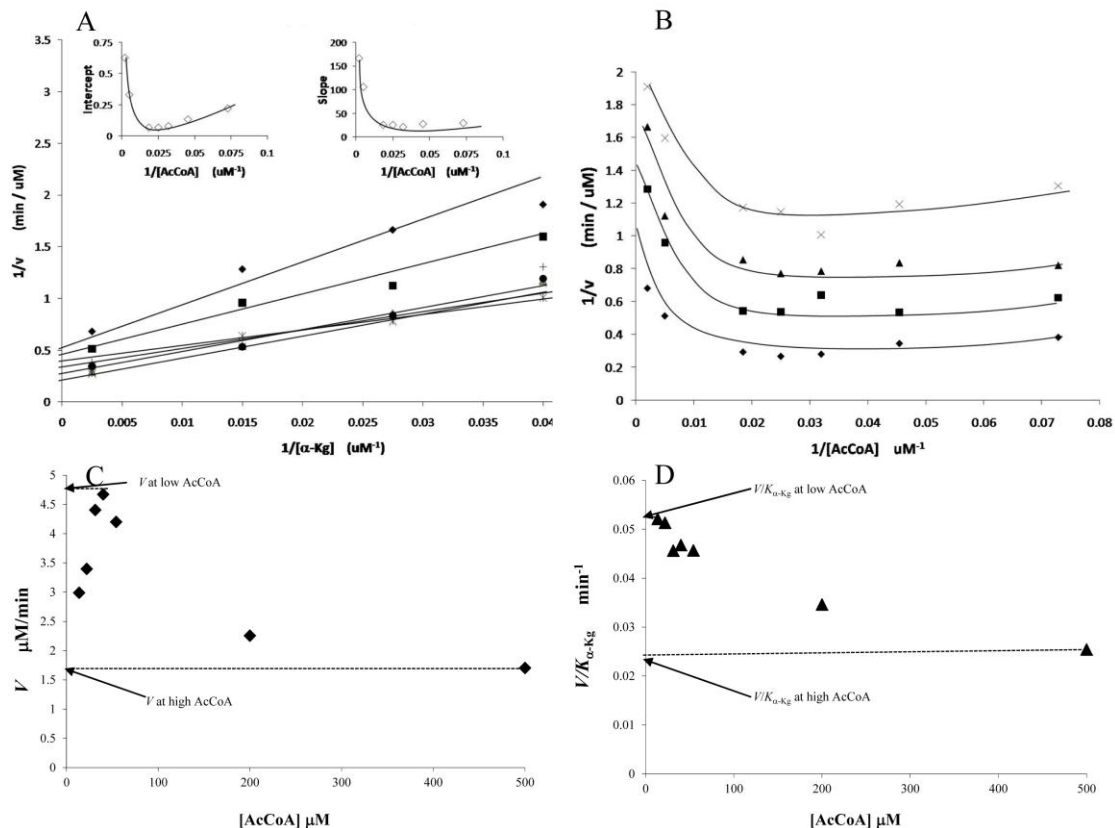
Figure 2.3  Initial Velocity Pattern with $Mg^{2+}$ as the Catalytic Divalent Metal Ion.  Initial rates were measured at pH 7.5 and 25 °C.  A) Data are plotted as a function of $\alpha$-Kg at different concentrations of AcCoA as follows: 14 (✳), 22 (✕), 31 ($\Delta$), 40 (●), 54 (+), 200 (■) and 500 (◆) $\mu$M.  B) Data are plotted as a function of AcCoA at different concentrations of $\alpha$-Kg as follows: 25 (✕), 36 (▲), 67 (■), and 400 (◆) $\mu$M.  The enzyme concentration was maintained at 1 $\mu$M.  C) and D) Plots of $V$ and $V/K_{\alpha\text{-}Kg}$ obtained from a fit of the individual saturating curves in A) (at each AcCoA concentration to the Michaelis Menten equation).  Note the apparent substrate inhibition exhibited in both replots.   Individual lines in A) are from a fit to eq. 1, while the curves in B) are drawn by hand.  Kinetic parameters listed in Table 2.2 were estimated as shown in C and D.

## 2.3.3 Inhibition studies.

In the presence of $Mg^{2+}$, or $Mn^{2+}$, product inhibition by the CoA, was competitive *vs* AcCoA with a $K_i$ of 26 ± 10 $\mu$M (data not shown), but was uncompetitive *vs* $\alpha$-Kg with a $K_i$ of 110 ± 30 $\mu$M.  **(**A value of 31 ± 8 $\mu$M, within error identical to the value of 26 $\mu$M, is obtained correcting the app$K_i$ for the fixed

concentration of AcCoA, 2.5 $K_{AcCoA}$; $K_i = (appK_i)/(1+A/K_a))$, Figure 2.4B. At high

concentrations of CoASH, curved double reciprocal plots were observed, Figure 2.4A.

Data are summarized in Table 2.3.

Oxalylglycine (OG), a α-Kg analog, is competitive $vs$ α-Kg, and $K_{iOG}$ is

independent of the concentration of AcCoA (data not show). Oxaloacetate was a slow

alternative substrate analog of α-Kg, with a $V/E_t$ of $0.0230 \pm 0.0006$ s$^{-1}$ and $V/K_{OAA}E_t$

of $0.065 \pm 0.019$ M$^{-1}$s$^{-1}$ (data not shown). Although the maximum rate with OAA is

only 5-fold lower than that with α-Kg, $V/K_{OAA}E_t$ is $3.5 \times 10^4$-fold lower than $V/K_{a-Kg}E_t$,

suggesting OAA binding is about 7000-fold weaker than α-Kg.[2]
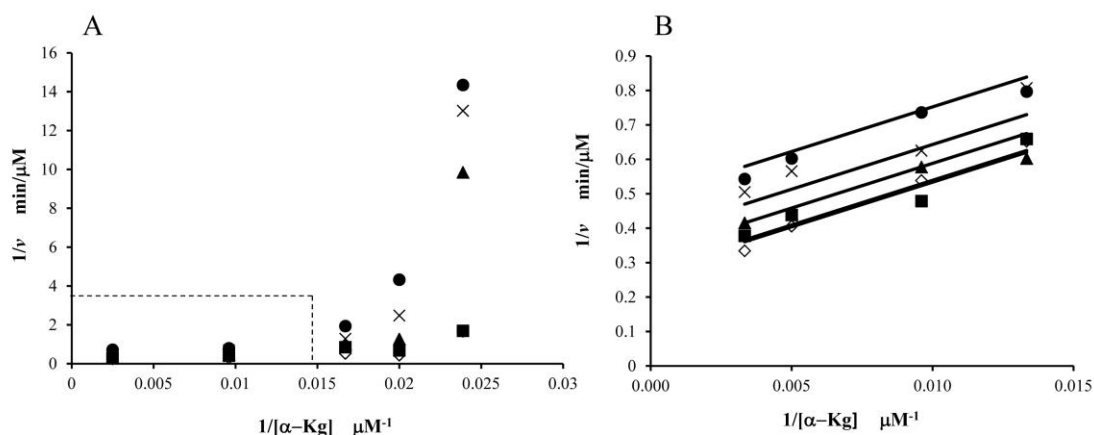


Figure 2.4 Inhibition by CoA at Variable Concentrations of α-Ketoglutarate. Initial rates were
obtained as a function of α-Kg concentration as shown with AcCoA fixed at 50 μM (A). The
concentrations of CoASH used are as follows: 0 (◊), 5 (■), 50 (▲), 100 (✕) and 200 (●) μM.
(B) Additional data for the concentration range shown in the dotted box in (A). The enzyme
concentration was maintained at 1 μM. Data at high concentration of α-Kg (>100 mM) were fit
to eq. 3.

Other analogs of α-Kg, including oxalate showed no significant inhibition at 1

mM with α-Kg fixed at 1.5$K_m$. Malonyl CoA and pantothenate, analogs of

AcCoA/CoASH, gave no inhibition at 1 mM concentration, with AcCoA fixed at $K_m$ and α-Kg fixed at a saturating concentration (1 mM). Data are summarized in Table 2.3.

Table 2.3  Summary of Inhibition Studies.

| Variable Substrate | Fixed Substrate | Inhibitor | $K_{is} \pm$ S. E. (mM) | $K_{ii} \pm$ S. E. (mM) | Pattern |
|---|---|---|---|---|---|
| AcCoA | α-Kg | CoASH | $0.026 \pm 0.01$ | - | C |
| α-Kg | AcCoA | CoASH | - | $0.11 \pm 0.03$ | UC |
| α-Kg | AcCoA | OG | $0.9 \pm 0.1$ | - | C |
| α-Kg | AcCoA | Lysine | Site 1 – $0.23 \pm 0.06$<br>Site 2 – $56 \pm 14$ | - | C |

Lysine, the final product of the aminoadipate pathway, exhibits feedback inhibition of HCS (*6*). Lysine is a competitive inhibitor *vs* α-Kg up to a concentration of 1 mM, Figure 2.5A. Inhibition by lysine is nonlinear, as shown by a Dixon plot of $1/v$ *vs* lysine at fixed concentrations of α-Kg ($16K_{a\text{-}Kg}$) and AcCoA ($2.5K_{AcCoA}$), Figure 2.5B. Data are suggestive of negative cooperativity in the binding of lysine. A fit of the data to eq. 4, gives well-defined $K_i$ values for binding the first and second molecules of lysine, Table 2.3. Inhibition by lysine is also competitive *vs* α-Kg in the high lysine concentration range, however the double reciprocal plots are concave upward at high lysine concentration, Figure 2.5C. Data suggest that the presence of high

concentrations of lysine induce positive cooperativity in binding α-Kg, as observed for

CoASH.
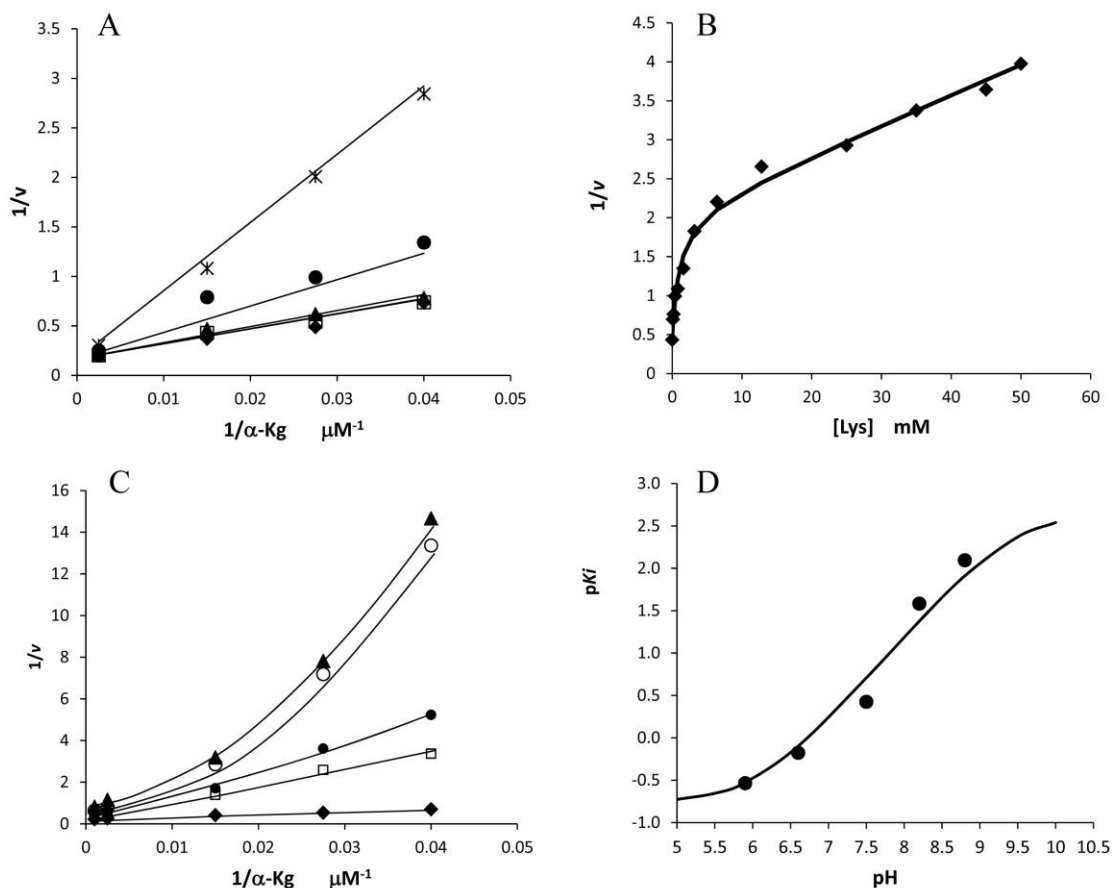


Figure 2.5  Inhibition by Lysine.  A) Double reciprocal plot of competitive inhibition by lysine against α-Kg concentration.  Data were obtained at pH 7.5 and 25 °C.   The rate was measured as a function of the α-Kg concentrations shown and AcCoA fixed at 50 μM, and lysine at different fixed concentrations as follows:  0 (◆), 1 (▢), 10 (▲), 100 (●) and 500 (✳) μM.  Points are experimental, while curves are theoretical based on a fit to eq. 3.  B)  Dixon plot of reciprocal initial rate *vs* the concentration of lysine with α-Kg and AcCoA concentrations fixed at 100 μM and 50 μM, respectively; lysine was varied from 0 to 50 mM.   The points are experimental, while the curve is theoretical based on a fit to eq. 5. C) Double reciprocal plot of competitive inhibition by lysine against α-Kg concentration as in A), with lysine in the high concentration range as follows: 0 (◆), 1 (▢), 3 (●), 5 (○) and 15 (▲) mM.  The enzyme concentration was maintained at 1 μM for all experiments.  D) Plot of the log (1/app $K_{iLys}$) *vs* pH.  Points were obtained from a Dixon analysis as shown in B) for the linear low concentration range.  The curve is theoretical based on a fit to eq. 10.

45

## 2.3.4 Primary substrate deuterium kinetic isotope effects.

Primary substrate deuterium kinetic isotope effects were measured with $Mg^{2+}$ as the divalent metal ion by direct comparison of initial rates at pH 7.5 with acetyl-$d_3$ CoA as the labeled substrate. An isotope effect of unity was obtained at low AcCoA concentration, but a kinetic isotope effect of about 2 is observed at high concentrations of AcCoA, Figure 2.6.
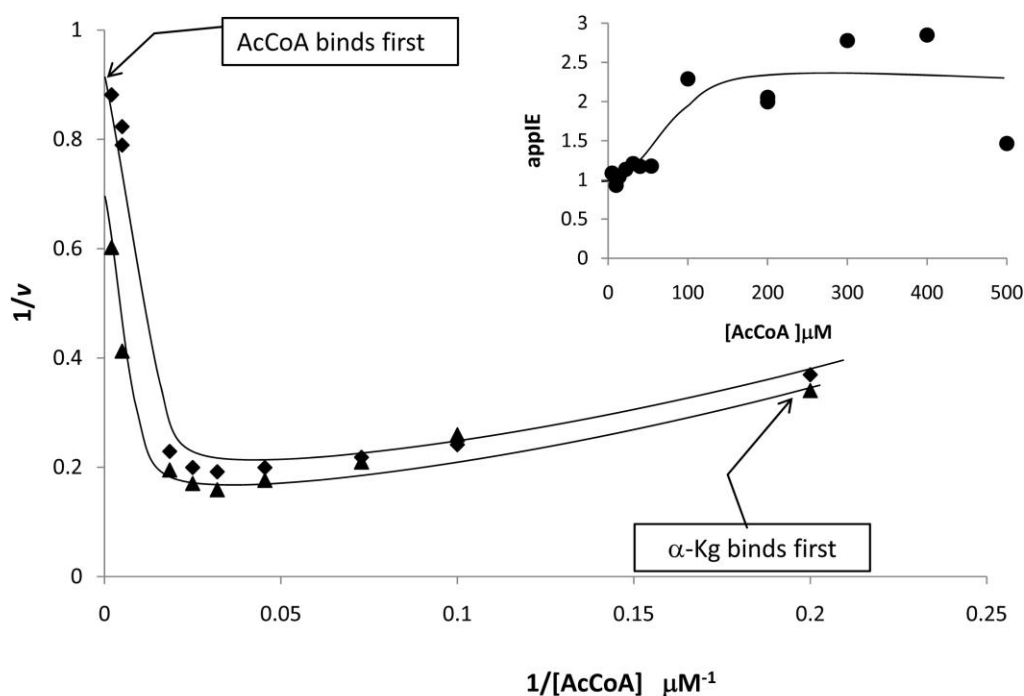


Figure 2.6 Primary Deuterium Kinetic Isotope Effect with AcCoA-$d_3$. Double reciprocal plot of initial rate as a function of AcCoA-$h_3$ (◆), and AcCoA-$d_3$) (▲); reactions with 400 μM α-Kg. The enzyme concentration was maintained at 1 μM. Inset shows the apparent isotope effect (appIE) *vs* the concentrations of AcCoA (the appIE is the ratio of the rates obtained with deuterated and undeuterated AcCoA). Curves are drawn by hand.

## 2.3.5 Solvent deuterium kinetic isotope effects.

Solvent deuterium kinetic isotope effects were measured in the presence of 200

µM Mg$^{2+}$ at pH(D) 7.5, in the pH independent region of the pH-rate profiles. Initial velocity patterns were obtained by measuring the initial rate at varying α-Kg concentrations and different fixed levels of AcCoA in $H_2O$ and $D_2O$, Figure 2.7A and B. Slope and intercept replots derived from the primary plot are shown in Figure 2.7C and D. Solvent isotope effects were unity at low concentrations of AcCoA, but were finite at high concentrations of AcCoA, with estimated values for $^{D2O}V$ of 1.7 and $^{D2O}(V/K_{AcCoA})$ of 2.8, Figure 2.7E.
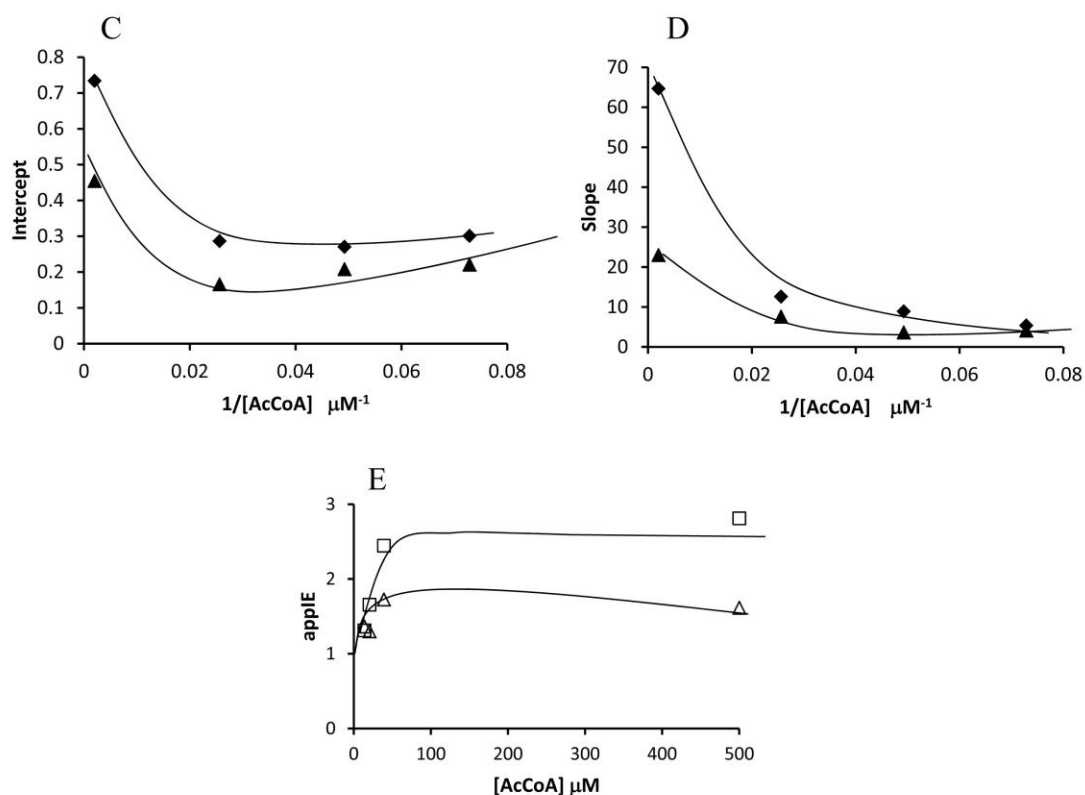


Figure 2.7 Solvent Deuterium Kinetic Isotope Effect. Double reciprocal plots of initial rate as a function of α-Kg at different concentrations of AcCoA as follows: 14 (O), 20 (Δ), 39 (▢) and 500 (◊) µM in $H_2O$ (A) and 14 (●), 20 (▲), 39 (■) and 500 (◆) µM in $D_2O$ (B). The enzyme concentration was maintained at 1 µM. Intercepts (C) and slopes (D) from (A) and (B) plotted against the reciprocal of AcCoA concentration in $D_2O$ and $H_2O$. E) Apparent isotope effect (appIE) *vs* concentration of AcCoA for slopes (▢) and intercepts (Δ), respectively (the appIE is the ratio of rates in $D_2O$ to $H_2O$).

47

**2.3.6 pH dependence of kinetic parameters.**

The pH dependence of kinetic parameters provides information on the optimal protonation state of functional groups on enzyme and/or substrate for binding and/or catalysis. To be certain that the kinetic mechanism of the enzyme does not change with pH and to obtain estimates of $K_m$ values for both substrates as a function of pH, initial velocity patterns were obtained with α-Kg and AcCoA concentrations varied at each pH. In presence of $MnCl_2$ with AcCoA as the varied substrate, $V$ is pH independent, while $V/K_{AcCoA}$ decreased at low pH with a slope of 1 giving a p$K_a$ of about 6.5 and at high pH with a slope of -1, giving a p$K_a$ of about 8.0, Figure 2.8. $V_{max}$ with $Mg^{2+}$ as the divalent metal ion is also pH independent (data not shown). The pH dependence of $V/K_{AcCoA}$ was not determined because of the large uncertainty in the values, Table 2.2, estimated from data similar to those in Figure 2.3.

An apparent $K_i$ for lysine inhibition was measured by Dixon plot for the low lysine concentration range, Figure 2.5B. Over the pH range studied, $K_{iLys}$ decreases from a constant value below pH 6.0 to another constant value above pH 8.8, Figure 2.5C. A value of 9.5 was assumed for the p$K_a$ obtained from the change in $K_i$ (see explanation in the Discussion), and data were fitted to eq. 10. The pH independent values of $K_{iLys}$ at high and low pH are 1.9 ± 0.4 μM and about 8 mM, respectively, and the p$K_a$ of the α-amine of lysine when it is bound to enzyme is 5.9 ± 0.2.
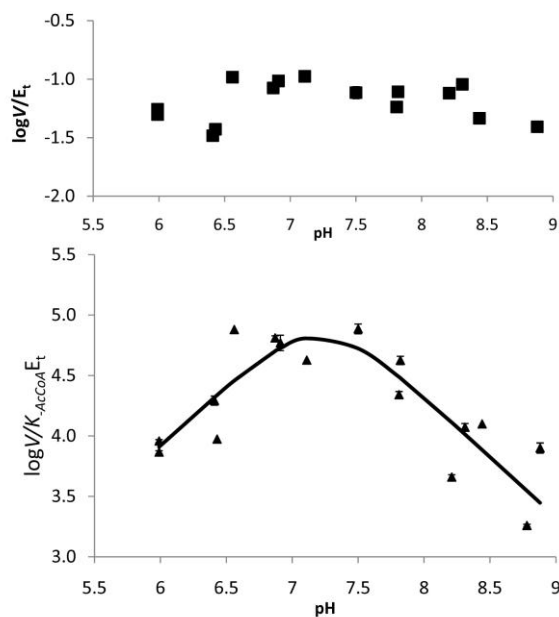
Figure 2.8  The pH Dependence of Kinetic Parameters with $Mn^{2+}$ as the Divalent Metal Ion. Data were obtained at $25^{\circ}C$.  At each pH, initial rates were obtained at a saturating concentration of $\alpha$-Kg ($10K_m$) as a function of AcCoA concentration.  The $V$ pH-rate profile is pH independent, while $V/K_{AcCoA}$ decreases at low and high pH giving limiting slopes of 1 and -1, respectively.  The points shown are the experimentally determined values, while the curve for $V/K_{AcCoA}$ is theoretical, and based on a fit to eq 9.


## 2.4 DISCUSSION

### 2.4.1 Divalent metal ion specificity.

The apo-enzyme of *Tt*HCS can be activated by $Mg^{2+}$ and $Mn^{2+}$, and is thus likely a Mg-dependent metal-activated enzyme.  Although $Mn^{2+}$ also activates the apo-enzyme to the same extent as $Mg^{2+}$, the total cellular levels of $Mn^{2+}$ are generally in the μM range (*21, 22, 29*) and it is thus unlikely that $Mn^{2+}$ is the physiologic activator. Interestingly, the initial velocity patterns obtained with $Mg^{2+}$ and $Mn^{2+}$ as the activator are different (see below), suggesting that the size of the metal ion and its coordination geometry, may contribute to this difference.  *Tt*HCS differs from the *Sc*HCS, which is a

49

Zn-metalloenzyme; $Zn^{2+}$ does not activate $Tt$HCS. A recent crystal structure (*10*) suggests $Co^{2+}$ is bound to $Tt$HCS in an apparent octahedral geometry with three ligands from enzyme, the side chains of Glu13, His197 and His 195, the C1-carboxylate and C2-oxo groups of α-Kg and a water molecule. However, these authors also showed significant activity of the enzyme in the presence of $Co^{2+}$, while no significant activation of $Tt$HCS was seen with $Co^{2+}$ in these studies. There was not enough information provided to determine how metal ion solutions were treated in the previous study (*10*), and activity could result from contaminating metal ions in the $Co^{2+}$ solution.

**2.4.2 Kinetic mechanism.**

The kinetic mechanism depends on the divalent metal ion and keto acid substrate used in the $Tt$HCS reaction. In the presence of $Mn^{2+}$, an initial velocity pattern is obtained that is near parallel at low concentrations of AcCoA, suggesting a $K_{i\alpha\text{-}Kg}/K_{\alpha\text{-}Kg}$ ratio that is low. Under these conditions the $K_{ia}K_b$ term in the sequential rate equation ( $v = \dfrac{V\mathbf{AB}}{K_{ia}K_b + K_a\mathbf{B} + K_b\mathbf{B} + \mathbf{AB}}$ ) becomes negligible and the rate equation reduces to the same as that for a ping pong mechanism. The replot of slope vs. 1/AcCoA is concave upward, Figure 2.2. However, the intercept replot is linear indicating substrate inhibition by AcCoA that is competitive vs α-Kg. Thus, the kinetic mechanism appears to be steady state ordered with α-Kg binding prior to AcCoA, Scheme 2.2, with a dead-end E-AcCoA complex allowed at high concentrations of AcCoA, described by eq. 1. It is interesting to note that the substrate inhibition constant for AcCoA is essentially equal to its $K_m$, 10 ± 5 μM compared to 27 ± 4 μM. At low, sub-saturating α-Kg, the E-

AcCoA complex will form at concentrations of AcCoA around 10 μM, decreasing the overall amount of productive enzyme, while at high, saturating concentrations of α-Kg, the reaction proceeds toward product at the same concentration of AcCoA. Thus, with $Mn^{2+}$ as the metal ion activator, α-Kg determines the rate of the *Tt*HCS reaction.
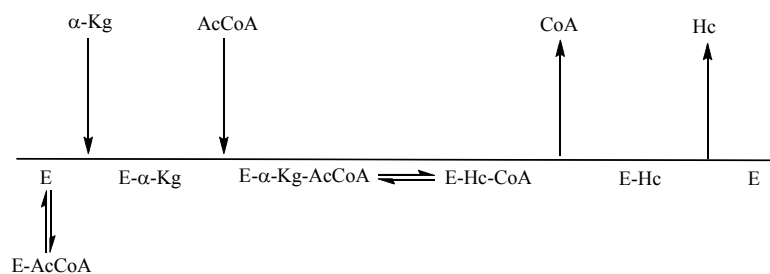


Scheme 2.2  Kinetic Mechanism Proposed for *Thermus thermophilus* Homocitrate Synthase with $Mn^{2+}$ as the Metal Ion.  An ordered kinetic mechanism is shown with a dead-end E-AcCoA complex.

The mechanism differs considerably in the presence of $Mg^{2+}$.  The initial velocity pattern obtained varying α-Kg at different fixed levels of AcCoA intersects to the left of the ordinate at low AcCoA, but slope and intercept replots exhibit curvature at high AcCoA concentrations, insets to Figures 2.3A. Note, however, that in the primary plot of $1/v$ *vs.* $1/[AcCoA]$, the pattern exhibits near parallel lines at low AcCoA, Figure 2.3B, with the extrapolated curves at high AcCoA, intersecting the ordinate at a finite value.  Data are indicative of a steady state random kinetic mechanism, Scheme 2.3.

The near parallel lines at low AcCoA suggest, as for data obtained with $Mn^{2+}$, a low $K_{i\alpha\text{-}Kg}/K_{\alpha\text{-}Kg}$ ratio.  The pathway to which this condition applies is that for α-Kg adding prior to AcCoA, the same pathway that is productive with $Mn^{2+}$ as the divalent metal ion.  Limits of the kinetic parameters were estimated as discussed above in

Results, Table 2.1.  The pathway with α-Kg adding prior to AcCoA is about 3-times faster than the pathway with AcCoA adding prior to α-Kg as shown by the ratio of the maximum rates obtained at low and high AcCoA.  The $K_m$ values for α-Kg and AcCoA are not significantly different for the two pathways, and thus the $V/K$ values for α-Kg and AcCoA mirror changes in $V$.

α-Kg     AcCoA

Products

E-α-Kg          E-α-Kg-AcCoA

E                                                      E*-α-Kg-AcCoA

E-AcCoA ⇌ E*-AcCoA

E-Lysine

AcCoA                      α-Kg
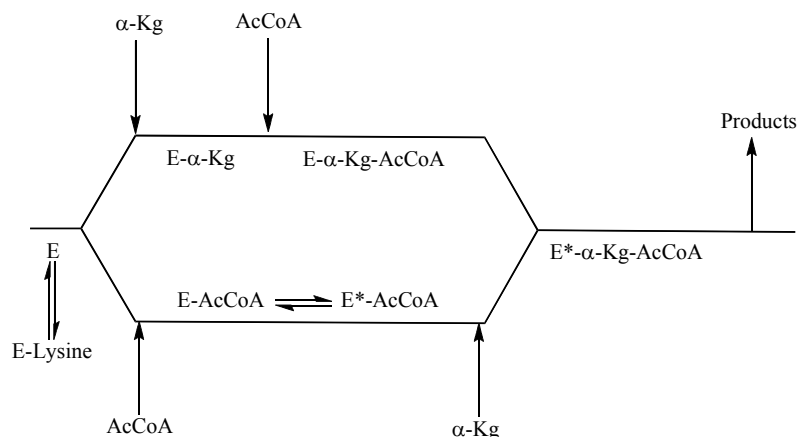
Scheme 2.3  Kinetic Mechanism Proposed for *Thermus thermophilus* Homocitrate Synthase with $Mg^{2+}$ as the Metal Ion.  A random kinetic mechanism is shown highlighting the conformational change that occurs upon AcCoA binding.  The conformations of the enzymes are denoted as E and E*.  Lysine binds to free enzyme competing with α-Kg, and generating a dead-end E-Lysine complex.

It is interesting to note that the pathway with AcCoA binding to free enzyme is productive with $Mg^{2+}$ as the divalent metal ion, while AcCoA exhibits substrate inhibition binding to E with $Mn^{2+}$ as the divalent metal ion.  (A small amount of activity at high AcCoA cannot be ruled out.)  Data certainly suggest something different about the active site with $Mg^{2+}$ and $Mn^{2+}$ bound.

Product inhibition by CoASH provides additional information on the kinetic mechanism of *Tt*HCS.  In the presence of $Mg^{2+}$, or $Mn^{2+}$, CoASH was competitive against AcCoA suggesting the binding of CoASH to the same enzyme form(s) as

AcCoA, free enzyme and the E-α-Kg complex (data not shown). Inhibition by CoASH *vs* α-Kg was uncompetitive, Figure 2.4B. In addition, at high concentrations of CoASH, curved double reciprocal plots were observed with α-Kg varied, Figure 2.4A. Data suggest induction of positive cooperativity of α-Kg binding, and this will be discussed below when lysine inhibition is considered. The CoASH inhibition patterns differ from those found for *Sc*HCS, which exhibits noncompetitive inhibition by CoASH *vs* AcCoA, and uncompetitive inhibition *vs* α-Kg (*4*). Data for the yeast enzyme were consistent with the ordered addition of a α-Kg prior to AcCoA and with binding of CoASH to the E-α-Kg and E-homocitrate (E-Hc) complexes. The CoASH inhibition patterns obtained for the *Tt*HCS are consistent with CoASH binding to E-α-Kg, but not to the E-Hc complex. Data suggest that release of homocitrate from the E-Hc complex does not contribute to rate-limitation of the bacterial enzyme.

The α-Kg analog, OG, is competitive as expected, but $K_{iOG}$ is independent of the concentration of AcCoA, suggesting binding of OG to E and E-AcCoA with equal affinity. The binding site for α-Kg apparently does not change whether or not the conformational change induced by the binding of AcCoA has taken place. The $K_i$ for OG is about 18-times lower than $K_{\alpha\text{-}Kg}$, suggesting somewhat stronger binding of OG. α-Kg binds in an extended conformation, but with the γ-carboxylate slightly twisted compared to its α-carboxylate, Figure 2.10A *(10)*. The stronger binding is thus likely the result of interaction between the amide nitrogen of OG with enzyme. Oxaloacetate, a methylene shorter than α-Kg, binds 700-fold weaker, indicating unfavorable interactions of the β-carboxylate with (a) group(s) on enzyme.

### 2.4.3 Inhibition by lysine.

Lysine is known to inhibit *Tt*HCS, suggesting end-product feedback regulation of the biosynthetic pathway (*8*). A Dixon plot of the reciprocal rate *vs* the concentration of lysine is biphasic, Figure 2.5, suggesting negative cooperativity of binding lysine, Figure 2.9. Lysine is a competitive inhibitor *vs* α-Kg at low concentrations, where it has the highest affinity for enzyme and at high concentrations, where it binds with lower affinity, Scheme 2.3. The difference in affinity for the two sites is about 250-fold, Table 2.3. At high concentrations, however, lysine induces positive cooperativity of α-Kg binding, similar to that observed with CoASH. The positive cooperativity is likely a result of the two sites generated by lysine binding, i.e. induced asymmetry in the enzyme dimer in the presence of lysine.
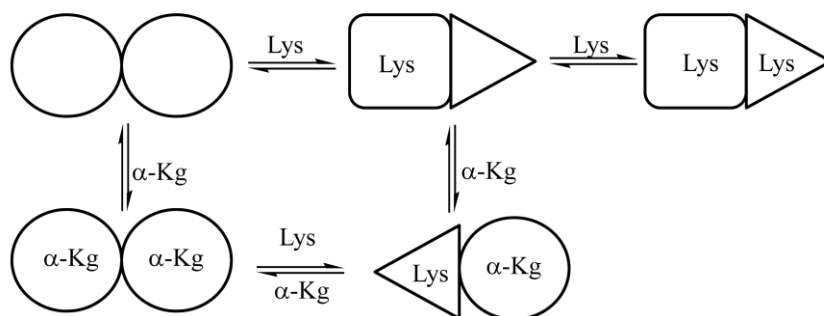


Figure 2.9 Lysine inhibition of *Tt*HCS. *Tt*HCS as a dimer depicted as circles. Change in conformation of enzyme on binding of Lys to one subunit shown as square and effect of which on the other subunit shown as a triangle. Binding of Lys to one subunit brings about a conformational change in the enzyme such that its affinity to bind the other subunit is lowered, thus making it relatively easier for α-Kg to compete.

By analogy a similar phenomenan likely occurs with CoASH. Since lysine and α-Kg compete for the same site, α-Kg can effectively compete for lysine at much lower concentrations at the low affinity site, but higher concentrations are required to compete

54

for lysine at the high affinity site. This would require that α-Kg competing with lysine at the weak site would decrease the affinity for lysine at the tight site, while increasing its own affinity for that site, i.e., the two ligands have opposing effects.

*Tt*HCS exists as a homodimer and this, in conjunction with the crystal structure of *Tt*HCS with lysine bound, Figure 2.10B (*10*), provide a possible molecular basis for the negative cooperativity of lysine binding. The competitive inhibition suggests, and the lysine-bound structure confirms, that lysine binding is at the active site. In fact, the α-amine and α-carboxylate of lysine occupy the same coordination positions on the active site $Mg^{2+}$ as the α-oxo and α-carboxylate of α-Kg occupy once bound. The hypothesis is that binding of the first molecule of lysine into the first active site brings about a conformational change in the enzyme such that its affinity for the second active site of the homodimer is reduced, resulting in the second phase observed in the Dixon plot, Figure 2.5. Binding of lysine results in dramatic structural changes (*10*). For example, helix 11 moves by about 44 Å from one side of the protein to the other. In addition, although lysine and α-Kg share some of the same active site binding determinants, there are a number of differences (see *Structure* below). The conformational change differs from the one(s) generated upon binding of reactants (see *Structure* or below).

In agreement with the above, and consistent with the structure, is the pH dependence of $pK_{iLys}$ for binding to site 1. Lysine is coordinated to the active site $Mg^{2+}$ by its α-amine and α-carboxylate. As a result, the α-amine must be neutral for optimum binding. The app $pK_{iLys}$ decreases from a constant value at high pH (above pH 9) and goes to a lower constant value at low pH (below pH 5.5). Thus, the group

with a p$K_a$ above 9 that must be unprotonated in order to coordinate to the metal ion is the a-amine of lysine, which has a p$K_a$ of about 9.5. A fit of the data to eq. 9 gives an estimate of about 6 for the p$K_a$ of the $\alpha$-amine of lysine bound to the active site $Mg^{2+}$. The $K_i$ for lysine changes by more than three orders of magnitude as the pH increases with the value above pH 10 reflecting the true $K_i$ (2 $\mu$M) for lysine with a neutral $\alpha$-amine binding to enzyme. Lysine with a protonated $\alpha$-amine binds 4000-fold weaker, and the p$K_a$ of the $\alpha$-amine has decreased by 3.6 pH units, reflecting the much lower proton affinity for lysine bound to the active site in the vicinity of the metal ion.

The negative cooperativity of lysine binding essentially results in decreasing activity of both active sites of the HCS dimer upon occupancy of a single subunit. The physiologic concentration of lysine can reach 5 mM (*23-28)*, a concentration at which the tight site of the *Tt*HCS is saturated ($K_i$ is 230 $\mu$M, Table 2.3). This suggests the activity of *Tt*HCS will depend on the concentration of $\alpha$-Kg. Although the physiologic concentration will likely not get high enough to allow binding to the loose site, the phenomenon of negative cooperativity in conjunction with the structural data available, aid in determining the mode of lysine binding.

**2.4.4 Rate-determining steps.**

In the presence of $Mg^{2+}$, isotope effect data are complex, but revealing. A substrate deuterium isotope effect of unity is measured with AcCoA-d$_3$, at low concentrations of AcCoA, but a finite primary kinetic isotope effect of about 2 is observed at high AcCoA. Data can be interpreted in terms of the steady state random kinetic mechanism proposed for *Tt*HCS (see **Kinetic Mechanism** above).

At low AcCoA, $\alpha$-Kg binds prior to AcCoA and this is the dominant pathway. The deuterium kinetic isotope effect reflects deprotonation of the methyl of AcCoA, while the solvent deuterium kinetic isotope effect reflects protons in flight in the rate-limiting transition state. Both isotope effects are unity for the pathway with $\alpha$-Kg binding first, indicating deprotonation of the methyl group of AcCoA does not contribute to rate-limitation, nor does hydrolysis of the homocitryl CoA that is produced in the Claisen condensation. As a result, we propose that a conformational change that likely follows the chemical steps limits the overall reaction (see below).

At high AcCoA, where it binds prior to $\alpha$-Kg, a finite primary kinetic isotope effect of about 2 is observed, Figure 2.6. We propose that binding of AcCoA to free enzyme elicits a conformational change that is slower than the one that must occur when AcCoA binds second. The difference between the two is the presence or absence of $\alpha$-Kg, which can pre-organize the active site for binding of AcCoA. Since an isotope effect is observed when AcCoA binds first, deprotonation of the methyl group of AcCoA must accompany the conformational change. The solvent deuterium kinetic isotope effects exhibits the same behavior as the substrate kinetic isotope effect, suggesting the conformational change that occurs when AcCoA binds first must have protons in flight in the transition state for the conformational change, giving an apparent solvent effect of about 1.7, Figure 2.7.

If the conformational change elicited by AcCoA binding after $\alpha$-Kg were slow, one would expect finite primary deuterium and solvent deuterium kinetic isotope effects. Thus, the slow step in the pathway with AcCoA binding after $\alpha$-Kg likely occurs after the chemical steps, i.e., release of the first product. The interpretation is

57

illustrated in Scheme 2.4. In the scheme, the mechanism is broken down to show the two pathways. Pathway A is the dominant pathway with $\alpha$-Kg binding before AcCoA, and the slow step is the conformational change that accompanies release of CoA. (Product inhibition by CoA is strictly competitive vs. AcCoA and uncompetitive *vs* $\alpha$-Kg, consistent with absence of binding of CoA to free enzyme or an E-Hc product complex. By analogy to the forward reaction, release of CoA before Hc is predicted, and data therefore suggest rapid release of Hc.) Pathway B, on the other hand, describes binding of AcCoA before $\alpha$-Kg, and the slow step in this case is the conformational change elicited upon binding of AcCoA, which includes deprotonation of the methyl of AcCoA.

**A**

E $\rightleftharpoons$ E-$\alpha$-Kg $\rightleftharpoons$ E-$\alpha$-Kg-AcCoA $\rightleftharpoons$ E*-$\alpha$-Kg-AcCoA $\xrightarrow{\textbf{D, D}_2\textbf{O}}$ E*-Hc-CoA $\xrightarrow{\text{CoA}}$ E-Hc $\xrightarrow{\text{Hc}}$ E

($\alpha$-Kg, AcCoA enter; Slow)

**B**

E $\rightleftharpoons$ E-AcCoA $\underset{\textbf{Slow}}{\overset{\textbf{D, D}_2\textbf{O}}{\rightleftharpoons}}$ E*-AcCoA $\rightleftharpoons$ E*-$\alpha$-Kg-AcCoA $\longrightarrow$ E*-Hc-CoA $\xrightarrow{\text{CoA}}$ E-Hc $\xrightarrow{\text{Hc}}$ E
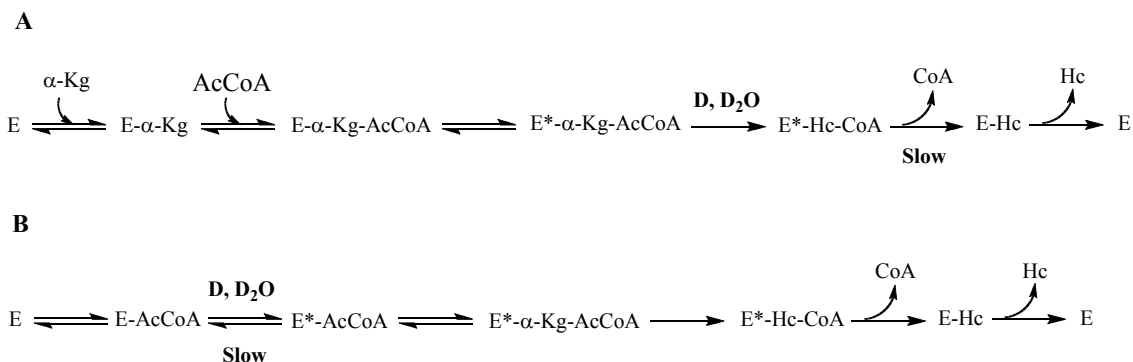
Scheme 2.4 The two pathways of the random mechanism shown in Scheme 2.3 are shown. Pathway A is the dominant pathway and exhibits rate-limiting release of CoA. The deuterium and solvent deuterium sensitive steps reflect the conversion of E*-$\alpha$-Kg-AcCoA to products. Pathway B occurs at high concentrations of AcCoA. The slow step in this case is the conformational change that accompanies AcCoA binding to give the E*-AcCoA complex. This step exhibits finite deuterium and solvent deuterium isotope effects.

## 2.4.5 pH dependence of kinetic parameters.

The pH dependence of $V/E_t$ is obtained at saturating concentrations of all

substrates. The *V* profile will thus reflect ionizable groups within the enzyme-substrate complex involved in catalysis. The $V/K\text{E}_t$ pH-rate profile reflects ionizable groups, on free substrate and the enzyme form to which it binds, required in an optimum protonation state for binding and/or catalysis. Data for the pH dependence of *V* and *V/K* were obtained in the presence of $Mn^{2+}$, however, the difference in kinetic mechanism with $Mg^{2+}$ and $Mn^{2+}$ lies in the competence of the E-AcCoA complex. Catalytic and binding groups, and the pH dependence of kinetic parameters for the pathway with α-Kg binding first should be very similar whatever the divalent metal ion used.

With $Mn^{2+}$ as the divalent metal ion, *V* is pH independent, while $V/K_{AcCoA}$ decreases at low and high pH giving $pK_a$ values of about 6.5 and 8.0, respectively. (The maximum rate obtained with $Mg^{2+}$ was also pH independent (data not shown).) The pH dependence of $V/K_{AcCoA}$ was not determined because of the large uncertainty in the values, Table 2.2, estimated from data similar to those in Figure 2.3. Data are consistent with the requirement for general base, general acid mechanism, as proposed for the *Saccharomyces* enzyme, *Sc*HCS. By analogy to *Sc*HCS, the base is proposed to accept a proton from the methyl of AcCoA to allow nucleophilic attack on the carbonyl of α-Kg, while the acid is proposed to donate a proton to the carbonyl oxygen to form homocitryl CoA (*6*). The active site residues of *Sc*HCS and *Tt*HCS are conserved, and will be further described below.

**2.4.6 Structure.**

  *Tt*HCS is a dimer comprised of a TIM barrel domain and C-terminal small domains (I and II) (*10*). Small domain II of one monomer is a 3-helix bundle that

covers the active site of the other monomer; the active site is on the C-terminal end of the TIM barrel. This arrangement, described as domain swapping, has also been observed in the case of *Schizosaccharomyces pombe* HCS (*Sp*HCS) (*19*). The substrate α-Kg and the feedback inhibitor lysine bind to the active site and share some of the same binding interactions (*10*).

α-Kg binds to the enzyme via several specific interactions. The C1-carboxylate and C2-oxo groups of α-Kg are coordinated to the bound divalent metal ion. The C1-carboxylate accepts a hydrogen bond from T166, while the C2-oxo group interacts with the guanidium group of R12. The side chains of A164 and L94 (not shown) make van der Waals contact with the C3 and C4 atoms of α-Kg, and the C5-carboxylate is stabilized by hydrogen bonds and ionic interactions with H72 and R133 and, via a water molecule, interacts with S135, Figure 2.10A. Lysine bound to the active site of *Tt*HCS is coordinated to the divalent metal ion via its α-carboxylate and α-amino, accepts a hydrogen bond from T166 and the aliphatic portion of the lysine side chain is stabilized by van der Waals contacts from A164 and L94, Figure 2.10B. It is these interactions that are in common with α-Kg binding. However, the α-amino of lysine is within hydrogen bonding distance to Tyr297* (the * indicates the residue is from the other subunit of the dimer), and the ε-amino group of lysine is stabilized by interactions with D92 and E193. The most significant difference in binding of α-Kg and lysine is in the displacement of residues surrounding the C5-carboxylate of α-Kg to accommodate binding of the ε-amino group. The overall rearrangement includes: 1) movement of R133 away from the active site with formation of an ion pair with E43; and 2)

movement of H72, which formed a hydrogen bond to the C5- carboxylate of $\alpha$-Kg, to stack with the side chain of R12, which formed a hydrogen bond to the C2-oxo group of $\alpha$-Kg. Given the contribution of residues from both subunits of the dimer to binding of lysine, cross talk between the two subunits of the dimer as lysine binds is not unexpected. We propose, that in the case of feedback inhibition by lysine in $Tt$HCS (and by analogy $Sp$HCS and $Sc$HCS), lysine binding to the first active site reduces the affinity for lysine binding to the second active site as a result of the crosstalk discussed above resulting in negative cooperativity as shown in Figure 2.5B. The specific active site interactions made by lysine as it binds result in substantial gross changes in the structure of the protein. Overall, there is a 44 Å displacement of the position of $\alpha$11 helix, which includes Y297*, moving it closer to the active site. The conformation of the enzyme in general and the active site specifically is quite different with $\alpha$-Kg or Lys bound.

Though there is no structure available with AcCoA bound, there is one with homocitrate bound, and this sheds some light on the residues involved in AcCoA binding. The C1-carboxyl of Hc, which is derived from AcCoA, is hydrogen bonded to H292*, which stacks with Y303*. H292* moves by 13 Å away from the active site upon binding of Lys (*10*). This large displacement indicates the conformation of the active site with Lys or AcCoA bound is different. It follows that the conformational change generated upon reactant binding is distinct from that with Lys bound at the active site. Lysine bound structure (PDB 3A9I) has one monomer in the asymmetric unit. Two-fold crystallographic symmetry makes the dimer. The Lys bound form has a different space group (C222$_1$) than the other structures (P6$_3$22) (*10*). This may result in

different crystal contacts at the active site.

All active site residues are conserved in *Sc*HCS, *Sp*HCS, *Li*CMS, and *Tt*HCS (*5, 9, 15*). In *Sc*HCS a catalytic dyad comprised of E155 and H309* was proposed as the base that deprotonates the methyl group of AcCoA, while Y320 contributed to providing the optimum orientation of the dyad and/or the reactant; E137 and H292* of *Tt*HCS correspond to the residues of the proposed catalytic dyad (E155 and H309* in *Sc*HCS) (*5*). A conserved arginine, R31 in *Sc*HCS (R12 in *Tt*HCS), is within hydrogen-bond distance to the carbonyl oxygen of α-Kg and may have a role of a general acid in the catalytic mechanism. Comparing the structures of *Tt*HCS and *Sp*HCS, the C-terminal small domain I is similar to that of the corresponding domain of *Sp*HCS (*10, 16*). Lysine binding in these structures is also similar with H72 in *Tt*HCS (H103 in *Sp*HCS) playing an important role by changing its side chain orientation to stabilize R12. H72 is conserved among lysine-sensitive HCSs, suggesting a role in feedback inhibition by lysine. In contrast, feedback inhibition by leucine in *Mycobacterium tuberculosis* IPMS (*Mt*IPMS) occurs by binding of the inhibitor to a separate regulatory domain linked to the C-terminal catalytic domain (*28*). A mechanism similar to that proposed for IPMS is expected for *Li*CMS since it also possesses a C-terminal regulatory domain.
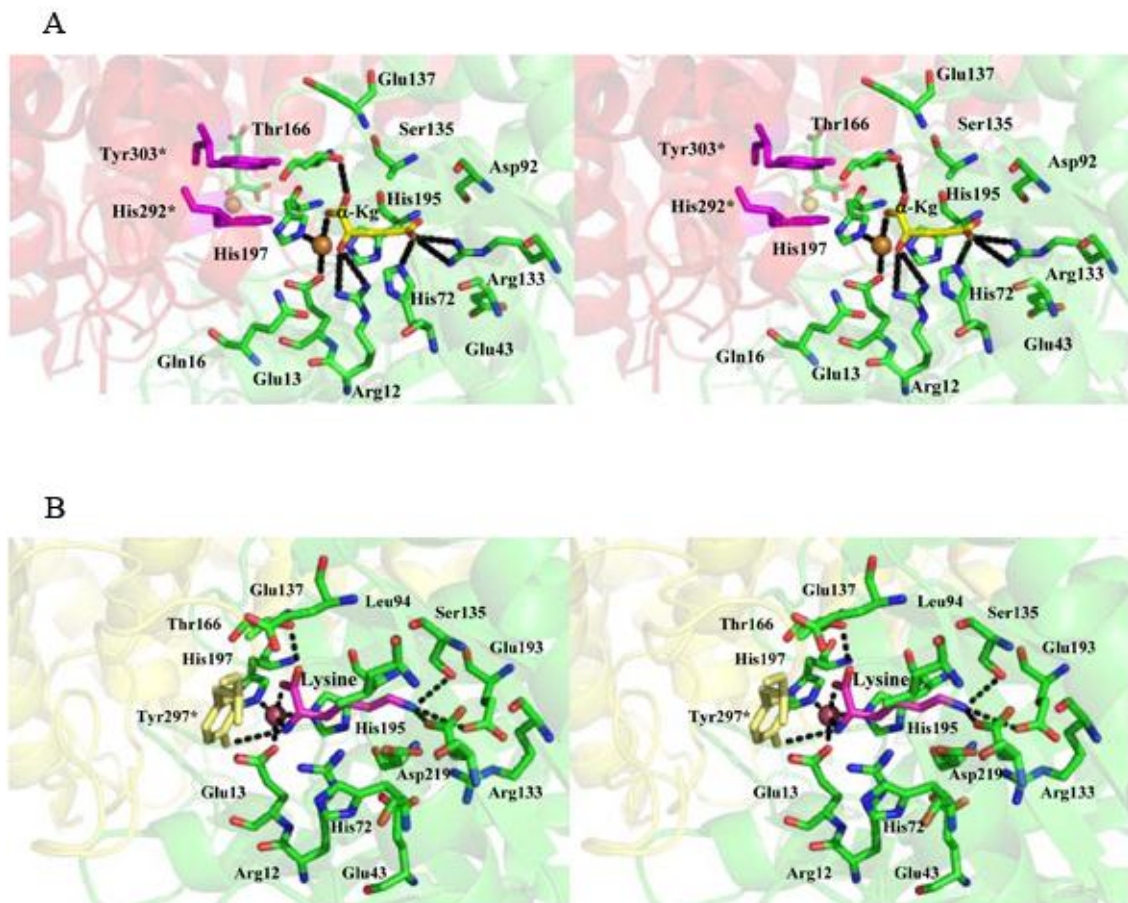
Figure 2.10  Close-up view of the Active Site of *Tt*HCS with Ligand Bound.  Active site residues and bound ligands are shown as stick models.  A putative $Co^{2+}$ ion is shown as a sphere in faint pink.  Hydrogen bonds are shown as dashed lines in black.  A) The structure with α-Kg bound (pdb 2ZTJ).  Distances for the hydrogen bonds for T166 - the C1 carboxyl group of α-Kg, Nη1 and Nη2 of R12 - the C2 keto group of α-Kg, the ε-amine of H72 - the C5 carboxyl group of α-Kg, Nη1 and Nη2 of R133 - the C5 carboxyl group of α-Kg are 2.6 Å, 2.3 Å, 3.1 Å, 3.0 Å, 2.7 Å, 3.3 Å, and 2.8 Å, respectively.  B) The structure with lysine bound (pdb 3A9I). Distances for the hydrogen bonds for T166 - the lysine α-carboxylate, Y297* (the * indicates the residue is from the other subunit of the dimer)- the lysine α-amino, S135 to the ε-amine of lysine, E193 to the ε-amine of lysine, and D92 to the ε-amine of lysine are 2.6 Å, 3.2 Å, 3.1 Å, 3.5 Å, and 2.6 Å, respectively.

## 2.5 REFERENCES

1. Tucci, A. F., and Ceci, L. N. (1972) Homocitrate synthase from yeast, *Arch. Biochem. Biophys.* 153, 742-750.

2. Gray, G. S., and Bhattacharjee, J. K. (1976) Biosynthesis of lysine in *Saccharomyces cervisiae*: properties and spectrophotometric determination of homocitrate synthase activity, *Can. J. Microbiol.* 22, 1664 – 1667.

3. Schöbel, F., Jacobsen, I. D., and Brock, M. (2010) Evaluation of lysine biosynthesis as an antifungal drug target: biochemical characterization of *Aspergillus fumigatus* homocitrate synthase and virulence studies, *Eukaryot Cell.* 6, 878-893.

4. Andi, B., West, A. H., and Cook, P. F. (2004) Kinetic mechanism of histidine-tagged homocitrate synthase from *Saccharomyces cerevisiae*, *Biochemistry* 43, 11790-11795.

5. Andi, B., West, A. H., and Cook, P. F. (2004) Stabilization and characterization of histidine-tagged homocitrate synthase from *Saccharomyces cerevisiae*, *Arch. Biochem. Biophys.* 421, 243-254.

6. Qian, J., Khandogin, J., West, A. H., and Cook, P. F. (2008) Evidence for a catalytic dyad in the active site of homocitrate synthase from *Saccharomyces cerevisiae*, *Biochemistry* 47, 6851-6858.

7. Andi, B., West, A. H., and Cook, P. F. (2005) Regulatory mechanism of histidine-tagged homocitrate synthase from *Saccharomyces cerevisiae*. I. Kinetic studies, *J Biol Chem.* 280, 31624-31632.

8. Qian, J., West, A. H., and Cook, P. F. (2006) Acid-base chemical mechanism of homocitrate synthase from *Saccharomyces cerevisiae*, *Biochemistry* 45, 12136-12143.

9. Wulandari, A. P., Miyazaki, J., Kobashi, N., Nishiyama, M., Hoshino, T., and Yamane, H. (2002) Characterization of bacterial homocitrate synthase involved in lysine biosynthesis, *FEBS Lett.* 522, 35-40.

10. Okada, T., Tomita, T., Wulandari, A. P., Kuzuyama, T., and Nishiyama, M. (2010) Mechanism of substrate recognition and insight into feedback inhibition of homocitrate synthase from *Thermus thermophilus*, *J Biol Chem* 285, 4195-4205.

11. Simon, E. J., and Shemin, D. (1953) The preparation of S-succinyl conenzyme A, *J. Am. Chem. Soc.* 75, 2520.

12. Qian, J. (2008) Chemical mechanism of homocitrate synthase from *Saccharomyces cerevisiae,* Ph.D. Dissertation, University of Oklahoma.

13. Cook, P. F. and Cleland, W. W. (2007) *Enzyme kinetics and mechanism.* Garland Science, New York. Chap. 6, 121-204.

14. Cleland, W. W. (1979) Substrate inhibition, *Methods Enzymol.* 63, 103-138.

15. Quinn, D. M.; Sutton, L. D. (1991) In *Enzyme mechanism from isotope effects*; Cook, P. F., Ed.; *CRC Press: Boca Raton, FL*, 73-126.

16. Karsten, W. E.; Lai, C. J. and Cook, P. F. (1995) Inverse solvent isotope effects in the NADmalic enzyme reaction are the result of the viscosity difference between D2O and H2O: Implications for solvent isotope effect studies, *J. Am. Chem. SOC.* 117, 5914-5918.

17. Lin, Y., West, A. H., and Cook, P. F. (2008) Potassium is an activator of homoisocitrate dehydrogenase from *Saccharomyces cerevisiae, Biochemistry.* 47, 10809-10815.

18. Bazelyansky, M., Robey, E. and Kirsch, J. F. (1986) Fractional diffusion-limited component of reactions catalyzed by acetylcholinesterase, *Biochemistry.* 25, 125-130.

19. Bulfer, S. L., Scott, E. M., Couture, J. F., Pillus, L., and Trievel, R. C. (2009) Crystal structure and functional analysis of homocitrate synthase, an essential enzyme in lysine biosynthesis, *J Biol Chem.* 284, 35769-35780.

20. Bulfer, S. L., Scott, E. M., Pillus, L., and Trievel, R. C. (2010) Structural basis for L-lysine feedback inhibition of homocitrate synthase, *J Biol Chem.* 285, 10446-10453.

21. Tholey, G., Ledig,M., Mandel, P., Sargentini, L., Frivold,A. H., Leroy, M., Grippo, A. A., and Wedler F. C. (1988) Concentrations of physiologically important metal Ions in glial cells cultured from chick cerebral cortex, *Neurochem Res*, 13, 45-50.

22. Jiang, Y, Zheng, W., Long, L., Zhao, W., Li, X., Mo, X., Lu, J., Fu, X., Li, W., Liu, S., Long, Q., Huang, J., and Pira, E. (2007) Brain magnetic resonance imaging and manganese concentrations in red blood cells of smelting workers: search for biomarkers of manganese exposure, *Neurotoxicology,* 28, 126-135.

23. Hans, M. A., Heinzle, E., and Wittman, C. (2001) Quantification of intracellular amino acids in batch-cultures of *Saccharomeyces cerevisiae, Appl. Microbiol. Biotechnol.* 56, 776-779.

24. Giuseppin,M. L., and von Riel, N. A. W. (2000) Metabolic modeling of *Saccharomyces cerevisiae* using the optimal control of homeostasis: A cybernetic model definition, *Metab. Eng.* 2, 14-23.

25. Hans, M. A., Heinzle, E., and Wittman, C. (2003) Free intracellular amino acid pools during autonomous oscillations in *Saccharomyces cerevisiae*, *Biotechnol. Bioeng.* 82, 143-151.

26. Ter Schure, E. G., Sillje, H. H. W., Verkleij, A. J., Boonstra, J., and Verrips, C. T. (1995) The concentration of ammonia regulates nitrogen metabolism in *Saccharomyces cerevisiae*, *J. Bacteriol.* 177, 6672-6675.

27. Feller, A., Ramos, F., Pierard, A., and Dubois, E. (1997) Repressor of Lys genes, is a pleiotropic regulatory factor identical to Mks1p, *Yeast* 13, 1337-1346.

28. Koon, N., Squire, C. J., and Baker, E. N. (2004) Crystal structure of LeuA from Mycobacterium tuberculosis, a key enzyme in leucine biosynthesis, *Proc. Natl. Acad. Sci. U.S.A.* 101, 8295−8300.

29. Hurwitz, C., and Rosano, C. L. (1967) The intracellular concentration of bound and unbound magnesium ions in *Escherichia coli*, *J. Biol. Chem.* 242 (16), 3719-3722.

## 2.6 FOOTNOTES

[1]Abbreviations: HCS, homocitrate synthase; Hc, homocitrate; IPMS, isopropylmalate synthase; CoA, coenzyme A; AcCoA, acetyl-CoA; AcCoA-$d_3$, deuterioacetylCoA; α-Kg, α-ketoglutarate; DCPIP, 2,6-dichlorophenolindophenol; EDTA, ethylenediaminetetraacetic acid; Mes, 2-morpholinoethanesulfonic acid; Taps, *N* [tris(hydroxymethyl)methyl]-3-aminopropanesulfonic acid; Hepes, 4-(2-hydroxyethyl)-1-piperazineethanesulfonic acid; Bis-tris, 2-bis(2-hydroxyethyl)amino-2-(hydroxymethyl)-1,3 propanediol.

[2]Oxaloacetate was not further characterized as a substrate in these studies, but will be considered in a future manuscript.

## ACKNOWLEDGEMENTS

# CHAPTER 3

# Catalytic residues in saccharopine dehydrogenase

Characterization of enzymes using kinetic parameters and isotope effects was done by me. Crystallization and structural studies were done by Thomas, L. M., Bobyk, K. D., Andi, B.

## 3.1 INTRODUCTION

Saccharopine dehydrogenase (N6-(glutaryl-2)-L-lysine: NAD oxidoreductase; EC 1.5.1.7) (SDH)[1] catalyzes the final step in the $\alpha$-aminoadipate (AAA) pathway for the *de novo* synthesis of L-lysine in fungi (*1, 2*). The enzyme catalyzes the reversible pyridine nucleotide dependent oxidative deamination of saccharopine to generate $\alpha$-Kg and Lys using NAD as an oxidant, Scheme 3.1 (*1*).

The proposed kinetic mechanism for the *Saccharomyces cerevisiae* SDH is ordered in the physiologic reaction direction with NAD binding before saccharopine (Sacc), while in the opposite direction $\alpha$-ketoglutarate ($\alpha$-Kg) and lysine (Lys) bind in random fashion once NADH is bound (*3*). A chemical mechanism involving two acid-base catalytic groups has been proposed on the basis of the pH dependence of kinetic parameters, Scheme 3.1 (*4*). Once the E·NADH·$\alpha$-Kg·Lys central complex is formed, the first base (B$_1$) accepts a proton from the $\varepsilon$-amine of Lys to allow nucleophilic attack on the carbonyl of $\alpha$-Kg (II). Nucleophilic attack gives a protonated carbinolamine with donation of a proton from the conjugate acid of B$_2$ to the carbonyl oxygen (III). The conjugate base of B$_2$ then accepts a proton from the carbinolamine nitrogen (IV) and this is followed by elimination of water to give the imine (V), which is reduced by NADH concomitant with protonation of the imine nitrogen by the conjugate acid of B$_1$.

A number of residues (E78, E122, K99, D319) in the active site of SDH have been mutated and mutant enzymes have been characterized (*5, 6*). To date, none appear to serve as acid-base catalytic residues.

In this study the roles of K77 and H96 have been determined by mutating them to M and Q, respectively. Mutations of K77 and H96 were prepared in the C205S mutant enzyme, which eliminates disulfide formation, so that 100% of the enzyme is in the "reduced" active form (*8*). A 1.6 Å X-ray structure the apo-wild-type SDH enzyme was solved by the Berghuis group (*7*) and showed a tertiary fold consisting of two domains (I and II) with a narrow cleft in between. Each domain can be described as a modified nucleotide-binding Rossman-like fold. The active site is located at the bottom of the cleft between the two domains. Three additional X-ray structures have been solved of SDH bound to a sulfate anion, adenosine monophosphate (AMP), and oxalylglycine (OxGly), respectively (*8*). The sulfate-bound structure revealed features of how the $\alpha$-keto acid substrate binds to R131 in the active site and showed a modest closure of the cleft between domains I and II. AMP was found to bind in the active site region expected to be occupied by the dinucleotide cofactor NAD. OxGly, an analogue of $\alpha$-Kg, was observed to bind to two arginines, R18 and R131 in the active site. A semi-empirical model was proposed based on these ligand-bound structures with NAD and Sacc modeled in the active site.

We now report a crystal structure of the ternary E•NADH•Sacc complex for the first time, which shows an enzyme form with a closed active site with K77 and H96 properly positioned to serve as acid-base catalysts. Mutant enzymes were characterized

via the pH dependence of kinetic parameters and isotope effects. Data are discussed in terms of the proposed mechanism of SDH.
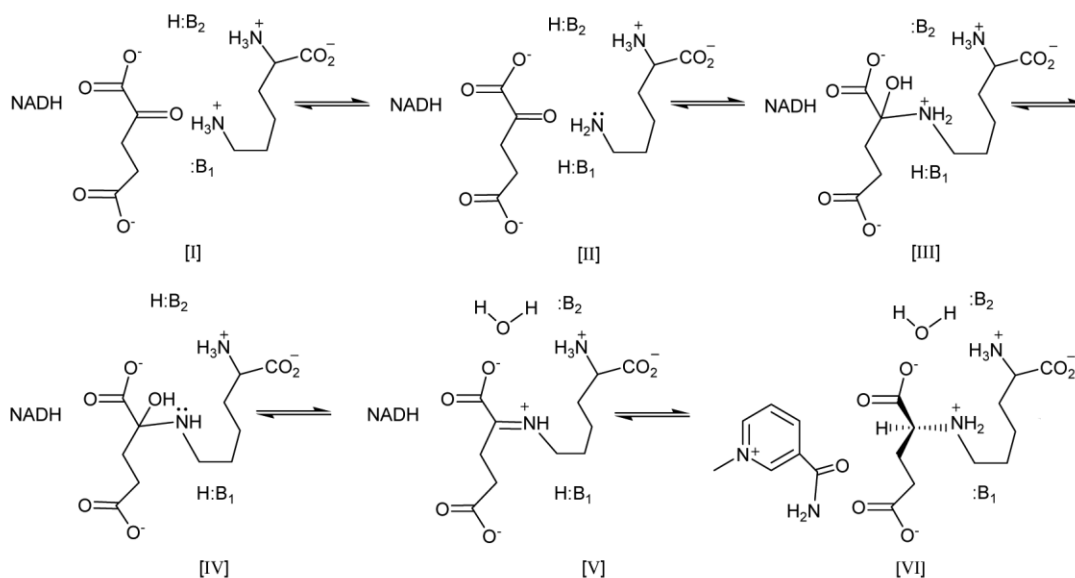


Scheme 3.1: Chemical Mechanism Proposed for Saccharopine Dehydrogenase. The reaction is written in the direction of Sacc formation. [I], protonated Lys; [II], the formed central complex E·NADH·α-Kg·Lys; [III], protonated carbinolamine; [IV], carbinolamine intermediate; [V], Schiff base intermediate; [VI], hydride transfer and formation of Sacc. With the exception of Sacc, no stereochemistry is implied.

## 3.2 MATERIALS AND METHODS

### 3.2.1 Chemicals.

Ampicillin, chloramphenicol, Sacc, Lys, α-Kg, AMP, OxGly, polyethylene glycol 3350, Bis-Tris propane, horse liver alcohol dehydrogenase, yeast aldehyde dehydrogenase, and the GenElute plasmid miniprep kit were obtained from Sigma. β-NADH, β-NAD, Luria-Bertani (LB) broth, LB-agar, and imidazole were purchased form U. S. Biochemical Corp. The buffers, Ches, Taps, Hepes, and Mes, were from Research Organics, while NiNTA resin was purchased from 5 Prime. Ethanol-$d_6$ (99 atom % D) and $D_2O$ (99.9 atom % D) were purchased from Cambridge Isotope Laboratories.

69

Ethanol (absolute, anhydrous) was from Pharmaco-Aaper. Polyethylene glycol monomethyl ether (PEG-MME) and Sodium Malonate were from Hampton Research. Isopropyl-β-D-1-thiogalactopyranoside was from Invitrogen. The QuikChange site-directed mutagenesis kit was from Stratagene, which includes PfuTurbo DNA polymerase and the *Dpn* I restriction enzyme. $4R$-4-$^2$H NADH (NADD) was prepared as described previously (*9*). The concentration of NADD was estimated using an $\varepsilon_{340}$ of 6220 $M^{-1}cm^{-1}$. All chemicals were obtained commercially, were of the highest grade available and were used without further purification.

### 3.2.2 Site-directed mutagenesis.

Template DNA used for site-directed mutagenesis was the plasmid containing the C205S mutation of SDH (*10*), to change K77 and H96 to M and E, respectively. The forward and reverse primers used to generate the K77M mutant enzyme are as follows:

K77$_f$, 5'-CATTATAGGTTTG**ATG**GAAATGCCTGAAACCG-3';

K77$_r$, 5'-CGGTTTCAGGCATTTC**CAT**CAAACCTATAA-3'.

Primers used to generate the H96Q mutant enzyme are as follows:

H96$_f$, CATCCAGTTTGCT**CAG**TGCTACAAAGACCAAGC-3';

H96$_r$, 5'-GCTTGGTCTTTGTAGCA**CTG**AGCAAACTGGATG-3'.

In addition, a double mutant enzyme was prepared using the K77M forward and reverse primers and the H96Q mutant gene to generate K77M/H96Q. The mutated codon is shown in bold. PCR followed by mutagenesis was carried out according to the instructions in the QuikChange site-directed mutagenesis kit as described previously

(*5*).  The XL-1-Blue competent cell strain of *Escherichia coli* was transformed with the plasmids containing mutations.  Plasmids were isolated and purified using the GenElute plasmid mini preparation kit.  Mutations were confirmed by sequencing the entire gene at the Sequencing Core of the Oklahoma Medical Research Foundation, Oklahoma City, OK.

### 3.2.3 Expression and purification.

Escherichia coli BL21 (DE3)-RIL cells were transformed with plasmids containing mutant genes and expression was carried out as reported previously (*3*) with some modifications.  Once cell density reached an $A_{600}$ of 0.3−0.4, induction of protein expression was carried out at 37°C by addition of 0.2 mM IPTG, followed by 3-4 h incubation.  Cells were harvested by centrifugation at 10,000*g* for 10 min, and then sonicated in 100 mM Hepes, pH 7.5, containing 300 mM NaCl, 5 mM imidazole.  Enzymes were purified by Ni-NTA affinity chromatography, with elution using 300 mM imidazole.  The enzymes were >95% pure as judged by SDS-PAGE.  The enzymes were stored at 4˚C in the elution buffer.

### 3.2.4 Enzyme assay.

Initial velocities were measured using a Beckman DU 640 UV-visible spectrophotometer.  All assays were performed at a temperature of 25°C.  Enzyme activity was measured in quartz cuvettes with a path length of 1 cm in the direction of Sacc formation by monitoring the decrease in $A_{340}$ ($\varepsilon_{340}$ = 6220 $M^{-1}$ $cm^{-1}$) as NADH is oxidized.  When NADH had to be maintained at high concentrations the reaction was

monitored at 366 nm ($\varepsilon_{366}$ = 3110 M$^{-1}$ cm$^{-1}$) using a path length of 0.4 cm. Reactions were initiated by addition of enzyme to a reaction mixture with a final volume of 0.5 mL containing 100 mM Hepes, pH 7.0, saturating NADH (0.5 mM) and variable concentrations of α-Kg and Lys.

### 3.2.5 pH Studies.

The pH dependence of $V$, $V/K_{Lys}$, and $V/K_{\alpha\text{-}Kg}$ was measured over the pH range 5–10 with NADH maintained at 0.5 mM, and either α-Kg or Lys maintained at saturation with the other varied. Buffers were maintained at 100 mM concentration in the following pH range; Mes, 5.5 - 7.0; Hepes, 7.0 - 8.0; Taps, 8.0 - 9.0; Ches, 9.0 – 10.0. None of the buffers had any effect on the activity of any of the mutant enzymes. The pH was recorded before and immediately after the reaction; no significant differences were detected. To be certain that the kinetic mechanism of the enzyme did not change with pH and to obtain estimates of $K_m$ values for both substrates at the pH extremes, initial velocity patterns were obtained at extreme pH values (5.5 and 10.0) with α-Kg and Lys concentrations varied, and NADH was maintained at a saturating concentration (0.5 mM).

### 3.2.6 Kinetic Isotope Effects.

Isotope effects were measured for K77M and H96Q mutant enzymes in the pH independent region of their pH-rate profiles (pH 9). Isotope effects on $V_2$ and $V_2/K_{Lys}$ were measured with NADH(D) (10$K_m$) and α-Kg (10$K_m$) maintained at saturation and Lys varied. Solvent deuterium kinetic isotope effects were measured at pH(D) 9, in the

pH independent region of the pH(D)-rate profiles. For rates measured in $D_2O$, substrates ($\alpha$-Kg and Lys) and buffers were first dissolved in a small amount of $D_2O$ and then lyophilized to replace exchangeable protons. The lyophilized powders were then re-dissolved in $D_2O$ to give the desired concentrations, and pD was adjusted using either DCl or NaOD. NADH was dissolved in $D_2O$ directly. Reactions were initiated by adding a small amount of each of the mutant enzymes in $H_2O$; the final concentration of $D_2O$ in the reaction mixture was about 98%. Multiple isotope effects were determined by direct comparison of the initial rates in $H_2O$ and $D_2O$ as for solvent deuterium effects, varying lysine at fixed saturating concentration of NADD and $\alpha$-Kg.

**3.2.7 Viscosity Effects.**

Initial velocities were determined in $H_2O$ at a relative viscosity of 1.24 at pH 8.0 and $25^O$C. Assays contained 9% glycerol (w/v) as the viscosogen, which generates the same relative viscosity as 100% $D_2O$ at 25 °C (*11*). The effect of viscosity on $V$ and $V/K$ ($^{\eta}V$ and $^{\eta}(V/K)$) were determined as the ratio of $V$ and $V/K$ in the absence and presence of glycerol.

**3.2.8 Data Analysis.**

Initial rate data were first analyzed graphically by double reciprocal plots to determine the quality of the data and the proper rate equation for data fitting. Data were then fitted using the appropriate equations (*12*) using the Marquardt-Levenberg algorithm (*13*), supplied with the EnzFitter program from BIOSOFT, Cambridge, U.K.

Kinetic parameters and their corresponding standard errors were estimated using a simple weighing method.

Data from saturation curves for pH-rate profiles and viscosity effects were fitted to eq. 1. Data obtained from the initial velocity patterns were fitted to eq. 2. Data for $V$ and $V/K$ deuterium isotope effects were fitted using eqs. 3 and 4. Equal isotope effects on $V$ and $V/K$ are assumed in eq. 3, while the isotope effects on $V$ and $V/K$ are allowed to be independent in eq. 4. The S.E. of a product or dividend was estimated using eq. 5.

$$v = \frac{V\mathbf{A}}{K_a + \mathbf{A}} \tag{1}$$

$$v = \frac{V\mathbf{AB}}{K_{ia}K_b + K_a\mathbf{B} + K_b\mathbf{A} + \mathbf{AB}} \tag{2}$$

$$v = \frac{V\mathbf{A}}{(K_a + \mathbf{A})(1 + F_i E_v)} \tag{3}$$

$$v = \frac{V\mathbf{A}}{K_a(1 + F_i E_{V/K}) + \mathbf{A}(1 + F_i E_V)} \tag{4}$$

$$\text{S.E.} \ \frac{x}{y} = \frac{x}{y}\left[\left(\frac{\text{S.E.} \ x}{x}\right)^2 + \left(\frac{\text{S.E.} \ y}{y}\right)^2\right]^{1/2} \tag{5}$$

In eqs. 1-4, $v$ and $V$ are initial and maximum velocities, respectively, $\mathbf{A}$, $\mathbf{B}$, are substrate concentrations, $K_a$ and $K_b$, are Michaelis constants for substrates A and B, respectively, and $K_{ia}$ is the dissociation constant for A from the EA complex. In eqs. 3 and 4, $F_i$ is the fraction of label in substrate or solvent, $E_v$, $E_V$ and $E_{V/K}$ are isotope effects minus 1 for the equal isotope effects on $V$ and $V/K$, and the independent isotope

effects on *V* and *V/K*, respectively.  In eq. 5, S.E. *x*, and S.E. *y* are computer generated

standard errors of values for kinetic parameters *x* and *y*.

Data for pH-rate profiles exhibiting a partial change on the acid side were fitted

to eq. 6.

$$\log y = \log\left[Y_L + Y_H\left(\frac{\mathbf{H}}{K_1}\right)\Big/\left(1+\frac{\mathbf{H}}{K_1}\right)\right] \qquad (6)$$

In eq. 6, *y* is the observed value of *V* or *V/K* at any pH, $\mathbf{H}$ is the hydrogen ion

concentration, $K_1$ is the acid dissociation constant of functional group required in a

given protonation state on enzyme or substrate for optimal binding and/or catalysis, and

$Y_L$ and $Y_H$ are pH-independent constant values of *y* at low and high pH, respectively.

### 3.2.9 Crystallization.

The purified SDH C205S mutant enzyme was crystallized based on fine

screening of the conditions described by Andi *et al.* (*8*) for the apo-SDH wild-type

enzyme.  The final reservoir conditions for crystallization of the SDH C205S enzyme

were 100 mM Tris (pH 7.0), 30% (w/v) PEG-MME 2000 at 4 °C using the hanging

drop vapor diffusion method.  The hanging drop contained equal volumes of protein

(14-18 mg/mL in 0.1 M Hepes, pH 7.0) and reservoir solution (2 μl each).  Trays were

cooled and setup at 4 °C.

Diffraction quality crystals could not be obtained by soaking Sacc and NADH

into the apo-C205S SDH crystals.  Likewise, co-crystallization trials with the SDH

C205S enzyme with Sacc and NADH using the original apo-SDH conditions did not produce diffraction quality crystals. New co-crystallization conditions were found based on broad screen crystallization trials carried out using the Mosquito liquid handler from TTP Labtech. A series of optimization screens were developed by varying the concentrations of polyethylene glycol (PEG) 3350 from 10 – 25 % w/v, malonate from 0 – 0.3 M with 0.1 M Bis-Tris Propane (pH 6.5). Trials were set up in 24 well VDX crystallization plates using a Rigaku Automation Alchemist II liquid handler. The final conditions that yielded diffraction quality crystals of the E·Sacc·NADH complex were 22% PEG 3350, 0.3 M malonate and 0.1 M Bis-Tris Propane (pH 6.5) at 4 °C.

### 3.2.10 X-ray data collection.

All data was collected at 100 K and crystals were cryo-protected by transfer through increasing concentrations of glycerol to a final concentration of 15%. All crystals were rapidly cryo-cooled in liquid nitrogen. X-ray data for the C205S apo-enzyme and E·Sacc·NADH complex crystals were collected at 100 K using CuKα (λ = 1.5418 Å) radiation on a Rigaku RU3HR rotating anode generator and RAXIS IV[++] image plate detector. Diffraction data were integrated using Mosflm, scaled and merged using SCALA and structure factors were calculated using TRUNCATE as found in the CCP4 program suite (*14*). Data collection statistics are given in Table 1.

### 3.2.11 Molecular replacement.

Initial phasing for both structures was done by molecular replacement using PHASER (*15*) The native apo-enzyme structure (PDB ID: 2Q99) was used as the initial

search model for the apo-C205S structure (*7*).  The resultant C205S structure was used as a search model in molecular replacement to solve the E·Sacc·NADH structure. There is a significant conformational change that occurs upon Sacc/NADH binding, and as a result the apo-enzyme model had to be edited by separating it into two halves at residues Phe135 and Pro326.  Refinement was conducted using REFMAC (*16*), with a round of simulated annealing done initially in PHENIX (*17*) to reduce model bias. Model visualization, rebuilding and the fitting of Sacc and NADH were done using COOT (*18*).  Water molecules were added toward the end of refinement using the Add Waters function in COOT and visually inspected after initial placement.   A glycerol molecule was also found in the ligand bound structure.  Refinement statistics are given in Table 1.

### 3.2.12 Molecular graphics.

Structure figures were prepared using *PyMOL*™ version 0.99 (*19*).

### 3.3 RESULTS

### 3.3.1 Cell Growth, Expression and Purification.

Expression of the K77M/C205S, H96Q/C205S and K77M/H96Q/C205S mutant enzymes was similar to that of the WT SDH.  All enzymes eluted from the Ni-NTA column with buffer containing 300 mM imidazole at pH 8.  Purity of the proteins was assessed by SDS-PAGE, and all of the mutant proteins were estimated to be >95% pure. The His-tagged mutant enzymes maintained stability and remained active for months when stored at 4 °C in 100 mM Hepes, 300 mM KCl, and 300 mM Imidazole at pH 8.

### 3.3.2 Structural studies.

The X-ray structure of the pseudo-WT C205S apo-enzyme (PDB ID code: 3UGK) was solved from crystals grown as described in **MATERIALS AND METHODS**. Diffraction data indicated a space group of $P2_12_12_1$ and the highest resolution shell was 2.01 Å, Table 1. The structure was solved by molecular replacement and initially built from the SDH model (PDB ID 2Q99) published by Berghuis and colleagues (7). The structure of the C205S apo-enzyme is virtually identical to that of the WT enzyme. A superimposition of the two structures gives an rmsd of 0.31 Å (data not shown).

Attempts to crystallize a ternary complex of the WT enzyme were unsuccessful, likely as a result of very weak binding of the cofactor to enzyme with an oxidized disulfide (5). A ternary complex structure was obtained by co-crystallization of the C205S enzyme with Sacc and NADH (PDB ID code: 3UH1). Diffraction data indicated a space group of $P4_3$ and the highest resolution shell was 2.17 Å, Table 1. The structure was solved by molecular replacement using the structure of the apo-C205S enzyme as discussed in **MATERIALS AND METHODS**. A superimposition of the E•Sacc•NADH ternary complex structure with the apo-C205S structure indicated significant changes that result in a closure of the active site, Figure 3.1A. In the ternary complex, there is a slight rotation and rigid body movement of almost 9 Å of domain I towards domain II that effectively closes the cleft region as shown in the CPK models in Figure 3.1B (apo) versus Figure 3.1C (ternary complex). The net displacement of K99 in the C97-K103 loop region is 8.8 Å in the ternary complex relative to the apo-enzyme.

Figure 3.2A shows a stereo view of an $F_o$-$F_c$ difference electron density map of the active site region to illustrate the positions of the bound NADH and Sacc molecules. Figure 3.2B is a mono view of the active site with hydrogen-bond and ionic interactions shown for protein side chains in contact with the ligands. The distances between enzyme side chain atoms and reactants are given in Table 4. The Nε atom of K77 and the Nε2 atom of H96 form hydrogen bonds with the Nε atom of Sacc. Other important contacts are made through R18, E122. Also shown is an ionic interaction between D227 and NADH.
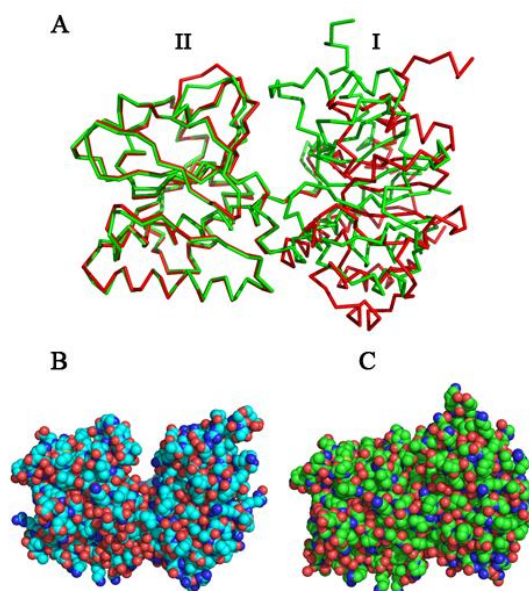


Figure 3.1 Overall Structures of the C205S Apo-enzyme and E·NADH·Saccharopine Ternary Complex. A. Superimposition of the apo-enzyme (red) and ternary complex (green) structures. Note the change in the position of the loop and helix in domain I (right) to close the active site. B. CPK model of the apo-enzyme with the active site entrance at the top (same orientation as in A). C. CPK model of the ternary complex structure in the same orientation as shown in B.

There are several hydrogen-bond interactions between the cofactor NADH and the substrate saccharopine.
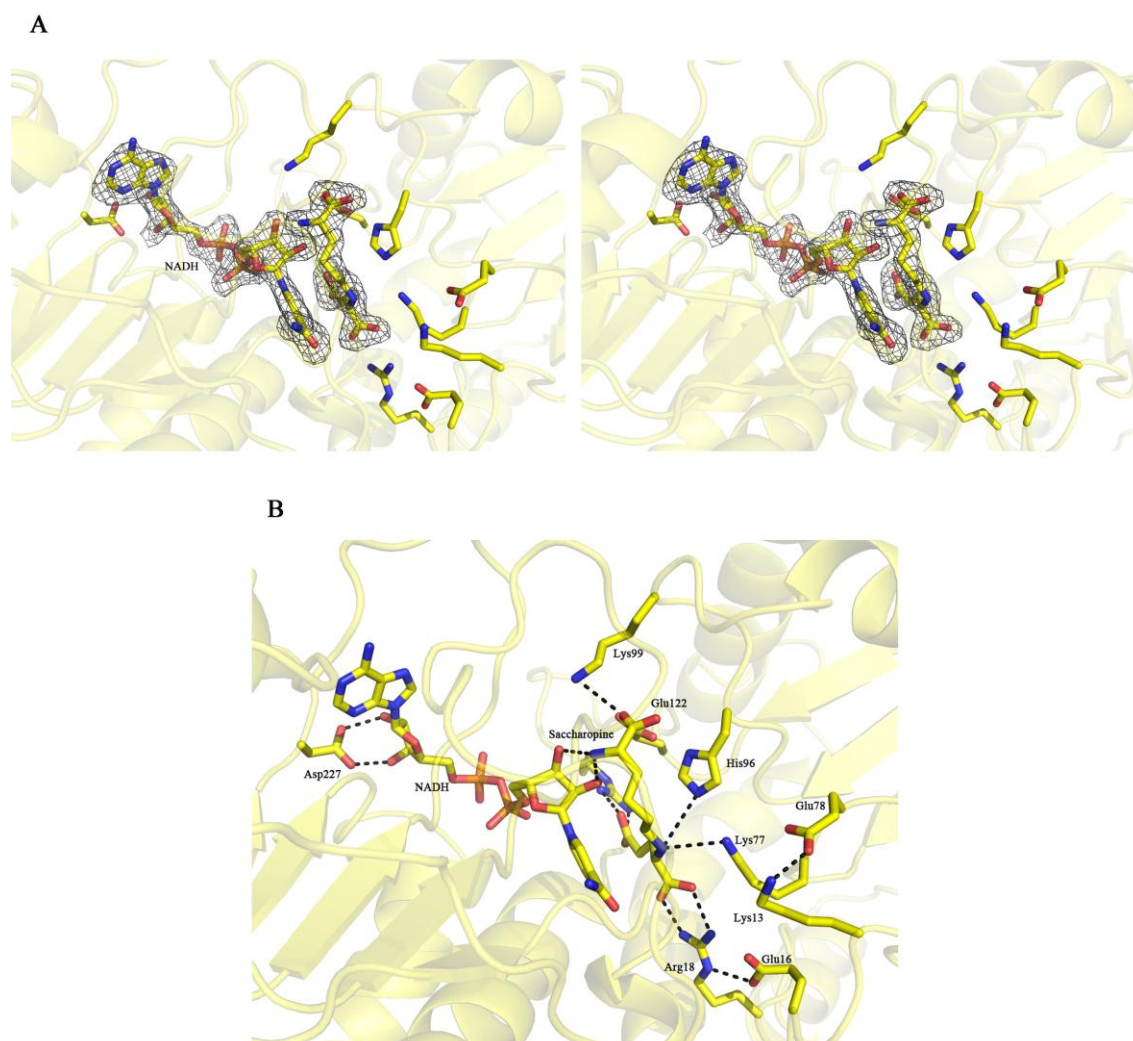


Figure 3.2 Close-up view of the Active Site of SDH in the Ternary Complex with NADH and Saccharopine. A. Stereoview of a $F_o$-$F_c$ difference electron density map contoured at $3\sigma$ with ligand atoms omitted. B. Mono view of the active site with NADH and Sacc bound. Residues within hydrogen bond distance (shown as a dashed line) to NADH and Sacc are shown. Distances represented by the dashes are given in Table 3.2.

We also attempted to co-crystallize SDH with NADH and lysine using the same screening conditions as for the E•Sacc•NADH ternary complex crystals. However, we

only observed density for NADH in the solved structure (PDB ID: 3UHA) and the enzyme was observed to be in the open conformation (data not shown).

### 3.3.3 Initial velocity studies.

Initial velocities were measured in the direction of Sacc formation for the K77M, H96Q and K77M/H96Q mutant enzymes. Replacing K77 with M resulted in a 145-fold decrease in $V_2/\mathbf{E_t}$ and $>10^4$-, and $>10^3$-fold decreases in $V_2/K_{\alpha\text{-}Kg}\mathbf{E_t}$ and $V_2/K_{Lys}\mathbf{E_t}$, respectively. This results in 28- and 90-fold increases in $K_{Lys}$ and $K_{\alpha\text{-}Kg}$, respectively. Replacing H96 with Q resulted in a 28-fold decrease in $V_2/\mathbf{E_t}$ and $>10^3$-fold decreases in $V_2/K_{\alpha\text{-}Kg}\mathbf{E_t}$ and $V_2/K_{Lys}\mathbf{E_t}$, respectively. The $K_{\alpha\text{-}Kg}$ and $K_{Lys}$ increased 80-, and 300-fold, respectively. The K77M/H96Q double mutant gave the largest changes in kinetic parameters, as expected, with 660-, $>10^6$-, and $\sim10^5$-fold decreases in $V_2/\mathbf{E_t}$, $V_2/K_{\alpha\text{-}Kg}\mathbf{E_t}$, and $V_2/K_{Lys}\mathbf{E_t}$, respectively; $K_{\alpha\text{-}Kg}$ and $K_{Lys}$ increased $>10^3$- and $10^2$-fold, respectively. Kinetic parameters are summarized in Table 3.3, and compared to those obtained for the pseudo-WT, C205S (*10*).

### 3.3.4 pH dependence of kinetic parameters.

The pH dependence of kinetic parameters provides information on the optimal protonation state of functional groups on enzyme and/or substrate for binding and/or catalysis. Studies were carried out with K77M and H96Q mutant enzymes in the direction of saccharopine formation, at 25 °C; the rate obtained with the double mutant enzyme were too low to allow data to be collected as a function of pH. Both mutant enzymes were active and stable over the pH range 5–10, and initial rate studies at pH

Table 3.1. Data Collection Statistics

| | C205S apo-enzyme | Sacc/NADH bound |
|---|---|---|
| space group | $P2_12_12_1$ | $P4_3$ |
| unit cell dimensions (Å) | 64.95, 75.23, 75.31 101.85 | 68.88, 68.88, |
| wavelength (Å) | 1.5418 | 1.5418 |
| temperature (K) | 100 | 100 |
| resolution (Å) | 41.71-2.01 | 35.2-2.17 |
| solvent content (%) | 43.9 | 57.3 |
| no. of observations | 98649 | 89656 |
| no. of unique reflections | 24396 | 25006 |
| completeness (%) | 97.1(81.8) [a] | 99.8(99.8) |
| average multiplicity | 4.0(2.6) | 3.6(3.4) |
| $<I/\sigma I>$ | 15.8(3.0) | 14.5(3.4) |
| $R_{merge}$ [b] | 0.052(0.295) | 0.063(0.300) |

Refinement Statistics

| | | |
|---|---|---|
| resolution range (Å) | 41.71-2.01 | 35.2-2.17 |
| no. of protein atoms | 2921 | 2884 |
| no. of solvent molecules | 152 | 134 |
| no. of ligand molecules | 0 | 3 |
| avg. B factor (all atoms) | 25.01 | 24.37 |
| $R_{cryst}$ [c] | 0.197 | 0.178 |
| $R_{free}$ [d] | 0.273 | 0.228 |
| rms deviation [e] | | |
|     bond length (Å) | 0.022 | 0.022 |
|     bond angle (°) | 1.74 | 1.89 |
| Ramachandran plot [f] | | |
|     favored | 97.8 | 97.5 |
|     allowed | 2.2 | 2.5 |
|     outliers | 0.00 | 0.00 |
|     disallowed | 0.00 | 0.00 |

[a] The data in parentheses refer to the highest resolution shell.
[b] $R_{merge} = \Sigma_h\Sigma_i |I_{hi} - <I_h>|/\Sigma_h\Sigma_i|<I_h>|$. $I_{hi}$ is the $i$th used observation for unique hkl h, and $<I_h>$ is the mean intensity for unique hkl h.
[c] $R_{cryst} = \Sigma||F_o|- |F_c||/\Sigma|F_o|$ where $F_o$ and $F_c$ are the observed and calculated structure factors, respectively.
[d] $R_{free}$ was calculated using 5% of randomly selected diffraction data which were excluded from the refinement.
[e] Ideal values taken from ref. *16*
[f] calculated using *MolProbity* (*20*).

5.5 and 10 suggest the kinetic mechanism did not change (data not shown). For the K77M mutant enzyme, $V_2/K_{Lys}\mathbf{E_t}$ is pH independent, while $V_2/\mathbf{E_t}$ exhibits a partial change on the acid side giving a p$K_a$ of about 7.4. pH independent values of $V_2/\mathbf{E_t}$ are $0.20 \pm 0.03$ s$^{-1}$ at low pH and $1.4 \pm 0.1$ s$^{-1}$ at high pH.

Table 3.2. Distances Between Enzyme Side Chains and Reactants

| Side Chain – Reactant | Distance (Å) |
|---|---|
| R18_NH1 – Sacc_O1 | 2.8 |
| R18_NH2 – Sacc_O2 | 2.8 |
| R131_NH1 – Sacc_O3 | 2.8 |
| R131_NH1 – Sacc_O4 | 2.6 |
| K77_N$^\varepsilon$ – Sacc_N$^\varepsilon$ | 3.4 |
| H96_N$^{\varepsilon 2}$ – Sacc_N$^\varepsilon$ | 3.5 |
| K13_N$^\varepsilon$ – Q78_O$^\gamma$ | 2.6 |
| D227_O1 – NAD_O2 | 2.6 |
| D227_O1 – NAD_O3 | 2.8 |
| [a]NAD_4C – Sacc_C8 | 3.6 |

[a]Numbering for Sacc is from C1 of the lysine
half to C11, the γ-carboxylate of the glutamate half.

The average pH independent value of $V_2/K_{Lys}\mathbf{E_t}$ is $0.8 \pm 0.5$. In the case of H96Q, $V_2/\mathbf{E_t}$ exhibits a decrease at low pH with a slope <1, giving an app p$K_a$ of about 6.7, while $V_2/K_{Lys}\mathbf{E_t}$ exhibits a partial change with a p$K_a$ of about 9, decreasing from a constant value at high pH to a lower constant value at low pH, Figure 3.3. The pH

independent value of $V_2/\mathbf{E_t}$ is $4.8 \pm 0.3$ s$^{-1}$, while values of $450 \pm 280$ and $4.5 \pm 2.9$ M$^{-1}$s$^{-1}$ are obtained for $V_2/K_{Lys}\mathbf{E_t}$ at high and low pH, respectively.

Table 3.3: Summary of the Kinetic Parameters.

| | C205S | K77M[a] | H96Q[a] | K77M/H96Q[a] |
|---|---|---|---|---|
| $V_2/\mathbf{E_t}$ (s$^{-1}$) | 106 | $0.73 \pm 0.02$ | $3.83 \pm 0.03$ | $0.16 \pm 0.02$ |
| $V_2/K_{\alpha\text{-}Kg}\mathbf{E_t}$ (M$^{-1}$s$^{-1}$) | $9.7 \times 10^5$ | $73 \pm 6$ | $435 \pm 116$ | $0.50 \pm 0.05$ |
| $V_2/K_{Lys}\mathbf{E_t}$ (M$^{-1}$s$^{-1}$) | $1.2 \times 10^5$ | $29 \pm 2$ | $14 \pm 3$ | $1.7 \pm 0.8$ |
| $K_{\alpha\text{-}Kg}$ (mM) | 0.11 | $10.0 \pm 0.8$ | $9 \pm 2$ | $267 \pm 60$ |
| $K_{Lys}$ (mM) | 0.89 | $25 \pm 2$ | $267 \pm 60$ | $96 \pm 9$ |

[a]Mutations prepared in the C205S background (*10*).

### 3.3.5 Isotope effects.

Isotope effects were measured for the K77M mutant enzyme at pH 9, the high pH independent region of the pH-rate profiles. Values of 1.8 and 2.0 were obtained for $^D V_2$ and $^D(V_2/K_{Lys})$, and both are greater than the value of 1.3 reported for the pseudo-WT enzyme (C205S). A small normal $^{D2O}V$ is observed, but $^{D2O}(V/K_{Lys})$ is inverse. Repeating the solvent effect with NADD gave only slight changes. On the other hand, a repeat of the primary deuterium effect in D$_2$O gives a decrease in the isotope effect on $V$ from 1.8 to 1.4, but no change in the isotope effect on $V_2/K_{Lys}$.
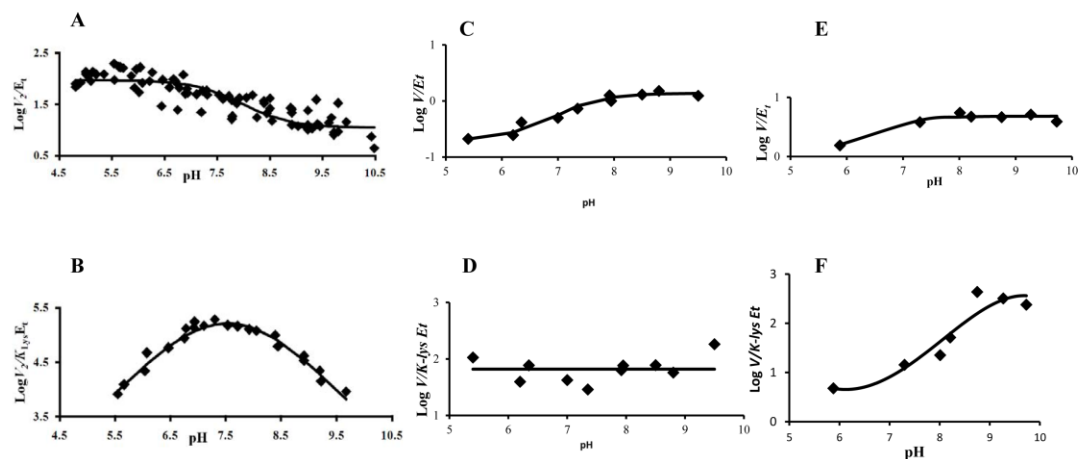
Figure 3.3: pH Dependence of Kinetic Parameters for SDH WTSDH (C205S), K77M/C205S and H96Q/C205S in the Direction of Saccharopine Formation. Data for WT SDH (C205S)(A and B) are from ref. (*4*), and are reproduced with permission, while (C and D) are data for the K77M/C205S, (E and F) are for H96Q/C205S mutant enzymes. Units for $V/E_t$ and $V/K\mathbf{E_t}$ are s$^{-1}$ and M$^{-1}$ s$^{-1}$, respectively. Points are the experimentally determined values. The curves are theoretical and based on fits to eq. 6 for panel C, E and F.


Table 3.4: Summary of the Kinetic Isotope Effects[a]

|  | C205S[b] | K77M[c, d] | H96Q[c, d] |
|---|---|---|---|
| $^{D}V$ | $1.3 \pm 0.2$ | $1.81 \pm 0.02$ | $1.17 \pm 0.40$ |
| $^{D}(V/K_{Lys})$ | $1.3 \pm 0.2$ | $2.03 \pm 0.04$ | $1.17 \pm 0.40$ |
| $^{D2O}V$ | $1.5 \pm 0.1$ | $1.45 \pm 0.01$ | $2.43 \pm 0.02$ |
| $^{D2O}(V/K_{Lys})$ | $1.5 \pm 0.1$ | $0.77 \pm 0.05$ | $2.43 \pm 0.02$ |
| $^{D2O}(V)_D$ | $1.5 \pm 0.1$ | $1.32 \pm 0.02$ | $2.24 \pm 0.05$ |
| $^{D2O}(V/K_{Lys})_D$ | $1.5 \pm 0.1$ | $0.62 \pm 0.07$ | $2.24 \pm 0.05$ |
| $^{D}(V)_{D2O}$ | ND | $1.42 \pm 0.01$ | $1.06 \pm 0.11$ |
| $^{D}(V/K_{Lys})_{D2O}$ | ND | $2.03 \pm 0.03$ | $1.06 \pm 0.11$ |

[a]Isotope Effects were measured at pH 9.
[b]From reference (*10*).
[c]Errors are standard error of the mean.
[d]Data for K77M were fitted to eq. 4, while data for H96Q were fitted to eq. 3.

For H96Q, the primary deuterium isotope effect is within error unity, whether measured in $H_2O$ or $D_2O$. The solvent deuterium kinetic isotope effect is 2.4 and there is no significant change when it is measured with NADD. Data are summarized in Table 3.4, and compared to those obtained for C205S mutant enzyme (*10*).

### 3.3.6 Viscosity effects.

In order to determine whether the SKIEs reflect the increased viscosity in $D_2O$, the initial rate was measured in the absence and presence of 9% glycerol, which gives a relative viscosity of 1.24, the same as 100% $D_2O$ (*21*). There was no effect of viscosity on $V$ and $V/K$ for the H96Q mutant enzyme; a value of $1.02 \pm 0.01$. For K77M, $^{\eta}V$ and $^{\eta}(V/K)$ were $1.18 \pm 0.03$ and $0.61 \pm 0.06$.

### 3.4 DISCUSSION

### 3.4.1 Structures.

Previous structures of apo-wild type SDH (*7*) and substrate analogue bound structures (*8*) showed an open or partially closed cleft between domains I and II. The E•NADH•Sacc ternary complex structure described here reveals a closed conformation in which reactants are tightly bound to the enzyme via hydrogen bond and ionic interactions and poised for acid-base catalysis. A slight rotation and 8.8 Å shift of domain I towards domain II is responsible for closing the active site.

On the basis of the ternary E•NADH•Sacc complex of SDH, there are a number of ionizable residues in the active site as discussed in the Introduction. Residues include R18, R131, K99, K77, K13, E122, E78, E16, and H96. A multiple sequence

alignment of the SDH from *Saccharomyces cerevisiae*, *Candida albicans*, *Aspergillus fumigatus*, *Cryptococcus neoformans*, *Magnaporthe grisea*, *Yarrowia lipolytica* and *Schizosaccharomyces pombe* indicated that all of these active site residues are conserved in these fungal species (data not shown), consistent with their importance in the mechanism.

As shown in Figure 3.2A, K77 and H96 are within hydrogen-bond distance (3.4 Å and 3.5 Å, respectively) to the secondary amine of saccharopine, and could serve as acid-base catalysts in the dehydrogenase reaction. The proposed mechanism suggests that one of the residues accepts a proton from the secondary amine in the hydride transfer step, while the second activates water for hydrolysis of the resulting imine. The lysine and imidazole side chains of K77 and H96 are in proper position to carry out these functions. Data presented in Results above are in agreement with this hypothesis and further discussed below.

### 3.4.2 Kinetic Parameters.

All three mutant enzymes, K77M, H96Q, and K77M/H96Q, were characterized in the direction of Sacc formation. Initial rates measured as a function of reactant concentration suggested the kinetic mechanism did not change compared to that proposed for the C205S pseudo-WT enzyme, i. e., binding of NADH first, followed by random addition of α-Kg or Lys (data not shown).

Mutating K77 to M decreases the positive charge in the site, while changing H96 to Q likely does not change the overall charge assuming the imidazole side chain is neutral at neutral pH. Mutation of K77 gives a 145-fold decrease in $V/E_t$, the largest

thus far observed for any site-directed mutation in SDH (*5, 6*).  The two order of magnitude decrease in the turnover number and 3 to 4 order of magnitude decreases in the second order rate constants are consistent with the K77 side chain playing a direct role as an acid-base catalyst in the SDH reaction.  Substitution of a glutamine for H96 leads to a 28-fold decrease in the turnover number of SDH and greater than 3 order of magnitude decreases in second order rate constants.  Although the decreases are not as great as those observed for the K77M mutant enzyme, the data are suggestive of a catalytic role for H96.  In agreement, the double mutant enzyme, K77M/H96Q, gives a nearly 3 order of magnitude decrease in $V_2/\mathbf{E_t}$ and 5 to 6 order of magnitude decreases in the second order rate constants.  These data, together with the position of the two residues in the site are consistent with their role as acid-base catalysts in the reaction.

### 3.4.3 Isotope effects.

Primary and solvent isotope effects are sensitive tools to investigate the slow step / rate determining steps in the reaction.  The primary deuterium kinetic isotope effect (PKIE) reflects the hydride transfer step (see Scheme 3.1) (*4*).  A solvent kinetic isotope effect (SKIE) is observed when protons are in flight in transition states that contribute to rate limitation.  In the WT and C205S enzymes, the SKIE was derived from protons in flight in the hydride transfer and imine hydrolysis steps, corroborated by a concave downward proton inventory (*4*).

The maximum rate for the C205S mutant enzyme is slightly pH dependent decreasing from a constant value at high pH to another constant value at low pH.  The isotope effects for the C205S enzyme reported in Table 4 were measured at pH 9 (*10*).

The effects obtained at pH 5.6 are about 2, similar to the value obtained for the K77M mutant at pH 9. The data suggest hydride transfer is slower for the K77M mutant enzyme. The slightly lower isotope effect on $V$ suggests release of NAD or isomerization of the E-NADH complex contributed to rate limitation. The SKIE on $V$ is similar to that obtained for C205S, but the effect on $V/K_{Lys}$ is unexpectedly inverse, and will be discussed further below. A repeat of the PKIE in $D_2O$ gives a value of $^D(V/K_{Lys})$ equal to that obtained in $H_2O$ suggesting that the hydride transfer step is rate-determining at pH 9, and the observed solvent deuterium isotope effect reflects changes that occur or have occurred once the transition state for hydride transfer is attained. The PKIE on $V$ in $D_2O$ decreases slightly consistent with a step in addition to hydride transfer contributing to rate limitation; the data are consistent with the suggestion that release of NAD or isomerization of the E-NADH complex contributed to rate limitation. A repeat of the SKIE with NADD fixed gives values that are either identical to or decreased slightly compared to the value in $H_2O$. Taken together, the data indicate hydride transfer as the step that is largely rate-determining at limiting Lys ($V/K_{Lys}$), and is a major contributor to rate limitation at saturating reactant concentrations. Thus, as suggested on the basis of structural studies and pH-rate profiles (see below) K77 is, in all likelihood, the base that donates a proton to the secondary amine of Sacc in the hydride transfer step as the imine is reduced.

Inverse SKIEs are expected for ionization of a thiol, hydrolysis of metal-$H_2O$, a medium effect (*21*), or an effect derived from the increase in viscosity generated by $D_2O$. Although there is a thiol in the vicinity of the dinucleotide-binding site, it is unlikely this ionization contributes to the chemistry in the site. If anything it would be

expected to decrease the affinity of enzyme for NADH, and this is not observed. There is no metal ion involved in the SDH reaction. It is thus possible that either a medium effect or an effect of viscosity is responsible for the observed inverse SKIE, and may reflect the conformational change to close the site to form the productive Michaelis complex upon binding of Lys. The viscosity effect is identical to the measured SKIE, consistent with a preference for the closed conformation because of the higher viscosity of $D_2O$.

The solvent isotope effects, listed in Table 3.4, are nearly identical to the viscosity effects obtained for K77M. Data strongly suggest the inverse isotope effect on $V/K$ is a consequence of the change in solvent viscosity in $D_2O$, i.e., the solvent deuterium isotope effect on $V/K$ is 1.0, while a slight normal isotope effect of about 1.23 ± 0.02 (1.45/1.18) is observed on $V$. Effects near unity suggest proton transfer steps do not contribute or contribute to a very small extent to the rate limitation in the reaction with Lys limiting. The reason for the increased rate in the presence of a viscosogen is not known at this point but likely results from stabilization of an enzyme conformation along the reaction pathway as suggested above. At saturating reactant concentrations, there is a slight contribution from diffusion (viscosity effect) and there is at least one proton in flight in a step that contributes to rate limitation. As suggested above, the step reflects either release of NAD or isomerization of the E·NADH complex, and the presence of a contribution from diffusion suggests that it is likely release of NAD.

Observation of an inverse viscosity effect is not unique to SDH. Similar observations have been made for the *Ascaris suum* NAD malic enzyme (*21*), and the homoisocitrate dehydrogenase from *S. cerevisiae* (*22*) using 9% glycerol as the

viscosogen. Inverse solvent deuterium isotope effects and viscosity effects of about 0.8 and 0.5 were estimated on $V$ and $V/K_{malate}$ for the malic enzyme. These results, with a larger inverse effect on $V/K$ than $V$, are qualitatively identical to those obtained in these studies. Data were interpreted in terms of stabilizing the closed form of the enzyme at higher viscosity. The increase in rate is thus a result of an increase in the concentration of the productive Michaelis complex. Isocitrate, a slow substrate for homoisocitrate dehydrogenase, also gave similar inverse solvent isotope and viscosity effects of 0.8 and 0.6 on $V$ and $V/K_{Ic}$. Data were again interpreted in terms of stabilizing an enzyme form along the reaction pathway.

Isotope effects measured for H96Q are very straightforward and easy to interpret. A primary deuterium effect near 1 indicates the hydride transfer step does not contribute to rate limitation. The SKIE is about 2.3 on $V$ and $V/K_{Lys}$, significantly greater than the value obtained for C205S. Data are consistent with the proposed role of H96 in formation of the imine prior to its reduction in the hydride transfer step.

Inverse SKIEs are expected for ionization of a thiol, hydrolysis of metal-$H_2O$, a medium effect (21), or an effect derived from the increase in viscosity generated by $D_2O$. Although there is a thiol in the vicinity of the dinucleotide-binding site, it is unlikely this ionization contributes to the chemistry in the site. If anything it would be expected to decrease the affinity of enzyme for NADH, and this is not observed. There is no metal ion involved in the SDH reaction. It is thus possible that either a medium effect or an effect of viscosity is responsible for the observed inverse SKIE, and may reflect the conformational change to close the site to form the productive Michaelis complex upon binding of Lys. The viscosity effect is identical to the measured SKIE,

consistent with a preference for the closed conformation because of the higher viscosity of $D_2O$.

The solvent isotope effects, listed in Table 2, are nearly identical to the viscosity effects obtained for K77M. Data strongly suggest the inverse isotope effect on $V/K$ is a consequence of the change in solvent viscosity in $D_2O$, i.e., the solvent deuterium isotope effect on $V/K$ is 1.0, while a slight normal isotope effect of about $1.23 \pm 0.02$ (1.45/1.18) is observed on $V$. Effects near unity suggest proton transfer steps do not contribute or contribute to a very small extent to the rate limitation in the reaction with Lys limiting. The reason for the increased rate in the presence of a viscosogen is not known at this point but likely results from stabilization of an enzyme conformation along the reaction pathway as suggested above. At saturating reactant concentrations, there is a slight contribution from diffusion (viscosity effect) and there is at least one proton in flight in a step that contributes to rate limitation. As suggested above, the step reflects either release of NAD or isomerization of the E·NADH complex, and the presence of a contribution from diffusion suggests that it is likely release of NAD.

Observation of an inverse viscosity effect is not unique to SDH. Similar observations have been made for the *Ascaris suum* NAD malic enzyme (*21*), and the homoisocitrate dehydrogenase from *S. cerevisiae* (*22*) using 9% glycerol as the viscosogen. Inverse solvent deuterium isotope effects and viscosity effects of about 0.8 and 0.5 were estimated on $V$ and $V/K_{malate}$ for the malic enzyme. These results, with a larger inverse effect on $V/K$ than $V$, are qualitatively identical to those obtained in these studies. Data were interpreted in terms of stabilizing the closed form of the enzyme at higher viscosity. The increase in rate is thus a result of an increase in the concentration

of the productive Michaelis complex. Isocitrate, a slow substrate for homoisocitrate dehydrogenase, also gave similar inverse solvent isotope and viscosity effects of 0.8 and 0.6 on $V$ and $V/K_{Ic}$. Data were again interpreted in terms of stabilizing an enzyme form along the reaction pathway.

Isotope effects measured for H96Q are very straightforward and easy to interpret. A primary deuterium effect near 1 indicates the hydride transfer step does not contribute to rate limitation. The SKIE is about 2.3 on $V$ and $V/K_{Lys}$, significantly greater than the value obtained for C205S. Data are consistent with the proposed role of H96 in formation of the imine prior to its reduction in the hydride transfer step.

### 3.4.4 pH dependence of kinetic parameters.

To further probe the role of K77 and H96, the pH dependence of kinetic parameters was measured. These studies allow a determination of the optimal protonation state of the functional groups on the enzyme and/or substrate involved in either binding and/or catalysis. On the basis of the above discussion, the proposed general base in the direction of Sacc formation is K77, which must accept a proton from the ε-amine of Lys as it attacks the α-carbonyl of α-Kg to form the imine. Histidine 96 is proposed to serve a role as a general acid in the reaction, first protonating the carbonyl oxygen to form the protonated carbinolamine, accepting a proton from the protonated carbinolamine to generate the neutral carbinolamine, and eventually protonating the leaving hydroxide to give water (III in Scheme 3.1).

Data for the C205S mutant enzyme (*10*) are shown in Fig. 1 as a reference for interpreting the pH-rate profiles for K77M and H96Q. $V_2$ decreases from a constant

value at low pH to a lower constant value at high pH. The $pK_a$ estimated for the change

is 7.5 and the ratio of the constant values is about 9. The pH dependence was attributed

to a conformational change in enzyme, with the low pH conformation the more active

of the two. (This aspect will be discussed further below.) The *V/K* for Lys exhibits a

bell-shaped pH-rate profile with $pK_a$ values of 7 and 8.1 attributed to the general base

and general acid in the SDH reaction.

Data for the K77M mutant enzyme differ considerably. The $V_2$ pH-rate profile

exhibits a partial change, but requires the group unprotonated, opposite the situation for

C205S. It is clear that the presence of the K77 side chain influences the $pK_a$ and

perhaps the group responsible for pH-dependent conformational change. On the basis

of the isotope effects presented in **RESULTS** and discussed above, the hydride transfer

step is slow for the K77M mutant enzyme, and we propose that K77 donates a proton as

the imine is reduced to the secondary amine in Sacc. The loss of the side chain of K77

results in a significant decrease in the rate at low pH, which increases with increasing

pH giving a $pK_a$ of about 7.5. The data obtained in these studies suggest an

interpretation that is alternative to a pH dependent conformational change. Although

chemistry contributes to rate limitation for the pseudo-WT enzyme, the conformational

changes required to close the site prior to catalysis and open it prior to product release

also make significant contributions (*5, 8*). The pH dependence observed in the $V_2$ pH-

rate profile may reflect two pathways that differ depending on the protonation state of

the ε-amino groups of the Lys substrate and the side chain of K77. For the C205S

mutant enzyme, the optimum protonation state exists when the substrate ε-amine is

protonated and the side chain of K77 is unprotonated. The proximity of the side chain

of Lys and K77, results in a decrease in the $pK_a$ of both ε-amino groups facilitating proton transfer from one to the other. As the pH increases, the proton shared between the two side chains is lost; the global $pK_a$ is about 7.5 for the Lys-K77 pair on the basis of the observed $pK_a$ values reported in Table 2. Once unprotonated, the rate decreases by 9-fold, likely as a result of a change in orientation of the Lys side chain. In the K77M mutant enzyme the protonation state of the substrate Lys ε-amine may also contribute to rate limitation at saturating reactants. Once bound the Lys ε-amine must be unprotonated to act as a nucleophile as it attacks the α-carbonyl of α-Kg to form the imine. Other active site side chains, e.g., E78, E16, or K13, must abstract the Lys ε-amine proton, perhaps via the intermediacy of a water molecule. As the pH increases the ε-amine of Lys becomes unprotonated (the $pK_a$ is around 7.5 for the bound substrate), can serve as a nucleophile, and the rate increases by about 10-fold.

The dominant forms of enzyme and substrate present when $V/K_{Lys}$ is measured is the E·NADH·α-Kg complex and free Lys. The $V/K_{Lys}$ is pH independent, while a bell-shaped pH-rate profile was obtained for C205S with $pK_a$ values of about 7 and 8. Since free Lys is dominant, the observed $pK_a$s are on enzyme; the $pK_a$ of the α- and ε-amino groups of Lys are 9.5 and 10.5, respectively. One of the $pK_a$ values likely reflects the K77 side chain, and intrinsic values are observed.[2] It is likely the group with a $pK$ of about 7 that reflects the K77 side chain, consistent with the discussion of the $pK_a$ of 7.5 in the $V_2/E_t$ pH-rate profile above. The $pK_a$ of the H96 side chain is thus about 8 and in the absence of the K77 side chain is perturbed to a pH higher than 9.5, perhaps resulting

from the influence of E78, which is in the vicinity and no longer neutralized by K77. The absence of the $pK_a$ of about 7 is consistent with its attribution to K77.

In the case of the H96Q mutant enzyme, interpretation will begin with the $V/K_{Lys}$ pH-rate profile. Note that the profile exhibits a partial change, decreasing from a constant value above pH 9 to a lower constant value below pH 6; the ratio of the constant values is about 100. The observed $pK_a$ of about 9 reflects the side chain of K77, while the $pK_a$ observed at high pH in C205S is absent consistent with assignment of H96 as this group. The loss of the H96 side chain resulted in an increase in the $pK_a$ of K77 from about 7.5 to 9, suggesting an influence of the imidazole side chain on the proton affinity of the K77 side chain. The H96 side chain must be protonated for optimum reaction in the direction of Sacc formation, and the proximity of the positive charge on the imidazole will certainly result in a decrease in the $pK_a$ of the ε-amino groups of K77. The finite rate obtained at low pH suggests K77 is important for catalysis, but is not absolutely essential. This is in agreement with the data obtained for the $V_2/E_t$ pH-rate profiles for C205S, K77M and H96Q (see below).

The $V_2/E_t$ pH-rate profile of H96 is similar to that of K77M at face value. However, since the K77 side chain is absent the $pK_a$ reflected is that of the bound substrate, Lys. Thus, the bound Lys has a $pK_a$ of about 7. As the pH increases and the ε-amino of bound Lys becomes neutral, the rate increases since the amine can now act as a nucleophile in the attack of the α-carbonyl of α-Kg to form the imine.

**3.4.5 Conclusions.**

A structure of a ternary complex between the C205S pseudo-WT enzyme, NADH, and Sacc provided a closed form of the enzyme and a more accurate description of the interactions between enzyme side chains and reactant functional groups compared to the semi-empirical model published previously (*6*). Importantly, the distance between C4 of the nicotinamide ring to C8 of Sacc is 3.6 Å as shown in Figure 3.2, a reasonable hydride transfer distance, compared to a distance of >4.5 Å estimated from the semi-empirical model, which was constructed from open forms of the enzyme. The side chains of H96 and K77 now appear properly positioned to act as acid-base catalysts.

Mutation of K77 to M results in 145-fold decrease in $V/\mathbf{E_t}$ and greater than three order of magnitude increase in the second order rate constants. Together with the large primary deuterium isotope effect (2.0) and small solvent deuterium isotope effect (1.45), data suggest rate limiting hydride transfer, consistent with the proposed general acid role of K77 in protonating the imine nitrogen concomitant with hydride transfer. In agreement with this proposal, $V_2/K_{Lys}\mathbf{E_t}$ is pH independent. The H96Q mutation, results in about a 28-fold decrease in $V_2/\mathbf{E_t}$ and $>10^3$-fold decreases in the second order rate constant. A primary deuterium isotope effect near unity and a large solvent deuterium isotope effect (2.4) is consistent with the proposed role of H96 in protonating the leaving hydroxyl as the imine is formed. Elimination of H96 results in a pH-rate profile for $V_2/K_{Lys}\mathbf{E_t}$ that exhibits the p$K_a$ for K77, which must be unprotonated in order to accept a proton from the ε-amine of the substrate Lys so that it can act as a

nucleophile.  The proposed roles of H96 and K77 are corroborated by the nearly 700-fold decrease in $V_2/\mathbf{E_t}$ and $>10^5$-fold decreases in the second order rate constants.

## 3.5 REFERENCES

1.	Xu, H., Andi, B., Qian, J., West, A. H., and Cook, P. F. (2006) The α-aminoadipate pathway for lysine biosynthesis in fungi, *Cell Biochem. Biophys. 46*, 43-64.

2.	Zabriskie, T. M., and Jackson, M. D. (2000) Lysine biosynthesis and metabolism in fungi, *Nat. Prod. Rep. 17*, 85-97.

3.	Xu, H., West, A. H., and Cook, P. F. (2006) Overall Kinetic Mechanism of Saccharopine Dehydrogenase from *Saccharomyces cerevisiae*, *Biochemistry 45*, 12156-12166.

4.	Xu, H., Alguindigue, S. S., West, A. H., and Cook, P. F. (2007) A proposed proton shuttle mechanism for saccharopine dehydrogenase from *Saccharomyces cerevisiae*, *Biochemistry 46*, 871-882.

5.	Ekanayake, D. K., Andi, B., Bobyk, K. D., West, A. H., and Cook, P. F. (2010) Glutamates 78 and 122 in the active site of saccharopine dehydrogenase contribute to reactant binding and modulate the basicity of the acid-base catalysts., *J Biol Chem. 285*, 20756–20768.

6.	Ekanayake, D. K., West, A. H., and Cook, P. F. (2011) Contribution of K99 and D319 to substrate binding and catalysis in the saccharopine dehydrogenase reaction, *Arch Biochem Biophys 514*, 8-15.

7.	Burk, D. L., Hwang, J., Kwok, E., Marrone, L., Goodfellow, V., Dmitrienko, G. I., and Berghuis, A. M. (2007) Structural studies of the final enzyme in the α-aminoadipate pathway-saccharopine dehydrogenase from *Saccharomyces cerevisiae*, *J Mol Biol. 373*, 745-754.

8.	Andi, B., Xu, H., Cook, P. F., and West, A. H. (2007) Crystal Structures of Ligand-Bound Saccharopine Dehydrogenase from *Saccharomyces cerevisiae*, *Biochemistry 46*, 12512–12521.

9.	Viola, R. E., Cook, P. F. and Cleland, W. W. (1979) Stereoselective preparation of deuterated reduced nicotinamide adenine nucleotides and substrates by enzymatic synthesis, *Anal Biochem 96*, 334-340.

10.     Bobyk, K. D., Kim, S. G., Kumar, V. P., Kim, S. K., West, A. H., and Cook, P. F. (2011) The oxidation state of active site thiols determines activity of saccharopine dehydrogenase at low pH., *Arch Biochem Biophys. 513*, 71-80.

11.     Quinn, D. M. S., L. D. (1991) *In Enzyme mechanism from isotope effects*, CRC Press: Boca Raton, FL.

12.     Cook, P. F. a. C., W. W. (2007) *Enzyme kinetics and mechanism*, Taylor & Francis Group, LLC, New York.

13.     Marquardt, D. W. (1963) An algorithm for least square estimation of nonlinear parameters, *J Soc Ind Appl Math 11*, 431-441.

14.     Winn, M., Ballard, C. C., Cowtan, K. D., Dodson, E. J., Emsley, P., Evans, P. R., Keegan, R. M., Krissinel, E. B., Leslie, A. G. W., McCoy, A., McNicholas, S. J., Murshudov, G. N., Pannu, N. S., Potterton, E. A., Powell, H. R., Read, R. J., Vagin, A. and Wilson, K. S. (2011) Overview of the CCP4 suite and current developments, *Acta Cryst. D67*, 235-242.

15.     McCoy, A. J., Grosse-Kunstleve, R. W., Adams, P. D., Winn, M. D., Storoni, L. C.,  and Read, R. J. . (2007) Phaser crystallographic software, *J. Appl. Cryst. 40*, 658-674.

16.     Murshudov, G. N., Skubak, P., Lebedev, A. A., Pannu, N. S., Steiner, R. A., Nicholls, R. A., Winn, M. D., Long, F. and Vagin, A. A. (2011) REFMAC5 for the refinement of macromolecular crystal structures, *Acta Cryst. D67*, 355-367.

17.     Adams, P. D., Afonine, P. V., Bunkoczi, G., Chen, V. B., Davis, I. W., Echols, N., Headd, J. J., Hung, L.-W., Kapral, G. J., Grosse-Kunstleve, R. W., McCoy, A. J., Moriarty, N. W., Oeffner, R., Read, R. J., Richardson, D. C., Richardson, J. S., Terwilliger, T. C. and Zwart, P. H. (2010) PHENIX: a comprehensive Python-based system for macromolecular structure solution, *Acta Cryst. D66* 213-221.

18.     Emsley, P. a. C., K. (2004) Coot: model-building tools for molecular graphics, *Acta Cryst. D 60*, 2126-2132.

19.     Delano, W. L. (2004) The PyMOL molecular graphics system (San Carlos, CA: Delano Scientific).

20.     Chen, V. B., Arendall III, W. B., Headd, J. J., Keedy, D. A., Immormino, R. M., Kapral, G. J., Murry, L. W., Richardson, J. S., and Richardson, D. C. (2010) MolProbity: all-atom structure validation for macromolecular crystallography. Acta Cryst. D66, 12-21, *Acta Cryst. D66*, 12-21.

21. Karsten, W. E. L., C. J. and Cook, P. F. (1995) Inverse solvent isotope effects in the NADmalic enzyme reaction are the result of the viscosity difference between D2O and H2O: Implications for solvent isotope effect studies., *J. Am. Chem. SOC. 117*, 5914-5918.

22. Lin, Y., Volkman, J., Nicholas, K. M., Yamamoto, T., Eguchi, T., Nimmo, S. L., West, A. H., and Cook, P. F. . (2008) Chemical Mechanism of Homoisocitrate Dehydrogenase from *Saccharomyces cerevisiae*, *Biochemistry 47*, 4169-4180.

## 3.6 FOOTNOTES

[1]Abbreviations: AAA, α-aminoadipate pathway; E, enzyme; SDH, saccharopine dehydrogenase; α-Kg, α-ketoglutarate; Sacc, L-saccharopine; Lys, L-lysine; NAD, β-nicotinamide adenine dinucleotide (the + charge is omitted for convenience); NADH, reduced β-nicotinamide adenine dinucleotide; NADD, reduced β-nicotinamide adenine dinucleotide with deuterium in the 4-R position; AMP, adenosine monophosphate; OxGly, oxalylglycine; WT, wild type; Mes, 2-(*N*-morpholino)ethanesulfonic acid; Taps, 3-[*N*-tris(hydroxymethyl) methylamino]-propanesulfonic acid; Hepes, *N*-(2-hydroxyethyl) piperazine-*N'*-(2-ethanesulfonic acid); Ches, 2-(*N*-cyclohexylamino) ethanesulfonic acid; PEG-MME, polyethylene glycol monomethyl ester; PKIE, primary kinetic isotope effects; SKIE, solvent kinetic isotope effects; MKIE, multiple kinetic isotope effects.

[2]A partial change was observed in the $V_2/E_t$ pH-rate profile of C205S, which was proposed to reflect a pH dependent conformational change (*10*). p$K_a$s for the catalytic groups are not observed suggesting optimum binding of only the correctly protonated forms of reactants and enzyme. In this case, intrinsic p$K_a$ values are observed (*12*).

# CHAPTER 4

## Supporting role of K13 and E16 in the acid-base mechanism of saccharopine dehydrogenase from *Saccharomyces cerevisiae*

### 4.1 INTRODUCTION

Saccharopine dehydrogenase (N6-(glutaryl-2)-L-lysine: NAD oxidoreductase; EC 1.5.1.7) (SDH)[1] catalyzes the final step in the $\alpha$-aminoadipate (AAA) pathway for the *de novo* synthesis of L-lysine in fungi (*1, 2*). The enzyme catalyzes the reversible pyridine nucleotide dependent oxidative deamination of saccharopine (Sacc) to generate $\alpha$-ketoglutarate ($\alpha$-Kg) and lysine (Lys) using NAD as an oxidant (*1*). The proposed kinetic mechanism for the *Saccharomyces cerevisiae* SDH (*Sc*SDH) in the physiological reaction direction is ordered with NAD binding before Sacc and random release of $\alpha$-Kg and Lys prior to NADH (*3*). An acid-base chemical mechanism has been proposed for *Sc*SDH, and is shown in the direction of Sacc formation in Scheme 4.1. Once the E·NADH·$\alpha$-Kg·Lys central complex is formed, the first base ($B_1$) accepts a proton from the $\varepsilon$-amine of Lys prior to imine formation (I). Resulting carbinolamine is protonated by the second acid ($B_2$) (II). The conjugate base $B_2$ then accepts a proton from the carbinolamine nitrogen which is then given to the leaving hydroxyl to form water (III). The imine then is reduced by NADH concomitant with protonation of the imine nitrogen by the conjugate acid of $B_1$ (IV) (*4*). On the basis of isotope effect studies and the pH dependence of kinetic parameters for the K77M and H96Q mutant enzymes, K77 was proposed as $B_1$, while H96 was proposed as $B_2$ (Chapter 3). On the basis of the structure of a dead-end E·NADH·Sacc ternary

complex, K77 and H96 are within hydrogen-bond distance (3.4 Å and 3.5 Å) to the secondary amine of saccharopine, supporting the proposed role of these residues, Figure 4.1 (Chapter 3).

In the crystal structure of apo-enzyme, a pair of thiols was observed in the dinucleotide binding site to form a disulfide, but were present as a dithiol in the AMP-bound structure (*5*).  A mutation at C205, one of the thiols, to S, gave a mutant enzyme with much higher rates at pH 7 compared to the WT enzyme.  The kinetic and chemical mechanisms of C205S remained qualitatively identical to the WT enzyme.  The C205S mutant enzyme is thus used as a pseudo-WT enzyme and the frame of reference for site-directed mutagenesis studies with mutations generated in a C205S background (*6*).

There are a number of ionizable residues (K99, E122, H96, R131, E78, K77, K13, E16, R18 and D319) in SDH active site (*5, 7*).  An alignment of the primary sequences from *C. albicans, Pichia guilliermondii, S. cerevisiae, A. fumigatus,* and *C. neoformans* SDHs indicated all of the ionizable residues are conserved (data not shown), suggesting they are important to the overall reaction.

According to the crystal structure of the E·NADH·Sacc tertiary complex (Chapter 3), K13 forms salt bridge with E78, thus neutralizing it, while E16 hydrogen-bonds to Nε of R18 which has strong H-bond interactions with carboxyl- and oxo-groups of $\alpha$-Kg, Figure 4.1 (Chapter 3).  In this study the roles of K13 and E16 have been determined by mutating them to M and Q respectively.  Elimination of K13 is expected to decrease positive charge in the active site, while mutation of E16 to Q would decrease negative charge, disrupting the overall charge balance in the active site. We hypothesize that these residues play a supportive role in catalysis and/or binding of

α-Kg and Lys on the basis of their positions in the active site (*5*) (Chapter 3). Mutant

enzymes were characterized via the pH dependence of kinetic parameters and isotope

effects. Data are discussed in terms of the proposed general acid - general base

mechanism of SDH.
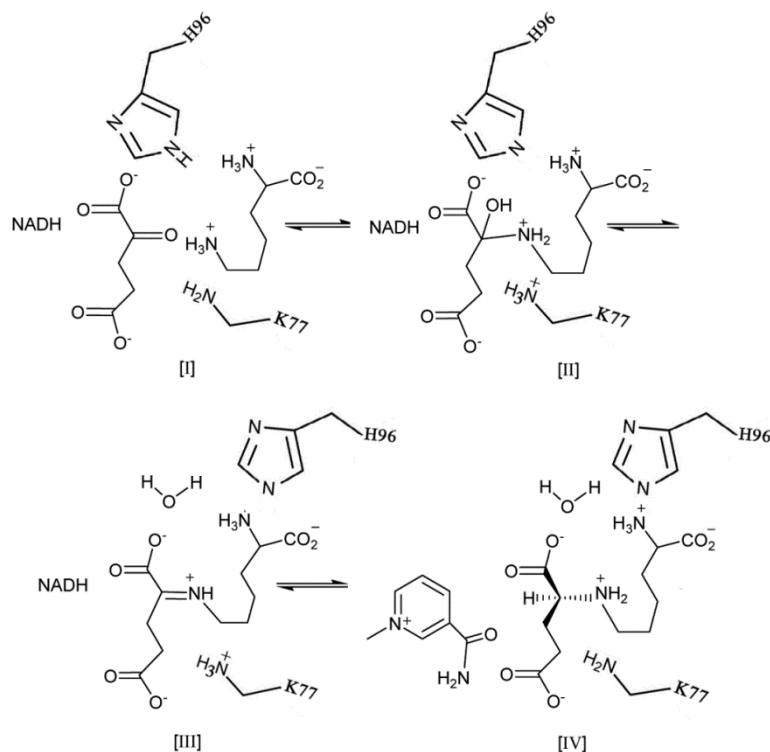


Scheme 4.1 Chemical Mechanism Proposed for Saccharopine Dehydrogenase. The reaction is written in the direction of Sacc oxidation. [I], the formed central complex E·NAD·Sacc once NAD and Sacc bind; [II], Schiff base intermediate; [III], carbinolamine intermediate; [IV], protonated carbinolamine; [V], the generated central complex E·NADH·α-Kg·Lys; [VI], protonated Lys. With the exception of Sacc, no stereochemistry is implied.

## 4.2 MATERIALS AND METHODS

### 4.2.1 Chemicals.

Ampicillin, chloramphenicol, Sacc, Lys, α-Kg, horse liver alcohol

dehydrogenase, and yeast aldehyde dehydrogenase were obtained from Sigma. β-

NADH, β-NAD, Luria-Bertani (LB) broth, LB-agar, and imidazole were purchased form U. S. Biochemical Corp. The buffers, Ches, Taps, Hepes, and Mes, were from Research Organics, while Ni-NTA resin was purchased from 5 Prime. Ethanol-d$_6$ (99 atom % D) and D$_2$O (99.9 atom % D) were purchased from Cambridge Isotope Laboratories. Ethanol (absolute, anhydrous) was from Pharmaco-Aaper. Isopropyl-β-D-1-thiogalactopyranoside was from Invitrogen, and the GenElute plasmid miniprep kit was from Sigma. The QuikChange site-directed mutagenesis kit was from Stratagene. 4$R$-4-$^2$H NADH was prepared as described previously (*8*). The concentration of NADD was estimated using an $\varepsilon_{340}$ of 6220 M$^{-1}$cm$^{-1}$. All chemicals were obtained commercially, were of the highest grade available and were used without further purification.
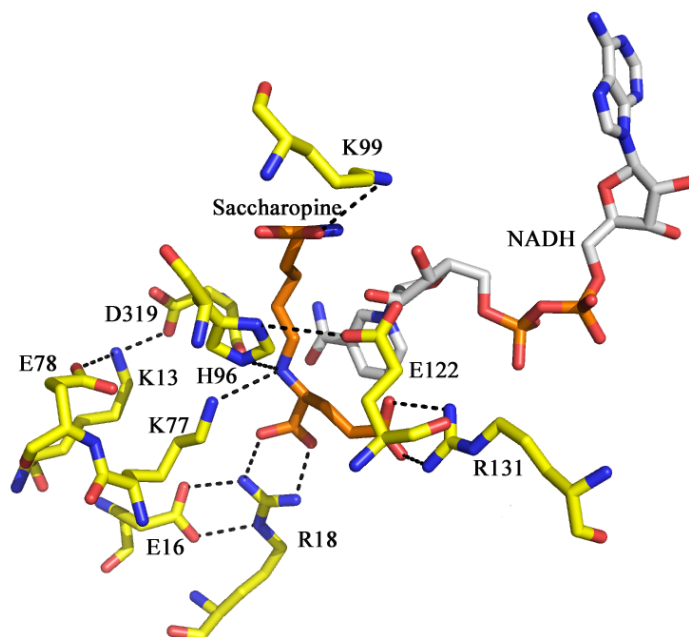


Figure 4.1 Close-up view of the Active Site of SDH in the Ternary Complex with NADH and Saccharopine. Residues within hydrogen bond distance (shown as a dashed line) to NADH and Sacc are shown. The average hydrogen-bond distance was 2.98 Å.

### 4.2.2 Site-directed mutagenesis.

Template DNA used for site-directed mutagenesis was the plasmid containing the C205S mutation of SDH, (*9*), to change K13 and E16 to M and Q, respectively.  The forward and reverse primers used to generate the K13M mutant enzyme are as follows:

K13$_f$, 5'-CTAAGAGCTGAAACT**ATG**CCCCTAGAGGCACGTG-3';

K13$_r$, 5'-CACGTGCCTCTAGGGG**CAT**AGTTTCAGCTCTTAG-3'.

Primers used to generate the E16Q mutant enzyme are as follows:

E16$_f$, 5'-GAAACTAAACCCCTA**CAG**GCACGTGCTGCC-3';

E16$_r$, 5'-GGCAGCACGTGC**CTG**TAGGGGTTTAGTTTC-3'.

Mutagenesis was carried out according to the instructions in the QuikChange site-directed mutagenesis kit as described previously (*10*).  The XL-1-Blue competent cell strain of *Escherichia coli* was transformed with the plasmids containing mutations. Plasmids were isolated and purified using the GenElute plasmid mini preparation kit. Mutations were confirmed by sequencing the entire gene at the Sequencing Core of the Oklahoma Medical Research Foundation, Oklahoma City, OK.


### 4.2.3 Expression and purification.

*Escherichia coli* BL21 (DE3)-RIL cells were transformed with plasmids containing mutant genes and expression was carried out as reported previously (*3*) with some modifications.  Once cell density reached an A$_{600}$ of 0.5−0.6, induction of protein expression was carried out at 37°C by addition of 0.1 mM IPTG, followed by 16 h incubation at 25°C.  Cells were harvested by centrifugation at 10,000$g$ for 10 min. Cells were sonicated in 100 mM Hepes, pH 7.5, containing 300 mM NaCl, 5 mM

imidazole.  Enzymes were purified by Ni-NTA affinity chromatography, with elution at

300 mM imidazole.  The enzymes were >95% pure by SDS-PAGE.  The enzymes were

stored at 4˚C in the elution buffer.


**4.2.4 Enzyme assay.**

Initial velocities were measured using a Beckman DU 640 UV-visible

spectrophotometer.  All assays were performed at a temperature of 25°C.  Enzyme

activity was measured in quartz cuvettes with a path length of 1 cm in the direction of

Sacc formation by monitoring the decrease in $A_{366}$ ($\varepsilon_{366}$ = 3110 $M^{-1}$ $cm^{-1}$) as NADH is

oxidized.  Reactions were initiated by addition of enzyme to a reaction mixture with a

final volume of 0.5 mL containing 100 mM Hepes, pH 7.5, saturating NADH (0.5 mM)

and variable concentrations of $\alpha$-Kg and Lys.


**4.2.5 pH Studies.**

The pH dependence of $V$, $V/K_{Lys}$, and $V/K_{\alpha\text{-}Kg}$ was measured over the pH range

5–10 with NADH maintained at 0.5 mM, and either $\alpha$-Kg or Lys maintained at

saturation with the other varied.  Buffers were maintained at 100 mM concentration

over the following pH range; Mes, 5.5 - 7.0; Hepes, 7.0 - 8.0; Taps, 8.0 - 9.0; Ches, 9.0

– 10.0.  None of the buffers had any effect on the activity of any of the mutant enzymes.

The pH was recorded before and immediately after the reaction; no significant

differences were detected.  To be certain that the kinetic mechanism of the enzyme did

not change with pH and to obtain estimates of $K_m$ values for both substrates at the pH

extremes, initial velocity patterns were obtained at pH 5.5 and 10.0 with $\alpha$-Kg and Lys concentrations varied, with NADH maintained at saturating concentration (0.5 mM).

**4.2.6 Kinetic Isotope Effects.**

Isotope effects were measured for K13M and E16Q mutant enzymes in the pH independent region of their pH-rate profiles (pH 7.2). Isotope effects on $V_2$ and $V_2/K_{\mathrm{Lys}}$ were measured with NADH(D) (0.5 mM) and $\alpha$-Kg ($10K_m$) maintained at saturation and Lys varied. Solvent deuterium kinetic isotope effects were measured at pH(D) 7.2, in the pH independent region of the pH(D)-rate profiles. For rates measured in $D_2O$, substrates ($\alpha$-Kg and Lys) and buffers were first dissolved in a small amount of $D_2O$ and then lyophilized to replace exchangeable protons. The lyophilized powders were then re-dissolved in $D_2O$ to give the desired concentrations, and pD was adjusted using either DCl or NaOD. NADH was dissolved in $D_2O$ directly. The pD was determined by adding 0.4 to the pH meter readings (*11*). Reactions were initiated by adding a small amount of each of the mutant enzymes in $H_2O$; the final estimated concentration of $D_2O$ in the reaction mixture was about 98%. Multiple isotope effects were determined by direct comparison of the initial rates in $H_2O$ and $D_2O$ as for solvent deuterium effects, varying lysine at fixed saturating concentrations of NADD and $\alpha$-Kg.

**4.2.7 Data Analysis.**

Initial rate data were first analyzed graphically by double reciprocal plot to determine the quality of the data and the proper rate equation for data fitting. Data were then fitted using the appropriate equations (*12*) and the Marquardt-Levenberg algorithm

(*13*), supplied with the EnzFitter program from BIOSOFT, Cambridge, U.K. Kinetic parameters and their corresponding standard errors were estimated using a simple weighing method.

Data for substrate saturation curves for pH-rate profiles and viscosity effects were fitted to eq. 1. Data obtained from the initial velocity patterns were fitted to eq. 2. Data for $V$ and $V/K$ deuterium isotope effects were fitted using eqs. 3; equal isotope effects are assumed on $V$ and $V/K$. The S.E. of a product or dividend was estimated using eq. 4.

$$v = \frac{V\mathbf{A}}{K_a + \mathbf{A}} \tag{1}$$

$$v = \frac{V\mathbf{AB}}{K_{ia}K_b + K_a\mathbf{B} + K_b\mathbf{A} + \mathbf{AB}} \tag{2}$$

$$v = \frac{V\mathbf{A}}{(K_a + \mathbf{A})(1 + F_i E_v)} \tag{3}$$

$$\text{S.E.}\ \frac{x}{y} = \frac{x}{y}\left[\left(\frac{\text{S.E.}\,x}{x}\right)^2 + \left(\frac{\text{S.E.}\,y}{y}\right)^2\right]^{1/2} \tag{4}$$

In eqs. 1-3, $v$ and $V$ are initial and maximum velocities, respectively, $\mathbf{A}$, $\mathbf{B}$, are substrate concentrations, $K_a$ and $K_b$ are Michaelis constants for substrates A and B, respectively, and $K_{ia}$ is the dissociation constant for A from the EA complex. In eq. 3, $F_i$ is the fraction of label in substrate or solvent, $E_v$, is isotope effect minus 1 for the equal isotope effects on $V$ and $V/K$. In eq. 4, S.E. $x$, and S.E. $y$ are computer generated standard errors of values for kinetic parameters $x$ and $y$.

Data for pH-rate profile that decreased with a slope of +1 at low pH and -1 at high pH were fitted to eq. 5, while pH-rate profile exhibiting a slope of +1 on the acid side were fitted to eq. 6.

$$\log y = \log \left[ C \Big/ \left( 1 + \frac{\mathbf{H}}{K_1} + \frac{K_2}{\mathbf{H}} \right) \right] \qquad (5)$$

$$\log y = \log \left[ C \Big/ \left( 1 + \frac{\mathbf{H}}{K_1} \right) \right] \qquad (6)$$

In eqs. 5 and 6, $y$ is the observed value of $V$ or $V/K$ at any pH, $\mathbf{H}$ is the hydrogen ion concentration, $K_1$ and $K_2$ are the acid dissociation constants of functional groups required in a given protonation state on enzyme or substrate for optimal binding and/or catalysis, and $C$ is the pH-independent value of $y$.

## 4.3 RESULTS

### 4.3.1 Cell Growth, Expression and Purification.

Expression of the K13M/C205S and E16Q/C205S mutant enzymes was similar to that of the WT SDH under similar conditions. All the enzymes were eluted from the Ni-NTA column with buffer containing 300 mM imidazole at pH 8. Purity of the proteins was assessed by SDS-PAGE, and all of the mutant proteins were estimated to be >95% pure. His-tagged mutant enzymes maintained stability and remained active for months when stored at 4 °C in 100 mM Hepes, 300 mM KCl and 300 mM imidazole at pH 8.

**4.3.2 Initial velocity studies.**

Initial velocities were measured in the direction of Sacc formation for the K13M and E16Q mutant enzymes. Replacing K13 with M resulted in a 14-fold decrease in $V_2/\mathbf{E_t}$ and ~200-, and ~12-fold decreases in $V_2/K_{\alpha-Kg}\mathbf{E_t}$ and $V_2/K_{Lys}\mathbf{E_t}$, respectively. This results in a 16-fold increase in $K_{Lys}$ and no significant change in $K_{\alpha-Kg}$. Replacing E16 with Q resulted in a 15-fold decrease in $V_2/\mathbf{E_t}$ and ~$10^3$- and ~200-fold decreases in $V_2/K_{\alpha-Kg}\mathbf{E_t}$ and $V_2/K_{Lys}\mathbf{E_t}$, respectively. The values of $K_{\alpha-Kg}$ and $K_{Lys}$ increased 70-, and 15-fold, respectively. Kinetic parameters are summarized in Table 4.1, and compared to those obtained for the pseudo-WT enzyme, C205S (*9*).

**4.3.3 pH dependence of kinetic parameters.**

The pH dependence of kinetic parameters provides information on the optimal protonation state of functional groups on enzyme and/or substrate for binding and/or catalysis. Studies were carried out with K13M and E16Q mutant enzymes in the direction of Sacc formation, at 25 °C. Both mutant enzymes were active and stable over the pH range 5–10, and initial rate studies at pH 5.5 and 10 suggested the kinetic mechanism did not change (data not shown). For the K13M mutant enzyme, $V_2/\mathbf{E_t}$ , $V_2/K_{Lys}\mathbf{E_t}$ and $V_2/K_{\alpha-Kg}\mathbf{E_t}$ are pH independent, Fig. 2, with average values of $8.1 \pm 0.7$ s$^{-1}$, $(1.2 \pm 0.3) \times 10^3$ M$^{-1}$ s$^{-1}$ and $(2.0 \pm 0.9) \times 10^3$ M$^{-1}$ s$^{-1}$, respectively. In the case of E16Q, Fig. 4.2, $V_2/E_t$ decreases at low and high pH with a slope of +1 and -1, giving p$K_a$ values of about 6.9 and 8.6; the pH independent value is $9.8 \pm 1.5$ s$^{-1}$. $V_2/K_{Lys}\mathbf{E_t}$ decreases with a slope of 1 on the acid side with a p$K_a$ of about 6.4 with a pH

independent value of $(4.0 \pm 0.2) \times 10^2$ $M^{-1}$ $s^{-1}$. $V_2/K_{\alpha-Kg}\mathbf{E_t}$ is pH independent with an average value of $(5.1 \pm 0.2) \times 10^2$ $M^{-1}$ $s^{-1}$.

Table 4.1: Summary of the Kinetic Parameters

|  | C205S | K13M[a] | E16Q[a] |
|---|---|---|---|
| $V_2/\mathbf{E_t}$ $(s^{-1})$ | 106 | $7.53 \pm 0.004$ | $6.87 \pm 0.05$ |
| $V_2/K_{\alpha-Kg}\mathbf{E_t}$ $(M^{-1}s^{-1})$ | 9.7 x $10^5$ | $(4.33 \pm 0.04) \times 10^3$ | $(8.95 \pm 0.93) \times 10^2$ |
| $V_2/K_{Lys}\mathbf{E_t}$ $(M^{-1}s^{-1})$ | 1.2 x $10^5$ | $(1.01 \pm 0.004) \times 10^4$ | $(5.27 \pm 0.78) \times 10^2$ |
| $K_{\alpha-Kg}$ (mM) | 0.11 | $1.74 \pm 0.02$ | $7.7 \pm 0.8$ |
| $K_{Lys}$ (mM) | 0.89 | $0.75 \pm 0.003$ | $13.1 \pm 1.9$ |

[a]Mutations prepared in the C205S background.

Table 4.2: Summary of the Kinetic Isotope Effects[a]

|  | C205S[b] | K13M[c, d] | E16Q[c, d] |
|---|---|---|---|
| $^{D}V_2$ and $^{D}(V_2/K_{Lys})$ | $1.3 \pm 0.2$ | $2.06 \pm 0.03$ | $2.17 \pm 0.06$ |
| $^{D2O}V_2$ and $^{D2O}(V_2/K_{Lys})$ | $1.5 \pm 0.1$ | unity | unity |
| $^{D}(V_2)_{D2O}$ and $^{D}(V_2/K_{Lys})_{D2O}$ | ND | $1.90 \pm 0.10$ | $2.09 \pm 0.04$ |

[a]Isotope Effects were measured at pH 8.2.
[b]From reference (9).
[c]Errors are standard error of the mean.
[d]Data for K13M and E16Q were fitted to eq. 3.

### 4.3.4 Isotope effects.

Isotope effects were measured for the K13M mutant enzyme at pH 8.2, within the pH independent region of the pH-rate profiles. All values of the PKIE are finite while the SKIE values are within error unity, Table 4.2. To be certain the SKIE was 1, the PKIE was repeated in $D_2O$; no significant difference was found.


### 4.4 DISCUSSION

### 4.4.1 Kinetic Mechanism.

A lower value of $k_{cat}$ was observed for both the K13M and E16Q mutant enzymes. Even though both mutant enzymes showed an increase in $K_{\alpha-Kg}$, the value was significant higher (~70-fold) for E16Q compared to WT. Isotope effects of about 2 suggested the hydride transfer step was rate limiting for both enzymes. This is corroborated by a SKIE of 1.0 measured with either NADH or NADD.

The deuterium isotope effects on $V_2$ and $V_2/K_{Lys}$ are equal for K13M and E16Q mutant enzymes, as found for the C205S pseudo-WT enzyme (9), indicating $K_{Lys}$ is equal to the $K_d$ for Lys from the E·NADH·α-Kg·Lys complex (14). The free energy of binding can thus be calculated for all three enzymes, C205S, K13M and E16Q ($\Delta G^{\circ'}$ = -RTln$K_{eq}$ = -RTln(1/$K_d$), where 1/$K_d$ is association constant, $K_s$). The $K_s$ values estimated from the data in Table 1, for C205S, K13M and E16Q mutant enzymes are $1.12 \times 10^3$ M$^{-1}$, $1.33 \times 10^3$ M$^{-1}$ and $0.08 \times 10^3$ M$^{-1}$, respectively, giving values of -4.16, -4.26 and -2.60 kcal/mol, respectively. There is no contribution of K13 to binding Lys indicated by the value of $\Delta\Delta G^{\circ'}$ of 0.1 kcal/mol, while a value of 1.56 kcal/mol for E16Q mutant enzyme suggests a modest contribution of E16 to binding Lys.

## 4.4.2 pH studies.

The role of K13 and E16 was probed further by measuring the pH dependence of kinetic parameters.  In the case of C205S, the maximum rate decreases from a constant value at low pH to another constant value at high pH giving a $pK_a$ of 7.5.  The group with a $pK_a$ of 7.5 needs to be protonated for optimum catalysis.  The pH dependence was attributed to a conformational change in the enzyme which is optimum at lower pH.  The pH dependence of $V_2/K_{Lys}\mathbf{E_t}$ is bell shaped and exhibits $pK_a$s of 7 and 8; one group is required protonated and the other unprotonated for optimum binding and/or catalysis.  $V_2/K_{\alpha\text{-}Kg}\mathbf{E_t}$ decreases below a $pK_a$ of 5.7, while at high pH a partial change is observed with a $pK_a$ of 7.5 .  The $pK_a$ of 5.7 could be as a result of pH dependent conformational change which was also observed in WT-SDH (*4, 9*).
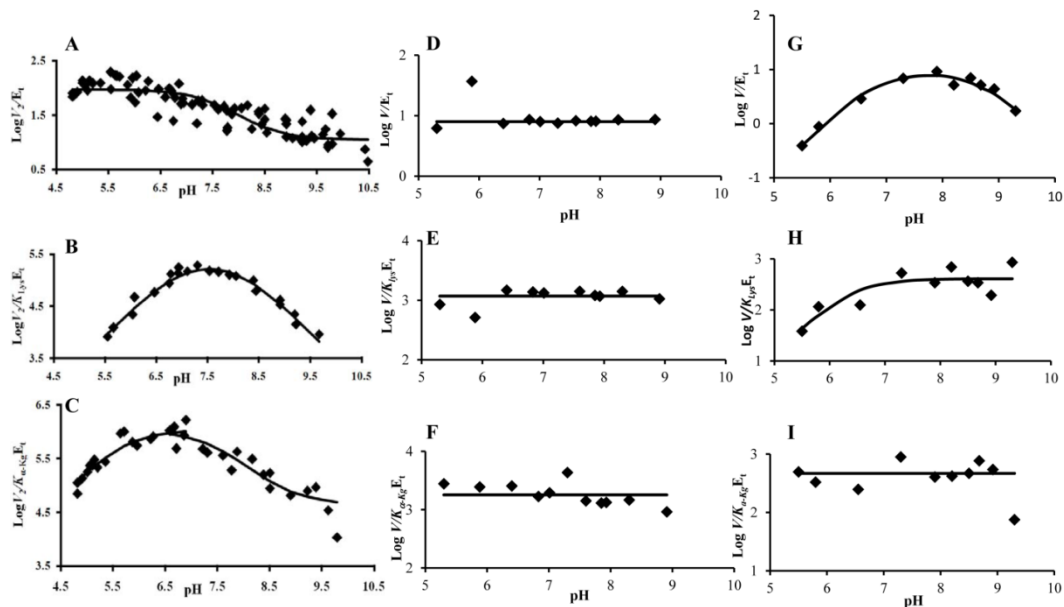


Figure 4.2: pH Dependence of Kinetic Parameters for SDH WTSDH (C205S), K13M/C205S and E16Q/C205S in the Direction of Saccharopine Formation. Data for WT SDH (C205S)(A to C) are from ref. (*9*) and are reproduced with permission, while (D to F) are data for the K13M/C205S, (G to I) are for E16Q/C205S mutant enzymes. Units for $V/E_t$ and $V/K\mathbf{E_t}$ are s$^{-1}$ and M$^{-1}$ s$^{-1}$, respectively. Points are the experimentally determined values. The curves are theoretical and based on fits to eq. 5 for panel G and eq. 6 for panel H.

The kinetic parameters observed for K13M are pH independent, Figure 4.2. K13 is positioned near K77 and hydrogen-bonds to E78 and E319. In the absence of K13, hydrogen-bonding with E78 and E319 are lost, increasing negative charge and likely resulting in a new hydrogen bond between K77 and E78, giving an increase in $pK_a$s of K77 and N$\varepsilon$ of Lys. In the case of H96, the increased $pK_a$ of N$\varepsilon$ of Lys, results in charge-charge repulsion when the imidazole is protonated, giving the perturbation of its $pK_a$ to a lower pH. From the data reported in RESULTS and the discussion above, K13 could be playing a significant role in balancing charge in the active site, thus achieving the optimal conformation for binding of substrates and catalysis.

The $V_2/\mathbf{E_t}$ profile for E16Q is bell shaped with the maximum rate decreasing below pH 6.9 and above pH 8.6. The two catalytic residues proposed for SDH are K77 and H96 (Chapter 3) with $pK_a$s of 7 and 8, the same groups seen in the $V_2/K_{Lys}\mathbf{E_t}$ profile for C205S. Thus, it is proposed that the two groups seen in the $V_2/\mathbf{E_t}$ profile for E16Q are the catalytic residues K77 and H96. When referring to the tertiary structure, the position of E16 is within hydrogen-bonding distance of 2.6Å from N$\varepsilon$ of R18. R18 has strong hydrogen bond/ ionic interactions with the $\alpha$-carboxylate of $\alpha$-Kg (Chapter 3). When apo-structure of SDH was superimposed onto the E·NADH·Sacc ternary complex structure, a repositioning of E16 and R18 was shown (Chapter 3). Mutating E16 to Q would affect the correct positioning of R18 for binding and holding $\alpha$-Kg in the correct position for optimum catalysis. Consistent with this is the 3 order of magnitude decrease in $V_2/K_{\alpha\text{-}Kg}\mathbf{E_t}$ resulting in a 70-fold increase in $K_{\alpha\text{-}Kg}$ in the case of E16Q mutant enzyme as compared to C205S enzyme. The $V_2/K_{Lys}\mathbf{E_t}$ profile for E16Q decreases below pH 6.4 and stays constant up to the maximum pH investigated, while

$V_2/K_{\alpha\text{-}Kg}\mathbf{E_t}$ profile is pH independent. The difference in these two conditions is the enzyme complex to which the limiting substrate binds. In the case of $V_2/K_{Lys}\mathbf{E_t}$, it is E·NADH·$\alpha$-Kg. When E·NADH·$\alpha$-Kg complex is formed, in absence of E16, to balance the positive charge in the active site the p$K_a$ for K77 might be slightly lowered. The group with p$K_a$ of 6.4 seen in $V_2/K_{\alpha\text{-}Kg}\mathbf{E_t}$ profile of E16Q could be K77. While in the case of $V_2/K_{\alpha\text{-}Kg}\mathbf{E_t}$, E·NADH·Lys complex is formed. Absence of E16 would affect $\alpha$-Kg binding to R18 as R18 is not positioned correctly. Perturbation of p$K_a$s could be as a result of ill-positioning of R18 resulting in lack of neutralization of the carboxylates of $\alpha$-Kg, thus changing the fine charge balance in the active site. Thus suggested role of E16 could be of correct positioning of R18 for optimal binding of $\alpha$-Kg and catalysis.

## 4.5 REFERENCES

1.    Xu, H., Andi, B., Qian, J., West, A. H., and Cook, P. F. (2006) The $\alpha$-aminoadipate pathway for lysine biosynthesis in fungi, *Cell Biochem. Biophys. 46*, 43-64.

2.    Zabriskie, T. M., and Jackson, M. D. (2000) Lysine biosynthesis and metabolism in fungi, *Nat. Prod. Rep. 17*, 85-97.

3.    Xu, H., West, A. H., and Cook, P. F. (2006) Overall Kinetic Mechanism of Saccharopine Dehydrogenase from *Saccharomyces cerevisiae*, *Biochemistry 45*, 12156-12166.

4.    Xu, H., Alguindigue, S. S., West, A. H., and Cook, P. F. (2007) A proposed proton shuttle mechanism for saccharopine dehydrogenase from *Saccharomyces cerevisiae*, *Biochemistry 46*, 871-882.

5.    Andi, B., Xu, H., Cook, P. F., and West, A. H. (2007) Crystal Structures of Ligand-Bound Saccharopine Dehydrogenase from *Saccharomyces cerevisiae*, *Biochemistry 46*, 12512–12521.

6.    Ekanayake, D. K., West, A. H., and Cook, P. F. (2011) Contribution of K99 and D319 to substrate binding and catalysis in the saccharopine dehydrogenase reaction, *Arch Biochem Biophys 514*, 8-15.

7.    Burk, D. L., Hwang, J., Kwok, E., Marrone, L., Goodfellow, V., Dmitrienko, G. I., and Berghuis, A. M. (2007) Structural studies of the final enzyme in the α-aminoadipate pathway-saccharopine dehydrogenase from *Saccharomyces cerevisiae*, *J Mol Biol. 373*, 745-754.

8.    Viola, R. E., Cook, P. F. and Cleland, W. W. (1979) Stereoselective preparation of deuterated reduced nicotinamide adenine nucleotides and substrates by enzymatic synthesis, *Anal Biochem 96*, 334-340.

9.    Bobyk, K. D., Kim, S. G., Kumar, V. P., Kim, S. K., West, A. H., and Cook, P. F. (2011) The oxidation state of active site thiols determines activity of saccharopine dehydrogenase at low pH., *Arch Biochem Biophys. 513*, 71-80.

10.    Ekanayake, D. K., Andi, B., Bobyk, K. D., West, A. H., and Cook, P. F. (2010) Glutamates 78 and 122 in the active site of saccharopine dehydrogenase contribute to reactant binding and modulate the basicity of the acid-base catalysts., *J Biol Chem. 285*, 20756–20768.

11.    Schowen, K. B. a. S., R.L. . (1982) Solvent Isotope Effects on Enzyme Systems, *Methods Enzymol. 87*, 551-606.

12.    Cook, P. F. a. C., W. W. (2007) *Enzyme kinetics and mechanism*, Taylor & Francis Group, LLC, New York.

13.    Marquardt, D. W. (1963) An algorithm for least square estimation of nonlinear parameters, *J Soc Ind Appl Math 11*, 431-441.

14.    Klinman, J. P. a. M., R. G. (1985) Calculation of substrate dissociation constants from steady-state isotope effects in enzyme-catalyzed reactions, *J. Am. Chem. Soc. 107*, 1058–1060.

## 4.6 FOOTNOTES

[1]Abbreviations: AAA, α-aminoadipate pathway; E, enzyme; SDH, saccharopine dehydrogenase; α-Kg, α-ketoglutarate; Sacc, L-saccharopine; Lys, L-lysine; NAD, β-nicotinamide adenine dinucleotide (the + charge is omitted for convenience); NADH, reduced β-nicotinamide adenine dinucleotide; NADD, reduced β-nicotinamide adenine dinucleotide with deuterium in the 4-R position; WT, wild type; Mes, 2-(*N*-morpholino)ethanesulfonic acid; Taps, 3-[*N*-tris(hydroxymethyl) methylamino]-propanesulfonic acid; Hepes, *N*-(2-hydroxyethyl) piperazine-*N'*-(2-ethanesulfonic acid);

Ches, 2-(*N*-cyclohexylamino) ethanesulfonic acid; PKIE, Primary kinetic isotope effects; SKIE, Solvent kinetic isotope effects; MKIE, Multiple kinetic isotope effects.

# APPENDIX 1

## Oxaloacetate as a substrate of homocitrate synthase

**Introduction**

Homocitrate synthase (HCS) catalyzes the condensation of Acetyl-CoA (AcCoA) and $\alpha$-ketoglutarate ($\alpha$-Kg) to give homocitrate and CoA. With $Mg^{2+}$ as the metal ion, a steady state random kinetic mechanism was proposed for *Thermus thermophilus* HCS (*Tt*HCS). (*Chapter 2*). The pathway with $\alpha$-Kg binding first was proposed to be three times faster than the one where AcCoA binds to free enzyme. Oxaloacetate (OAA) is a $\alpha$-Kg analog and serves as a slower substrate for *Tt*HCS. The kinetic mechanism for ScHCS exhibited some randomness i.e. a productive E·AcCoA complex was formed (*1*).

Oxaloacetate was used to identify and characterize slower steps involved in catalysis.

**Methods**

*Initial velocity studies.* Initial rates were measured as a function of AcCoA concentrations at different fixed concentrations of OAA. The reaction mixture typically consisted of 50 mM Hepes, pH 7.5, 0.1 mM dichlorophenol indophenol (DCPIP), 200 $\mu$M $MgCl_2$, 2 $\mu$M *Tt*HCS and variable concentrations of OAA and AcCoA.

*Isotope effects.* Primary deuterium kinetic isotope effects were measured by direct comparison of initial velocities, where deuterioacetyl-CoA (AcCoA-$d_3$) was used as the deuterated substrate and OAA was fixed at saturated concentration (10 mM). AcCoA-

d$_3$ was prepared as described in Chapter 2. Solvent isotope effects with were carried out by comparing initial velocity patterns in H$_2$O and D$_2$O at pH(D) 7.5.

*Dependence of initial rate on solution viscosity.* The initial rate was measured as a function of the concentration of OAA at different fixed levels of AcCoA at pH 7.5 and 25 $^o$C in the presence of 9% glycerol. A glycerol concentration of 9% gives a relative viscosity of 1.24, identical to that obtained with 100% D$_2$O.

## Data processing

Data for initial rate studies were fitted to eq. 1 while isotope effects obtained were fitted using eq. 2.

$$v = \frac{V\mathbf{AB}}{K_{ia}K_b + K_a\mathbf{B} + K_b\mathbf{A} + \mathbf{AB}} \qquad (1)$$

$$v = \frac{V\mathbf{AB}}{K_a\mathbf{B}\left(1 + \dfrac{\mathbf{B}}{K_{IB}}\right) + K_b\mathbf{A} + \mathbf{AB}} \qquad (2)$$

$$v = \frac{V\mathbf{A}}{K_a\left(1 + F_i E_{V/K}\right) + \mathbf{A}\left(1 + F_i E_V\right)} \qquad (3)$$

In eqs. 1-3, $v$ and $V$ are initial and maximum velocities, respectively, **A** and **B**, are substrate concentrations, $K_a$ and $K_b$ are Michaelis constants for substrates A and B, respectively. $K_{ia}$ is the dissociation constant for A from the EA complex. $K_{IB}$ is the substrate inhibition constant for B. In eq. 3, $F_i$ is the fraction of deuterium in D$_2$O or in AcCoA-d$_3$, and $E_{V/K}$ and $E_V$ are the isotope effects minus 1 on $V/K$ and $V$, respectively.

## Results

*Initial velocity studies.* OAA is a slow alternative substrate analog of α-Kg. The

initial velocity pattern obtained with OAA and AcCoA is intersecting with no demonstrable substrate inhibition by AcCoA (Figure 2A) for the concentration range tested (0.2 – 200 μM  AcCoA).  Kinetic parameters are summarized in Table 1.

**Table 1. Summary of Kinetic parameters with 200 μM Mg$^{2+}$**

|  | H$_2$O | D$_2$O |
|---|---|---|
| $V/\mathbf{E_t}$ (s$^{-1}$) | 0.0230 ± 0.0006 | 0.028 ± 0.002 |
| $V/K_{OAA}\mathbf{E_t}$ (M$^{-1}$s$^{-1}$) | 0.065 ± 0.019 | UD$^a$ |
| $V/K_{AcCoA}\mathbf{E_t}$ (M$^{-1}$s$^{-1}$) | 0.74 ± 0.06 | 2.0 ± 0.4 s$^{-1}$ |
| $K_{OAA}$ (μM) | 350 ± 50 | 19 ± 20 |
| $K_{AcCoA}$ (μM) | 31 ± 3 | 14 ± 3 |
| $K_{I\,AcCoA}$ (μM) |  | 11 ± 12 |

*Primary Isotope effect.* Primary substrate deuterium kinetic isotope effects were measured with Mg$^{2+}$ as the divalent cation by direct comparison of initial rates at pH 7.5 with perdeuterio-acetyl CoA as the labeled substrate.   The isotope effect is dependent on the AcCoA concentration, the maximum apparent deuterium kinetic isotope effect is about 2.24, Figure 1B.   Fitting the data to eq. 3 resulted in the following values: $^{D}V = 1.72 ± 0.29$;  $^{D}(V/K_{AcCoA}) = 0.90 ± 0.37$

*Solvent isotope effect.*   Initial velocity patterns, measuring the initial rate as a function of OAA concentration at different fixed levels of AcCoA, were obtained in H$_2$O and D$_2$O, Figure 2A, B. The patterns give near parallel lines in H$_2$O and D$_2$O, but substrate inhibition by AcCoA is observed in D$_2$O.   Replots of the slope and intercept vs. the reciprocal of AcCoA concentration are shown in Figure 2C, D.   The intercept

replot indicates $^{D2O}V$ is $1.03 \pm 0.05$, while $^{D2O}(V/K_{AcCoA})$ is equal to about 0.5. The slope

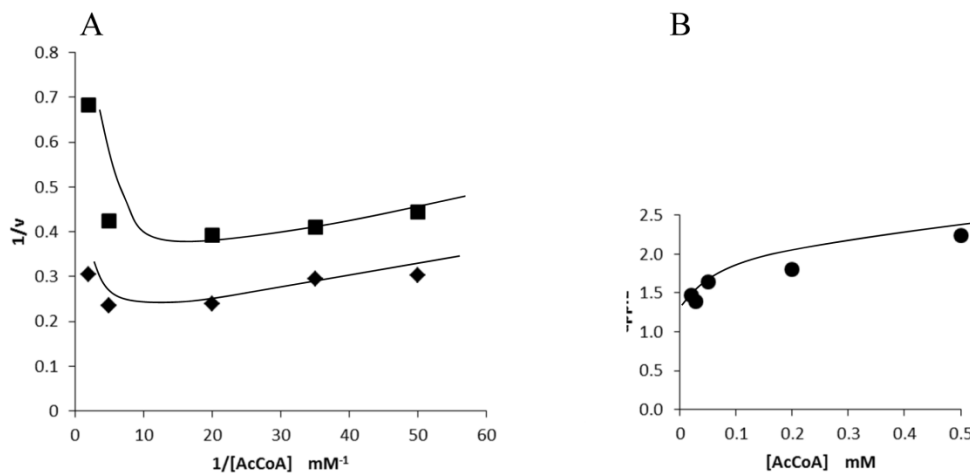replot indicates a large apparent isotope effect as a result of the substrate inhibition.



Figure 1. Primary isotope effects with OAA and AcCoA-d₃. A. Double reciprocal plot for reactions with 10 mM OAA and variable concentrations of AcCoA-h₃ (♦), and AcCoA-d₃ (■). B. The apparent isotope effect (appIE) *vs* concentrations of AcCoA (the appIE is the ratio of data with deuterated and undeuterated AcCoA). Curves are drawn by hand.

In the presence of glycerol as a viscosogen, there is a significant increase in $V/K_{AcCoA}$ and a decrease in the value of $V$. The ratio of kinetic parameters determined in the absence and presence of 9% glycerol, the resulting value of $^{D2O}V$ is $1.40 \pm 0.06$, while the value of $0.14 \pm 0.03$ and $0.76 \pm 0.103$ are observed on $^{D2O}(V/K_{AcCoA})$ and $^{D2O}(V/K_{OAA})$, respectively.

**Discussion**

The kinetic mechanism with OAA as a substrate in place of α-Kg is sequential, similar to that seen for α-Kg and AcCoA in presence of $Mn^{2+}$ as the divalent cation. Competitive substrate inhibition by AcCoA is observed in $D_2O$ ($\geq 200$ μM AcCoA), as

121

well as in $H_2O$ at very high concentration ($\geq$ 500 $\mu M$) suggesting ordered addition of

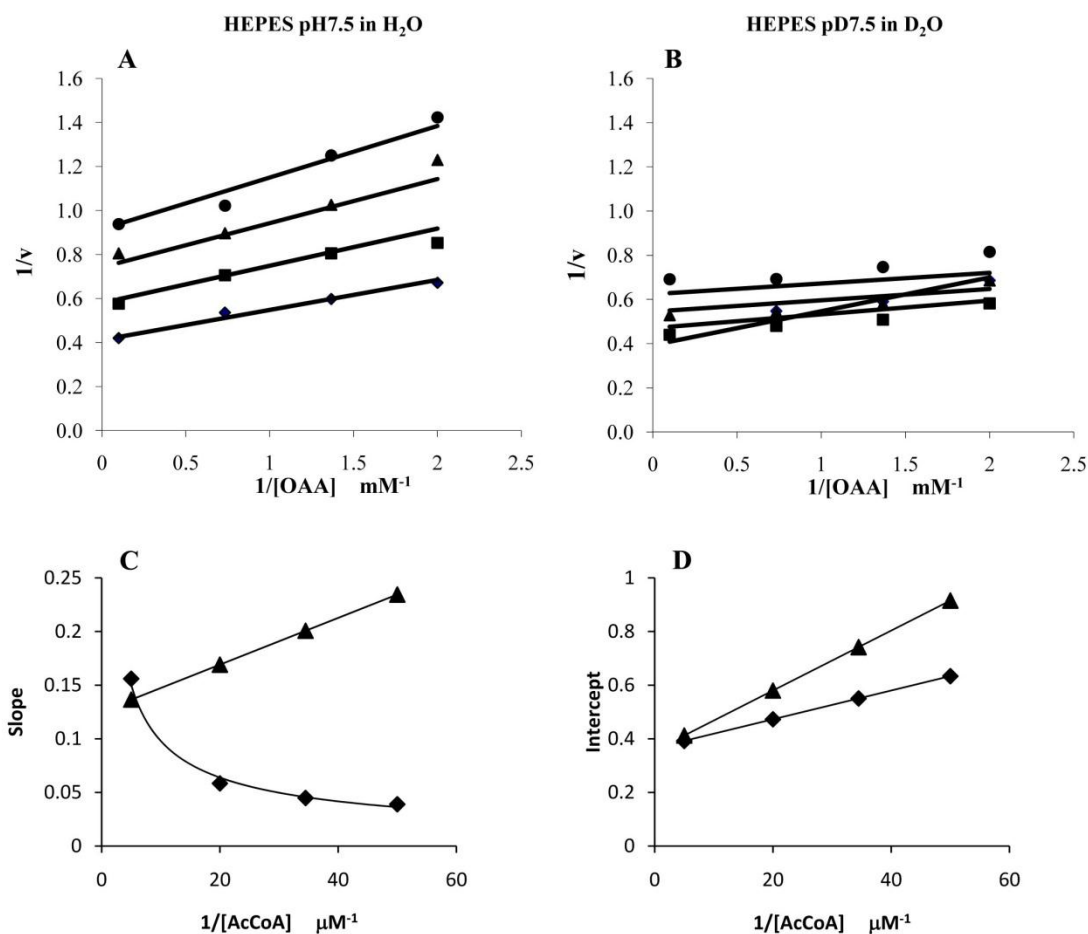OAA prior to AcCoA with a dead-end E·AcCoA complex (Figure 3)



Figure 2. Solvent isotope effects with OAA and AcCoA.
Initial Velocity Pattern at pH 7.5 and 25 $^o$C. Data are plotted as a function of OAA at different concentrations of AcCoA as follows: 20 (●), 29 (▲), 50 (■) and 200 (♦) $\mu M$ in $H_2O$ (A) and $D_2O$ (B). C) and D) are replots of slopes and intercepts obtained from the primary plots vs. the reciprocal of AcCoA concentration in $H_2O$ (▲) and in $D_2O$ (♦). Note the apparent substrate inhibition exhibited in the slope replot in $D_2O$.
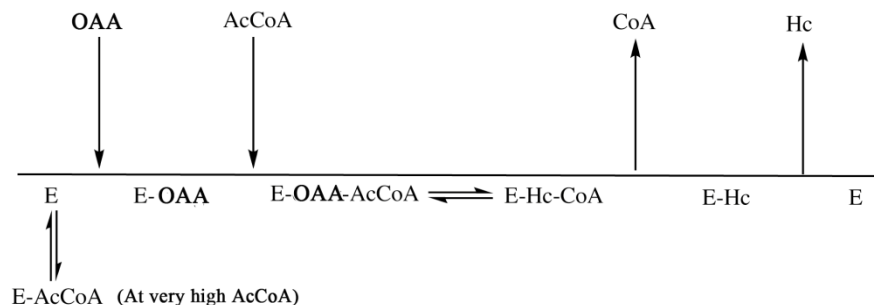
Figure 3. Proposed Kinetic Mechanism for *Thermus thermophilus* Homocitrate Synthase. An ordered kinetic mechanism is shown with a dead-end E·AcCoA complex.

A substrate deuterium isotope effect of 1.4 is measured with AcCoA-$d_3$, at low concentrations of AcCoA, for the pathway in which OAA binds before AcCoA. However, at high AcCoA, where it binds prior to OAA, a finite primary kinetic isotope effect $\geq$ 2.2 is observed (Figure 1). Data suggest the presence of a slow step contributing to rate limitation that occurs after AcCoA binds to enzyme, likely a conformational change in the enzyme. For the pathway in which $\alpha$-Kg binds prior to AcCoA, the conformational change still occurs as AcCoA binds, but no isotope effect is observed. Thus, deprotonation of the methyl group of AcCoA must occur together with the conformational change, which contributes to rate limitation when AcCoA binds first, but not when $\alpha$-Kg binds first (Chapter 2). On the basis of primary kinetic isotope effects, similar conclusions can be made for the reaction with OAA and AcCoA.

A solvent deuterium isotope effect of unity is obtained on *V*, but an inverse isotope effect of about 0.5 is observed on $V/K_{AcCoA}$. There are a number of reasons for observing an inverse solvent isotope effect, including ionization of a thiol, hydrolysis of metal water, and a medium effect that may reflect a structural change in enzyme (*2*). However, it is also important to consider the effect of solvent viscosity when carrying

out solvent deuterium isotope effects (*3, 4*). Viscosity can affect the reaction in a number of ways (*2*). Increased viscosity is routinely used to slow down diffusion-controlled steps, such as the binding of reactant or release of product. If these steps contribute to rate-limitation, a decrease in the limiting rate constants, *V* (release of product) and *V/K* (addition of reactant), will be observed. It is also possible to speed up or slow down structural changes in the protein at higher viscosity (*3, 4*). Substitution of $D_2O$ for $H_2O$ results in an increase in solvent viscosity ($\eta_{rel}$) to 1.24, a value identical to that in the presence of 9% glycerol (*4*). A large inverse viscosity effect (0.14) was observed on *V/K$_{AcCoA}$*, indicating a step becomes faster in $D_2O$ compared to $H_2O$. A logical possibility for the step affected is the conformational change that is proposed upon binding of AcCoA to enzyme. Interestingly, a small normal viscosity effect of 1.4 is observed on *V*, consistent with a solvent kinetic isotope effect of unity. Data for *V* suggest little or no effect of either solvent deuterium or 9% glycerol, consistent with product inhibition experiments that suggest no contribution of product release to rate-limitation at saturating reactant concentrations. The inverse viscosity effect on *V/K$_{AcCoA}$* is consistent with an increased rate of a conformational change to give the active Michaelis complex upon binding of AcCoA to the E·OAA complex. An inverse isotope effect is observed suggesting that the proposed conformational change in the enzyme on binding of AcCoA is faster in $D_2O$ compared to $H_2O$. An inverse viscosity effect on *V/K$_{AcCoA}$* is consistent with this hypothesis, and suggests the active conformation is stabilized at higher viscosity.

## References

1.      Andi, B., West, A. H., and Cook, P. F. (2004) Kinetic mechanism of histidine-tagged homocitrate synthase from *Saccharomyces cerevisiae*, *Biochemistry 43*, 11790-11795.

2.      Quinn, D. M. S., L. D. (1991) *In Enzyme mechanism from isotope effects*, CRC Press: Boca Raton, FL.

3.      Karsten, W. E. L., C. J. and Cook, P. F. (1995) Inverse solvent isotope effects in the NADmalic enzyme reaction are the result of the viscosity difference between D2O and H2O: Implications for solvent isotope effect studies., *J. Am. Chem. SOC. 117*, 5914-5918.

4.      Lin, Y., West, A. H., and Cook, P. F. (2008) Potassium is an activator of homoisocitrate dehydrogenase from *Saccharomyces cerevisiae*, *Biochemistry 47*, 10809-10815.

# APPENDIX 2

## Pyridine 2,6-dicarboxylate as an inhibitor of homocitrate synthase

### Introduction

The first step in the α-aminoadipate pathway for lysine biosynthesis is catalyzed by homocitrate synthase (HCS). Inhibition studies with dead-end inhibitors aid significantly in determination of kinetic mechanism and binding determinants in the active site (*1*). Pyridine 2,6-dicarboxylate (Pyr), an analog of α-Kg, was used as a dead-end inhibitor in this study.

### Methods

*Inhibition studies*. Inhibition patterns were obtained by measuring initial rates at different concentration of one reactant at a fixed concentration of the other in the absence and presence of inhibitor. AcCoA was varied from $15 - 100$ μM and α-Kg was varied from $25 - 400$ μM and this was repeated in the presence of different concentrations of Pyr. The reaction mixture typically consisted of 50 mM Hepes, pH 7.5, 0.1 mM dichlorophenol indophenol (DCPIP), 200 μM $MgCl_2$, 1 μM *Tt*HCS and variable concentrations of Pyr ( including zero), α-Kg and AcCoA.

### Results

Pyridine 2,6-dicarboxylate is competitive *vs* α-Kg with slight activation at lower concentrations, suggesting binding of the inhibitor to two distinct sites on enzyme, one as an activator and to the same site as α-Kg as an inhibitor (Figure 1 and 2) (*1*).
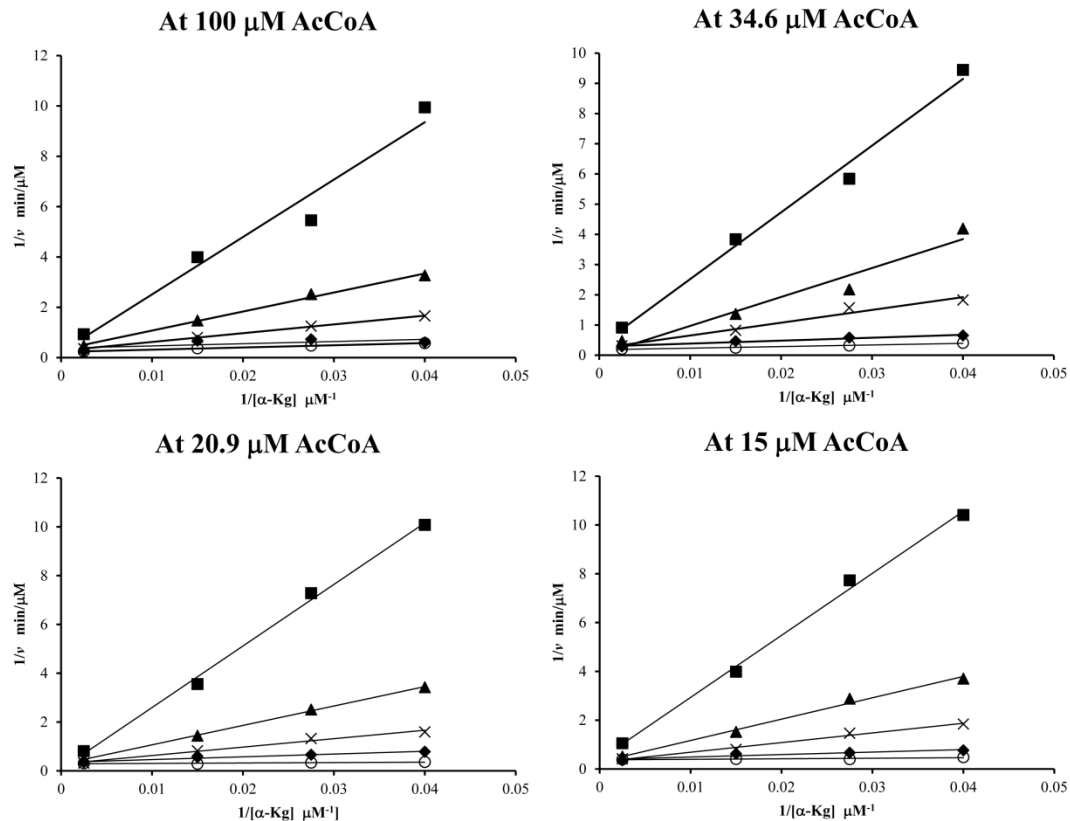
Figure 1. Inhibition pattern with AcCoA varied from 15 – 100 µM and α-Kg varied from 25 – 400 µM. Concentrations of Pyr used were 15 mM (■), 7.5 mM (▲), 5 mM (×), 1 mM (○) and 0 mM (◆).
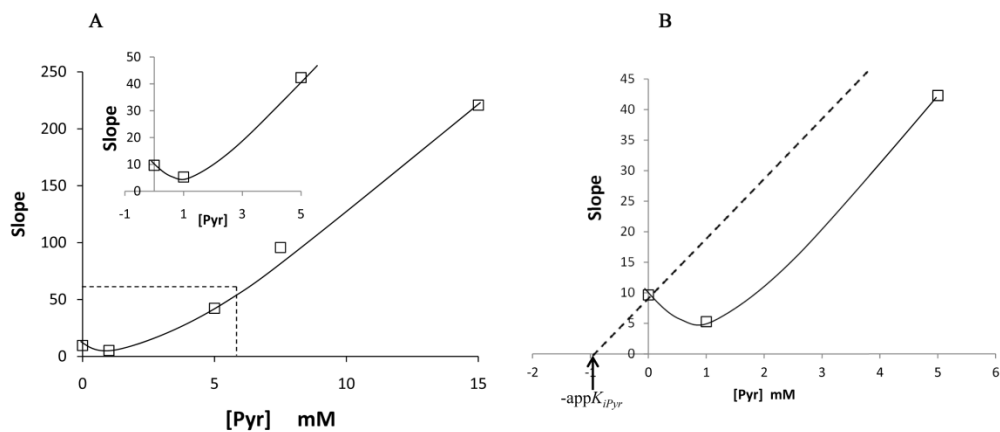


Figure 2. Slope Replot for Inhibition by Pyridine 2,6-dicarboxylate (Pyr). The initial rate was measured as a function of α-Kg concentration (25 to 400 µM) with AcCoA fixed at 100 µM at different fixed levels of Pyr (plot not shown). A. The slope of the double reciprocal plot *vs* Pyr is shown. The inset gives an expansion of the low concentration region to show what appears to be a slight activation by the analog. Curves were drawn by hand. B. Graphical analysis of the data.

127

**Discussion**

Pyridine 2,6-dicarboxylate exhibits a combination of activation at low concentrations and competitive inhibition *vs* α-Kg at higher concentrations. Data indicate the binding of two molecules of the inhibitor, one as an activator and a second to the α-Kg site of free enzyme. Data should adhere to the following rate equation:

$$slope = slope_o \left| \frac{1 + \dfrac{\mathbf{Pyr}}{K_i}}{\left(1 + \dfrac{\mathbf{Pyr}}{K_{act}}\right)\left(1 + \dfrac{\mathbf{Pyr}}{K_{Id}}\right)} \right| \qquad (1)$$

where *slope* is the observed value at any concentration of Pyr, *slope$_o$* is the values in the absence of Pyr, $K_i$ is the inhibition constant for Pyr binding to the α-Kg site, $K_{act}$ is the activation constant, and $K_{Id}$ is a constant that causes *v* to go to a constant value at infinite Pyr (in the absence of inhibition). Attempts to fit the data in Figure 1 were unsuccessful, so the inhibition constant for Pyr was estimated from Figure 1 as follows. The inhibition by Pyr for the activated enzyme is exhibited for the rates at ≥ 5 mM. Assuming Pyr has equal affinity for the less active and activated enzyme, the line obtained from the three points in the graph from 5-15 mM Pyr will be parallel to a line that passes through the point on the *slope* axis at zero Pyr. The abscissa intercept is then equal to the apparent $K_{iPyr}$, which must be corrected for the α-Kg concentration (Figure 1B). Thus, the slope of the line obtained for data ≥ 5 mM Pyr divided by the intercept of the plot gives an app$K_{iPyr}$ of about 60 μM, which gives a value of about 20 μM, correcting for α-Kg equal to $2K_{\alpha\text{-Kg}}$. A rough estimate of the ratio of $K_{Id}$ to $K_{act}$ can be obtained from the data at 1 mM Pyr. At 1 mM Pyr, [*slope$_o$*(1 + Pyr/$K_i$)] will be equal to (10)(1 + 1 mM/0.06 mM), approximately 177. The actual value of slope is 5

from Figure 3, and will be equal to $177/\left(1+\dfrac{\textbf{Pyr}}{K_{act}}\right)\left(1+\dfrac{\textbf{Pyr}}{K_{Id}}\right)$.   A value of about 50 is

obtained for $K_{Id}/K_{act}$.  In order to see any activation by Pyr, the value of $K_{act}$ must be of

the same order of magnitude as the $K_i$ for inhibition, i. e., in the vicinity of 10 μM,

while $K_{Id}$ will be about 50-times greater.   The binding site for Pyr activation is not

known, but it must be on free enzyme, since activation and inhibition are only observed

at low concentrations of both substrates.   Data are suggestive of conformational

heterogeneity with Pyr binding to some site on enzyme stabilizing a more active form of

the enzyme.   The complex inhibition patterns observed in these studies were not

observed for *Saccharomyces cerevisiae* HCS, which exhibited linear inhibition in all

cases (*2*).


**References**

1.     Cook, P. F. a. C., W. W. (2007) *Enzyme kinetics and mechanism*, Taylor & Francis Group, LLC, New York.

2.     Qian, J., West, A. H., and Cook, P. F. (2006) Acid-base chemical mechanism of homocitrate synthase from *Saccharomyces cerevisiae, Biochemistry 45*, 12136-12143.

# APPENDIX 3

## Homocitrate synthase from *Candida albicans*

**Introduction**

Candidiasis represents a major health threat for patients with cancer, AIDS patients, and transplant patients undergoing immunosuppressive treatment. *Cryptococcus neoformans, Aspergillus fumigatus* and *Candida albicans* are human pathogens. These human pathogens in addition to the non-pathogenic yeast *Saccharomyces cerevisiae* and plant pathogen *Magnaporthe grisea* have α-aminoadipate pathway for biosynthesis of lysine (*1, 2*). With essentiality of the lysine biosynthetic pathway reported in *Aspergillus fumigatus* for its survival *in vivo (3),* we could expect the pathway being essential also in the other human pathogen such as *Candida albicans.* Homocitrate synthase being the first and committed step of α-aminoadipate pathway could be a very good target enzyme for drug development against candidiasis. It catalyzes the condensation of Acetyl-CoA (AcCoA) and α-ketoglutarate (α-Kg) to give homocitrate and CoA (Figure 1).
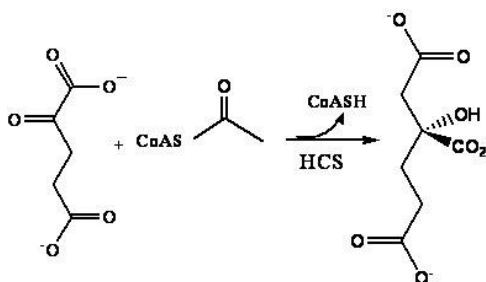


Figure 1. Reaction catalyzed by Homocitrate Synthase (HCS)

**Methods**

*Cloning, protein expression and purification. Candida albicans* homocitrate synthase (*Ca*HCS) *lys*1gene has been listed under putative gene function. The *lys*1 gene was cloned into the pET16b vector (which was provided by Prof. Paula R. Sundstrom, Dartmouth Medical School) and was expressed as a N-terminal histidine tagged 48 kDa protein in the *BL21*(DE3)RIL star strain of *E. coli*.

When the bacterial culture is grown in Luria Bertani Broth at 37°C and induced at various temperatures (37°C for 2-4 hrs, 18°C for 16 hrs, 25°C for 16 hrs) with different combinations of concentrations (0.5 and 1 mM) of IPTG, the protein was expressed as inclusion bodies. In order to get soluble protein, the culture was grown in Magic Media from Invitrogen at 37°C for 16 hrs.

Soluble fractions of the protein were purified using the Ni-NTA resin with buffer containing 50 mM Hepes at pH 7.5, KCl 300 mM with concentrations of imidazole from 30 – 300 mM. *Ca*HCS was eluted at 300 mM imidazole. The isolated enzyme was stored in stabilization buffer containing 100 mM guanidine hydrochloride, 600 mM ammonium sulfate, 100 mM α-cyclodextrin along in the elution buffer (*4*).

*Protein stability at 4°C.* In order to check the stability of the protein stored in stabilization buffer at 4°C, the enzyme activity was tested at regular intervals upto 20 days.

*Enzyme Assay.* HCS activity was measured using the enzyme assay described in Chapter 2.

*Initial Velocity Studies.* To determine the kinetic mechanism, initial velocity patterns were obtained by measuring the initial rate as a function of AcCoA

concentration at different fixed concentrations of α-Kg. The reaction typically consisted of 50 mM Hepes, pH 7.5, 0.1 mM dichlorophenol indophenol (DCPIP), 0.3 μM *Ca*HCS and variable concentrations of α-Kg and AcCoA. Data were plotted as double reciprocal plot of initial rate *vs* substrate concentration. Data could not be obtained in the reverse direction due to the irreversibility of the reaction.

*pH Studies.* To confirm that the enzyme is stable for the duration of the assay time over the pH range tested, the enzyme was preincubated at the given pH and aliquots were taken out at regular time intervals and assayed at pH where the enzyme is known to be stable (pH 7.5 in case of *Ca*HCS). *Ca*HCS was stable between pH 6.0 – 9.0. The effect on the kinetic parameters was also tested at the extreme end of the pH range e.g. pH 6 and pH 9. This information aided in deciding the concentration of substrates to be used while testing the entire pH range. The pH dependence of *V* and *V/K* was obtained by measuring the initial rate as a function of AcCoA, maintaining the α-Kg at a fixed concentration (24 mM). Different buffers were used at different pH ranges at 50 mM concentration – Bis-Tris, 6.0 - 7.0; Hepes, 7.0 - 8.0; TAPS and Ches, 8.0 - 9.0. The pH of the reaction mixture was recorded before and after the reaction. The data was then analyzed by plotting log*V* or *V/K vs* pH.

*Data Processing.* All data were fitted to the appropriate rate equation and the EnzFitter program from BIOSOFT, Cambridge, UK. Initial velocity data were fitted to eq. 1 while the pH dependence of $V/E_t$ was fitted to eq. 2.

$$v = \frac{V\mathbf{AB}}{K_{ia}K_b + K_a\mathbf{B} + K_b\mathbf{A} + \mathbf{AB}} \qquad (1)$$

$$\log y = \log\left[ C \Big/ \left(1 + \frac{\mathbf{H}}{K_1} + \frac{K_2}{\mathbf{H}}\right) \right] \qquad (2)$$

132

In eqs. 1, $v$ and $V$ are initial and maximum velocities, respectively, **A** and **B**, are substrate concentrations, $K_a$ and $K_b$ are Michaelis constants for substrates A and B, respectively. $K_{ia}$ is the dissociation constant for A from the EA complex. In equation 2, $y$ is the observed value of $V/E_t$ at any pH, $C$ is the pH-independent value of $y$, **H** is the hydrogen ion concentration, and $K_1$ and $K_2$ are the acid dissociation constants of functional groups required in a given protonation state on enzyme for optimal catalysis.

## Results

*Protein expression and purification.* *Ca*HCS was expressed as a soluble protein when grown for 16 hours in Magic Media at 37°C. Nearly 95% pure protein was obtained using Ni-NTA column (Figure 2). ~3mg of protein was purified from 5 g of wet cell mass. The protein was stored in stabilization buffer at 4°C composition of which was mentioned earlier.
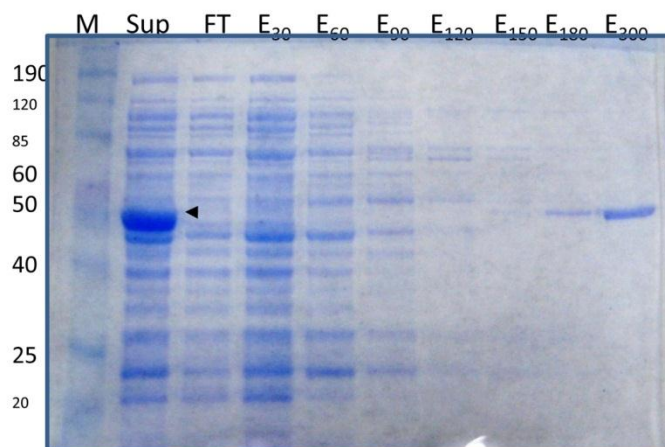


Figure 2. Purification of *Ca*HCS using Ni-NTA column. Most of the CaHCS protein was eluted at 300 mM imidazole to about 95% purity estimated by SDS-PAGE.

*Stability of CaHCS in storage buffer at 4°C.* Activity of the stored enzyme was measured at different time intervals at saturating concentrations of both the substrates. There was a sharp drop in activity in the first few days and then the activity stabilized and not much loss was seen until 20 days (Figure 3).
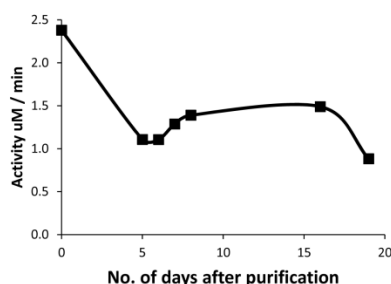


Figure 3. Stability of *Ca*HCS in storage buffer. Aliquots of enzyme were tested for activity at saturated concentrations of α-Kg and AcCoA at pH 7.5 and 25°C temperature.

*Initial Velocity Studies.* Initial velocity patterns were obtained at varying concentrations of α-Kg (0.5 – 20 mM) at different fixed concentrations of AcCoA (3.36 - 200 μM) (Figure 4). The lines intersect to the left of the vertical axis suggesting a sequential Bi Bi kinetic mechanism. The kinetic parameters are listed in Table 1.

**Table 1. Summary of Kinetic parameters for *Ca*HCS.**

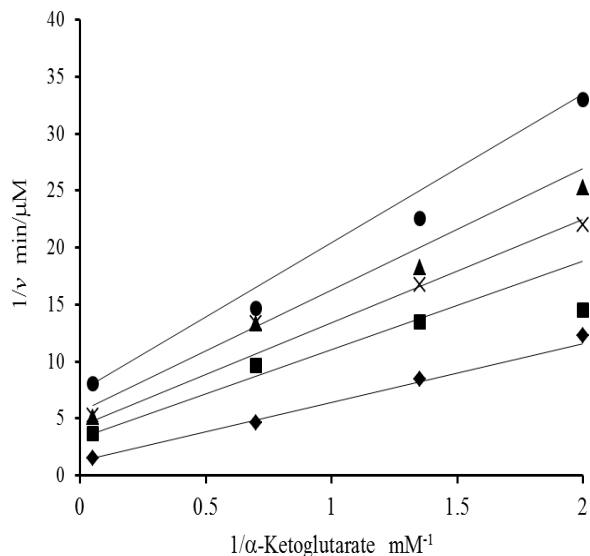| Parameter | Value ± S.E. |
|---|---|
| $V/E_t$ (s$^{-1}$) | $0.0513 \pm 0.0004$ |
| $V/K_{\alpha\text{-}Kg}E_t$ (M$^{-1}$s$^{-1}$) | $11.20 \pm 0.88$ |
| $V/K_{AcCoA}E_t$ (M$^{-1}$s$^{-1}$) | $1740 \pm 113$ |
| $K_{\alpha\text{-}Kg}$ (mM) | $4.6 \pm 0.36$ |
| $K_{AcCoA}$ (mM) | $0.03 \pm 0.002$ |
| $K_{i\ \alpha\text{-}Kg}$ (mM) | $1.26 \pm 0.25$ |

Figure 4. Initial velocity pattern of *Ca*HCS with varying concentrations of α-Kg at different fixed concentrations of AcCoA at pH 7.5 and 25 °C. Data are plotted as a function of α-Kg at different concentrations of AcCoA as follows: 5 (●), 7.4 (▲), 9.8 (×), 14.3 (■) and 200 (♦) μM. Points in the plot are experimental, while the solid lines are theoretical based on a fit to eq 1.

*pH dependence of kinetic parameters.*

The pH dependence of log $V/E_t$ *vs* pH is obtained at saturating concentrations of the reactants while log$V/K$ profile is obtained with one reactant at limiting concentrations and the other saturating. The $V/E_t$ profile will give p$K_a$ values of residues that are important for catalysis, while $V/K$ will reflect groups either on enzyme or on substrate important for binding and/or catalysis. In the case of the $V/K_{AcCoA}$ pH-rate profile, the groups are for E·α-Kg and/or AcCoA.

The $V/E_t$ profile exhibits slopes of 1 and -1, indicating the requirement for one group to be unprotonated and one protonated for optimum catalysis (Figure 5). A group with a p$K_a$ of 7.2 ± 0.2 must be unprotonated while a group with a p$K_a$ of 8.3 ± 0.2 must be protonated. These groups also can be in reverse protonation states. By analogy to

135

the chemical mechanism of *Sc*HCS (*5*) the group with p$K_a$ of 7.2 would likely function as a general base to accept a proton from the methyl group of AcCoA. The group with p$K_a$ of 8.3 is likely a general acid that donates a proton to the α-Kg carbonyl as the nucleophilic attack by the methyl of AcCoA occurs. $V/K_{AcCoA}$ profile is pH independent for the pH range tested. The p$K_a$ of groups involved in binding of AcCoA could be outside the tested range and hence are not detected (Figure 7). The pH independent value for $V/\mathbf{E_t}$ and $V/K_{AcCoA}$ $\mathbf{E_t}$ are $0.06 \pm 0.01$ s$^{-1}$ and $(7.03 \pm 0.01) \times 10^2$ M$^{-1}$ s$^{-1}$, respectively.
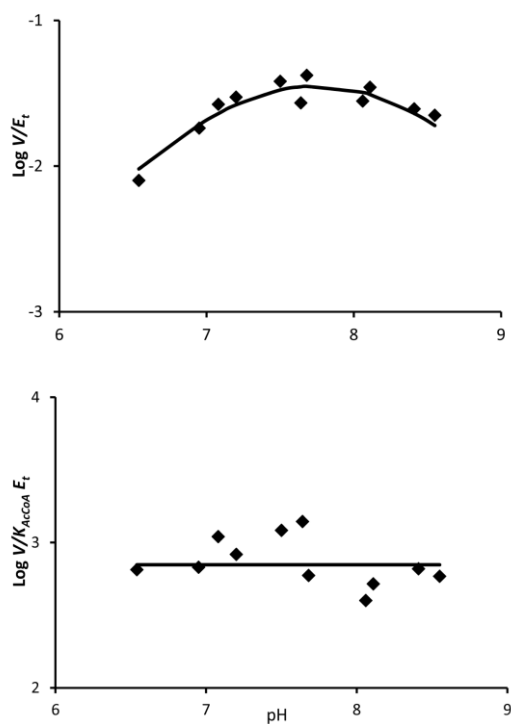


Figure 5. pH dependence of kinetic parameters for the *Ca*HCS reaction. The points shown are the experimentally determined values, while the curve for $V/\mathbf{E_t}$ profile is theoretical based on fit of the data using equation 2.

136

**Discussion**

*Candida albicans* homocitrate synthase and *Sc*HCS are 89% identical at the amino acid level. This study was to see the differences between *Sc*HCS and *Ca*HCS if any and carry out detailed biochemical investigation of *Ca*HCS.

*Ca*HCS was successfully over-expressed and purified in an active form. Soluble form of the protein was obtained when grown in Magic Media at 37 °C. *Ca*HCS was found to be very unstable as isolated. It was amenable to short term storage at 4°C in presence of the stabilization buffer, the condition same as the one for *Sc*HCS (*4*). Lower stability of the enzyme limited the kind of biochemical characterization that can be carried out. Even in presence of the stabilization buffer, the enzyme would lose activity rapidly initially and then maintain its activity for about 2 months.

Initial velocity patterns at pH 7.5 exhibited the lines intersecting to the left of the ordinate suggesting an ordered sequential kinetic mechanism, similar to that proposed for *Sc*HCS. The values for the kinetic parameters were similar to those in the case of *Sc*HCS. The pH profile for $V/\mathbf{E_t}$ indicated presence of two groups required for optimum catalysis. The group with $pK_a$ 7.2 needs to be unprotonated and is speculated to function as a general base aiding extraction of proton from methyl of AcCoA. The second group with a $pK_a$ of 8.3 might function as a general acid donating a proton to form an alcohol as the methyl of AcCoA attacks. The profile for $V/K_{AcCoA}$ was pH independent for the range of pH tested. From the data in this study, it is concluded that the biochemical parameters tested are similar to *Sc*HCS (*4-6*). As *Ca*HCS is also unstable, it is not suitable for crystallographic studies.

# References

1.      Xu, H., Andi, B., Qian, J., West, A. H., and Cook, P. F. (2006) The α-aminoadipate pathway for lysine biosynthesis in fungi, *Cell Biochem. Biophys. 46*, 43-64.

2.      Zabriskie, T. M., and Jackson, M. D. (2000) Lysine biosynthesis and metabolism in fungi, *Nat. Prod. Rep. 17*, 85-97.

3.      Liebmann, B., Muhleisen, T. W., Muller M, Hecht, M., Weidner, G., Braun, A., Brock M., and Brakhage, A. A. . (2004) Deletion of the *Aspergillus fumigatus* lysine biosynthesis gene lysF encoding homoaconitase leads to attenuated virulence in a low-dose mouse infection model of invasive aspergillosis., *Arch Microbiol. 181*, 378 - 383.

4.      Andi, B., West, A. H., and Cook, P. F. (2004) Stabilization and characterization of histidine-tagged homocitrate synthase from *Saccharomyces cerevisiae*, *Arch Biochem Biophys. 421*, 243-254.

5.      Qian, J., West, A. H., and Cook, P. F. (2006) Acid-base chemical mechanism of homocitrate synthase from *Saccharomyces cerevisiae*, *Biochemistry 45*, 12136-12143.

6.      Andi, B., West, A. H., and Cook, P. F. (2004) Kinetic mechanism of histidine-tagged homocitrate synthase from *Saccharomyces cerevisiae*, *Biochemistry 43*, 11790-11795.

This is just the beginning...